ENGINEERING RESEARCH INSTITUTE

THE EFFECTS OF TURBULENCE AND WIND SPEED ON THE RATE OF EVAPORATION OF A FUEL SPRAY

by

R. G. Fledderman

A. R. Hanson

REPORT NO. CM667

Project M604-3

CONTRACT NOrd 7924, TASK UMH-3D

U. S. NAVY DEPARTMENT, BUREAU OF ORDNANCE

June 20, 1951

UNIVERSITY OF MICHIGAN • ANN ARBOR

ACKNOWLEDGMENTS

The authors are pleased to express their gratitude to Dr. Arnold M. Kuethe for guidance and encouragement from the very beginning of this investigation. Dr. Kuethe supervised the project from its inception, and all phases of the work were stimulated and improved through his contributions. During the year 1949-50 the project was supervised by Prof. W. C. Nelson, and it is a pleasure to thank him for his interest and cooperation.

Drs. J. L. York and J. T. Banchero of the Chemical Engineering Department are to be thanked for discussions and help on spray photography and the treatment of mass- and heat-transfer processes. Dr. R. C. F. Bartels of the Mathematics Department offered valuable suggestions on certain points of theory. Dr. W. W. Hagerty of the Engineering Mechanics Department generously supplied information on the measurement of spray velocities.

Mr. Eugene Turner kindly examined the portions of Section 4 dealing with lens errors and offered valuable criticism. Mssrs. J. B. Cooper, Jr., R. B. Ridenour, and H. V. Talbot contributed a great deal to the photographic work, both in ideas and processing of the film.

Mr. William Fetchik helped extensively in the taking and reduction of data.

Thanks are also due to Mr. P. B. McKee, who collaborated in the early stages of the work on the design and construction of the wind tunnel.

TABLE OF CONTENTS

LIST OF FIGURES

LIST OF TABLES

THE EFFECTS OF TURBULENCE AND WIND SPEED ON THE RATE OF EVAPORATION OF A FUEL SPRAY

SUMMARY

This report describes an experimental investigation of the effect of turbulence and relative velocity upon the evaporation of a liquid-fuel spray.

A hollow-cone spray was injected downstream into the test section of a wind tunnel in such a way that the axis of the spray cone coincided with the centerline of the tunnel. The total mass passing through any transverse plane of the test section was measured by means of a rack of open-end collector tubes. By making collections at various distances downstream from the tip of the nozzle it was possible to determine the mass of the spray evaporated as a function of this distance. The relative velocity between the spray and the airstream was varied by changing the velocity of the airstream. Turbulence intensity, on the other hand, could be changed independently of velocity by introducing grids of various-sized wires upstream of the test section. Downstream traverses made at different velocities and turbulence levels permitted a comparison of the amount of spray evaporated under the influence of these parameters.

A hot-wire anemometer was used in the usual manner to measure the intensity and scale of turbulence in the tunnel test section.

The measurement of the diameters of individual spray drops was carried out by photographing a small volume element of the spray at some position in its path through the test section of the tunnel. From the measured sizes of many drops it was possible to calculate a mean diameter. Such a mean diameter was determined for two different levels of turbulence intensity.

A correlation of the present data with existing theory has been carried out. Although the theory has, in the past, been verified only for single drops of moderately volatile substances, the results reported here indicate that the form of the equation is correct for sprays of highly volatile liquids, but that an empirical constant occurring in the evaporation equation needs checking.

1. INTRODUCTION

1.1 Statement of the Problem

In studying combustion it is important to know which aerodynamic parameters dominate the process of evaporation of a spray which is injected into a moving airstream. Free-stream turbulence and the relative velocity between spray and airstream appear to be the most important of these parameters, and the present experimental study was designed to measure their influence.

No attempt has been made to assess the numerous factors which enter into the turbulence and velocity fields which might be produced by particular types of combustion chambers or air inlets. Rather, the aim here has been to explore the extent to which existing theory, verified for simpler systems of moderately volatile substances, agrees with experiment for a complex spray of a highly volatile liquid.

The problem also embraces the use of photography in the study of sprays, with particular emphasis on the numerous errors which are of utmost importance if the method is to yield results of any value.

1.2 Properties of Sprays

For the purposes of discussion and definition, certain properties and terms will be reviewed briefly.

a) Size Distribution. -- Liquid fogs and sprays in general consist of dispersed drops of a range in sizes. The various sizes of drops are present in different abundances, with the most plentiful size lying somewhere between the maximum and minimum. A number of useful mathematical descriptions of the size distribution have been given. Important among these are those of Rosin-Rammler and Nukiyama-Tanasawa, which have been discussed by Bevans[1*] and are, respectively,

$$\frac{dN}{d\delta} = a\,\delta^{q-4}\,e^{-b\delta^q} \qquad (1.1)$$

and

$$\frac{dN}{d\delta} = a\,\delta^{2}\,e^{-b\delta^q} \qquad (1.2)$$

where a, b, and q are constants, δ is the drop diameter, and N is the number of drops larger than δ. Eqs 1.1 and 1.2 are empirical in nature but have been

---

*For bibliographic references, see Bibliography, end of text.

found to describe atomizing processes quite well. There are other distribution functions which could be used except that they are more complicated and render evaluation of the constants more difficult without a significant increase in accuracy.

When the distribution of drop sizes in a spray is known, it becomes possible to compute a "mean" drop diameter $\bar{\delta}$. This mean diameter may be based on surface area, the ratio of surface area to volume, mass, or volume. For example, the volume mean, defined by the relation,

$$\bar{\delta} = \left\{ \frac{\int_0^N \delta^3 \, dN}{\int_0^N dN} \right\}^{1/3} , \tag{1.3}$$

gives

$$\bar{\delta} = \frac{1}{b^{1/q}} \left\{ \frac{\Gamma(6/q)}{\Gamma(3/q)} \right\}^{1/3} \tag{1.4}$$

for the Nukiyama-Tanasawa distribution, and

$$\bar{\delta} = \frac{1}{b^{1/q}} \left\{ \frac{1}{\Gamma(1 - 3/q)} \right\}^{1/3} \tag{1.5}$$

for the Rosin-Rammler distribution, where $\Gamma(\ )$ denotes the complete gamma function.

b) Mass Distribution. -- Most nozzles develop a spray which is closely conical in shape. Depending upon the nozzle design, the concentration of drops may be a maximum along the axis and gradually decrease to zero at the edge of the conical surface; or the concentration may be a minimum along the axis, rise to a maximum, and then fall to zero with increasing distance from the axis. The latter, called a "hollow-cone" spray, is the type used in the present work. Most of the mass of the hollow-cone spray passes through an annular strip concentric with the spray axis, and the width of this annulus will be referred to as the "sheath thickness".

c) Spray Angle. -- In the case of conical sprays the spray angle is defined as that total included angle which takes in some specified fraction, say 90 per cent, of the total mass in the spray. In the present experiments the spray angles were measured from photographs of the spray; the angle could also be determined from the spray-collection data described later.

d) Drop Velocity. -- The velocities with which drops issue from the nozzle orifice depend upon the design of the nozzle and the operating conditions.

Although few data are available, it seems certain[2] that there is a distribution of velocities among the drops. Whether this distribution arises during the formation of the spray is not clear; nevertheless, it could still be produced after the drops were formed because of the dependence of drag coefficient on diameter through the Reynolds number. It is worth noting that the initial drop velocity can be far different from the average nozzle-exit velocity. The calculations and measurements of Section 6 show that the initial drop velocity is only a few per cent of the average nozzle-exit velocity calculated from the rate of mass flow. Diffusion of the liquid after it leaves the orifice and the effects of the swirl are major factors responsible for the discrepancy.

e) Spray Formation. -- Very briefly, a spray is formed from a jet or sheet of liquid by virtue of an instability which produces waves on the surface. These waves increase in amplitude, an effect which, together with the action of the viscosity of the air, tears the liquid into fine ligaments. The ligaments in turn break apart into segments of various lengths which are drawn into drops by surface tension.

Many different nozzle designs have been developed to exploit the factors favorable to rapid and fine jet break-up. The one used in the present work has a swirl insert which imparts rotation to the liquid before it emerges from the orifice. This rotation greatly increases the spray angle and thus accelerates the atomization process.

1.3 Methods of Spray Measurement

A considerable number of methods and techniques for spray measurement have been developed and perfected over the past twenty-five or thirty years. Most of these methods employ mechanical sampling coupled with optical or electrooptical devices to count and measure the drops sampled. The rotating cylinder method is entirely mechanical. Except for those methods which are purely optical or electrooptical, they all disturb the normal pattern of the spray to some extent. All devices which mechanically extract a spray sample are certain to be more or less selective in their sampling action and that to a degree which is aggravated when the drops are carried in a moving airstream. The various methods will be discussed briefly with a view to bringing out their limitations in the present application.

a) Prepared Surfaces. -- Many studies of atomization have been made using plane surfaces which have been treated so as to capture drops or to retain a permanent impression of their impacts. Lee,[3] for example, used glass plates which had been coated with soot. He exposed the plates to a liquid spray and then measured with a microscope the diameters of the circular impressions left by the drops upon the sooted surface. Lee's work was done under experimental conditions which confined the spray to a test chamber in which the air was at rest.

Other investigators have used glass slides coated with greases or oils. Houghton[4] and Houghton and Radford[5] studied fog drops by catching them on slides

coated with vaseline applied by a special technique. Before appreciable evaporation could take place, the drops were photographed through a microscope. Measurements of the drops were made by projecting the negatives on a ground-glass screen at a 10X magnification.

Kinoshita and Uchiyama[6] used oiled slides to sample fog drops and then photographed the slides through a microscope. Their method was therefore essentially the same as that employed by Houghton and Radford.

The procedures just described are well suited to the study of fog drops, but there are a number of reasons why they are inadequate for the present work. First, the presence of a glass plate in a spray carried by a moving airstream will disturb the local spray and flow pattern considerably. Moreover, the plate will not catch a representative sample of drops but will tend to catch more of the larger drops having greater inertia. Second, a fuel-like liquid, such as hexane, will dissolve vaseline and a wide variety of oils and greases. Third, even if the surface were covered with soot or some other insoluble material, the highly volatile drops, especially the smaller ones, might evaporate without leaving a visible trace. A fourth difficulty is that of determining the "flattening" of the drop due to impact with the slide. While this difficulty is not peculiar to the present problem, it is certainly made more severe by the higher impact velocities.

b) Collector Tubes. -- The collector tube has been used extensively in the present investigation and is therefore discussed fully in Section 3.

c) Photometric Method. -- Sauter[7] was the first to utilize the attenuation of a beam of light by the action of a spray to determine the mean diameter of the drops. On the assumption that each drop is opaque to the light, he derives the relation

$$\bar{\delta} = \frac{150\,\Psi_f\,L}{\Psi_a\,J} , \qquad (1.6)$$

where Ψ_f is the volume of fuel atomized per second, L is the length of the light path, Ψ_a is the volume rate of air flow, and J is the per cent diminution of light intensity through the spray. As here defined, the mean drop diameter applies to a fictitious spray having the same ratio of volume to surface area as the actual spray. Eq 1.6 holds only for relatively "thin" sprays, that is, for $J < 20$ per cent.[7] For the case of dense sprays where some drops are shaded by others, Sauter[7] gives

$$\bar{\delta} = \frac{150\,\Psi_f\,L}{\Psi_a\,j} , \qquad (1.7)$$

where j is related to J by the expression

$$J = 100\,(1 - e^{-j/100}) ,$$

from which

$$j = -100 \ln (1 - J/100) \qquad (1.8)$$

It appears that Eqs 1.7 and 1.8 cover the general case of sprays of any density.

The experimental arrangement employed by Sauter made use of a visual, bench type of photometer to measure the intensity of the light transmitted by the spray. If I_o is the incident light intensity and I the intensity of the transmitted light, then $J = 100\ I/I_o$.

Schmidt[8] has recently used Sauter's method, but measured light intensities with a photoelectric photometer. He does not report any details on the accuracy of his instrument beyond stating that it is suitable for rapid, comparative measurements of atomization to check the effects of changes in design parameters.

On the basis of Schmidt's results it was decided in the initial stages of the present work to use this method to measure the mean drop size of the spray. Accordingly, a photometer of similar type was built and tested. The reproducibility and sensitivity proved to be inadequate, and the amount of work involved in developing a better instrument made use of the collector-tube and photographic methods more expedient.

d) Photography. -- Those methods which make use of prepared surfaces or collection cells usually rely upon a photographic record for final measurement of the drop diameters. This is also true, of course, when photographs are taken of the spray directly without the use of sampling devices. The subject of spray photography is taken up in some detail in Section 5.

e) Corona Method. -- Coronas can occur in nature when fog, smoke, or clouds exist between the observer and the sun or moon. Such coronas consist of circular, colored bands which closely and concentrically surround the sun or moon and are due to diffraction of light around the drops. In dealing with sprays and artificial fogs in the laboratory the phenomenon can sometimes be observed by viewing a pinhole source of light through a volume of the spray or fog. If monochromatic light is used the bands are no longer colored, but rather the entire corona becomes a system of alternate bright and dark rings. The bright rings are called maxima, the dark minima. The peak intensity of the successive maxima decreases rapidly. For example, relative to the intensity of the central disc the intensity of the first maximum is 2 per cent, with still smaller values for the higher orders.[9]

The theory of coronas[9] leads to the basic relation

$$\sin \theta_n = (n + 0.22) \frac{\lambda}{\delta} , \qquad (1.9)$$

where n is the order of the minimum,* θ_n is the angular distance from the center of the corona to the nth minimum, λ is the wavelength of light, and δ is the diameter of the drops. The derivation of Eq 1.9 assumes that all the drops have the same diameter. It is evident that, when a fog or spray consists of drops having a distribution in size, the corona rings will tend to diffuse. In fact, if the size distribution is relatively broad, separate rings are not discernible.

Eq 1.9 is not valid when d approaches the wavelength λ, and Wilson[10] finds that it holds only when δ is larger than about 10 microns. Below this size, "Tyndall scattering"[9] takes place. On the other hand, as δ increases θ_n decreases until for large values of δ the value of θ_n becomes too small to measure. For example, if δ = 200 microns, the corresponding value of θ_n for the first minimum is 12.2 minutes when λ = 580 millimicrons, a wavelength in the yellow region of the spectrum. Due to the rapid decrease of light intensity with increasing order, it is usually possible to see only three or four minima.

Schmidt[11] has tried this method on sprays produced by various types of nozzles and finds that the corona can be observed only with certain hollow-cone nozzles. This latter type of nozzle evidently develops drops which are sufficiently small and uniform to produce definite diffraction rings. After comparing the results of the corona and other methods of measuring mean drop size, Schmidt observes that there is poor agreement among them and, further, that the corona mean drop size does not even fall near the maximum of the distribution curve.

In the course of the present work an attempt was made to use the corona method. Although a slight brightening occurred around the light source, distinct diffraction rings could not be seen. This failure to produce a corona is presumably due to the range of drop sizes in the spray.

f) Collection Cells. -- Efforts to capture drops without splattering or appreciable distortion have led to the development of what may be called the collection cell. A sample of the spray is allowed to fall into a shallow dish or cell containing an emulsifying liquid. The technique has been perfected by Hausser and Strobl,[12] Woeltjen,[13] Rupe,[14] and others. Collection cells are excellent for studying certain sprays in a static atmosphere, but obvious practical difficulties rule out their use in the airstream of a wind tunnel.

g) Electronic Counting from Photographs. -- Ordinary visual measurement of drop sizes from photographic films or plates involves much tedious and time-consuming work. To overcome this drawback, Rupe[14] has devised a system which automatically analyzes photographic drop images and sorts them into size groups. This is done by means of a scanning device which utilizes photocells to actuate counting circuits.

---

*The order of a maximum or minimum is found by counting the number of bright or dark rings from the center out to the ring in question.

The necessary image sharpness was not obtainable with the lenses available in the present study. Moreover, the spray was thinned out by injection into the airstream to such an extent that very few drops appeared on any one negative. Rupe collected spray in small cells which he later photographed, a technique which is not practicable in an airstream.

h) Impingement on Wires. -- An electronic method for counting individual particles and determining their sizes has been devised by Guyton.[15] In this system the particles are sucked by vacuum into the open end of a cylindrical glass probe equipped with an internal conical nozzle, which directs the particles towards a fine wire passing through the probe. The wire is connected to the input of a vacuum-tube amplifier whose output can be viewed on an oscilloscope or used to actuate an electromechanical counter. The potential applied to the wire depends on the nature of the particles. For solid particles it is zero, while for water drops the sensitivity of the device is poor unless the wire is at a potential of several hundred volts. When a particle or drop impinges on the wire, or passes close by, a voltage pulse is developed which is fed into the amplifier.

This method appears promising, but since its limitations have not been investigated, a considerable amount of work would be required before its accuracy could be checked.

In addition to the methods discussed above, there are certain others which, for one reason or another, are impracticable in the present application. Rotating cylinders have been used extensively[16,17] to study atmospheric clouds and icing due to deposition of water drops. However, this method presents formidable problems if applied to sprays of highly volatile liquids which do not freeze on impact. A procedure that might be called the "Rainbow Method" uses an electrooptical instrument to measure the light intensity of an artificially created rainbow. It seems likely that this type of instrument could be adapted to spray studies in a wind tunnel. However, at the time the rainbow-recorder design was published,[18] the present investigation was well under way and was committed to the use of collector tubes and photography. Lastly, mention may be made of the Tyndallmeter, which is essentially a photometer arranged to measure the intensity of light which is scattered along the normal to the incident beam by small particles. Such an instrument has been used by Tolman, et al.[19] in the study of smokes and liquid suspensions of particles. They found that the Tyndallmeter reading is a function of particle size. However, the two derived equations are merely limiting forms valid for particles which are classed as "very small" or "large". A rough quantitative agreement was found between the theory and experiment, but the method is not accurate enough for the present work.

The investigation reported here makes use of collector tubes and direct photography of the spray. These two methods are therefore discussed in some detail in Sections 3 and 4.

2. DESCRIPTION OF EQUIPMENT

2.1 Wind Tunnel

A general view of the wind tunnel is shown in Fig. 1. Air is drawn from within the room through the bellmouth at the left and exhausted outdoors through the wall on the right. Heaters in the room permit control of the air temperature during a run to within about ± 1°C for usual outdoor temperatures.

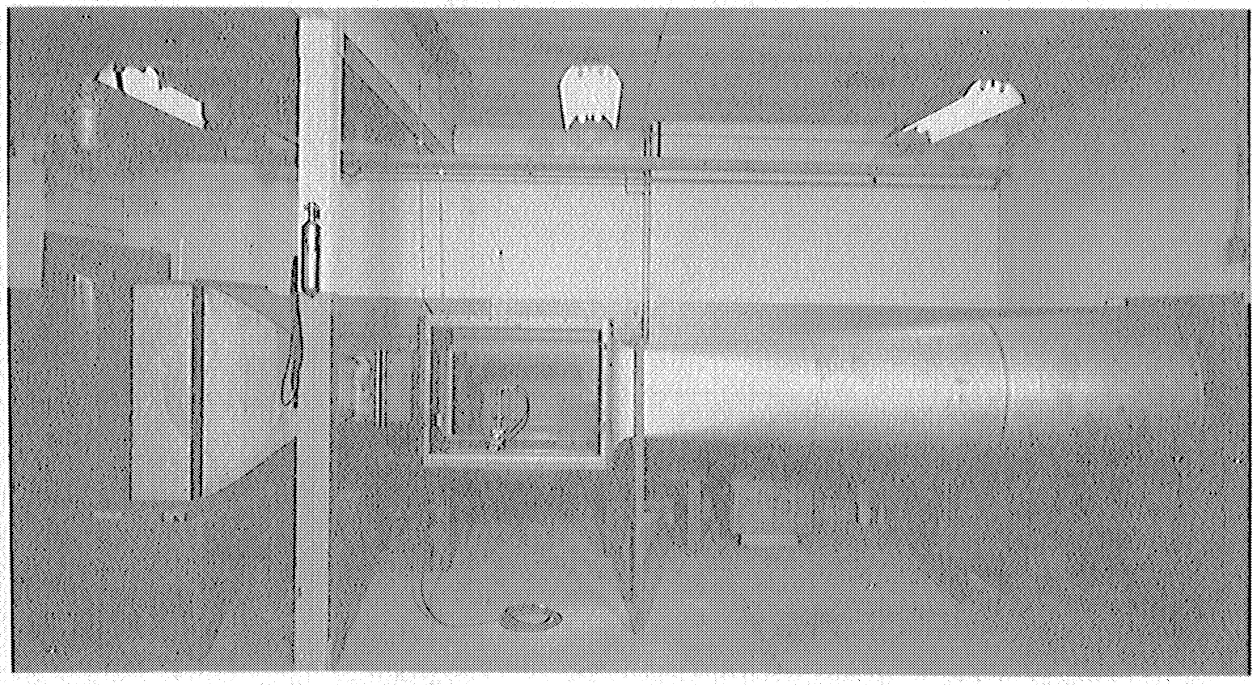

Fig. 1. Overall View of Wind Tunnel and Test Section

Connecting the bellmouth and contraction sections is a settling chamber, 3 ft by 3 ft in section and 1 ft long, which contains five 40-mesh screens for the purpose of reducing the initial turbulence. Variation of the turbulence level is accomplished by inserting screens held between removable frames located 8 in. upstream of the entrance to the test section. Four screens were used in all, three of these being 2-mesh of 0.148-in., 0.105-in., and 0.072-in. wire diameters, while the fourth was a 2.5-mesh of 0.148-in. diameter wire, to which cloth streamers were tied in a regular pattern. The spray nozzle unit is located near the downstream end of the straight section, the tip of the nozzle being approximately in the entrance plane of the test section. Spray is injected downstream along the axis of the tunnel.

The test section itself is 3 ft long and 2 ft by 2 ft in a section normal to the airflow; it is equipped with removable glass sides. A 9-ft diffuser joins the downstream end of the test section and the fan housing.

2.2 Spray Nozzle and Pressure System

An exploded view of the nozzle unit is shown in Fig. 2. The mounting strut, made of stainless steel, is shaped in the form of a symmetrical airfoil to minimize the turbulent wake. A central body to contain the nozzle proper was machined from stainless steel; it was slotted so that it could be slipped over the strut and silver-soldered at the midpoint. Fuel flows to the nozzle through a hole drilled along the strut from the threaded end to the central body.

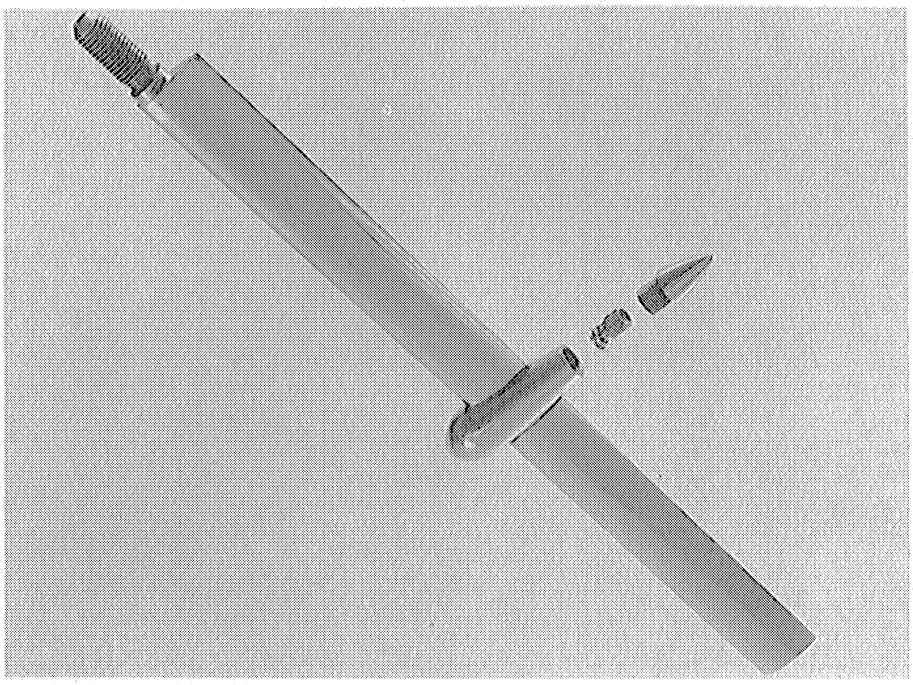

Fig. 2. Exploded View of Nozzle Assembly

The orifice diameter of the nozzle is 0.030 in. and has a length-to-diameter ratio of approximately 3. The hole was drilled and then lapped to make it uniform and smooth. In order to accommodate the nozzle insert, a hole 0.25 in. in diameter and 0.5 in. deep was drilled in the nozzle section, a tapered section connecting this hole with the orifice. A shallow 30° chamber fits the bevel on one part of the insert and seats it properly. The insert is in two sections. The lower section is a brass cylinder, 0.25 in. in diameter and 0.25 in. long, on which sixteen fine V-threads have been cut. This insert fits snugly into the nozzle and imparts swirl to the liquid. A beveled section screws into the swirl cylinder and positions it properly in the nozzle. Four radial holes in the stem of this beveled section connect with an axial hole drilled from the top end and serve to feed the liquid to the swirl cylinder. There is a cup-shaped region at the bottom of the swirl chamber, which acts as a mixing chamber for the liquid before it is ejected from the orifice.

Fig. 3. shows the mounted nozzle system in operation.

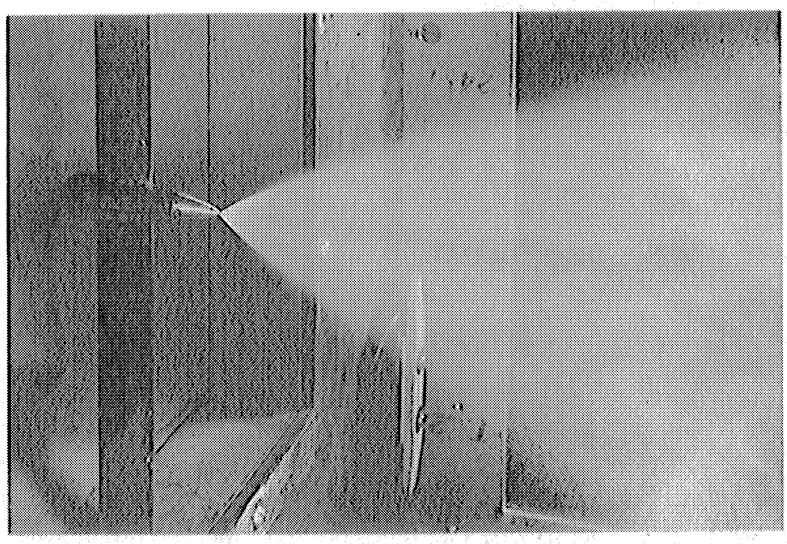

Fig. 3. Nozzle in Operation

The pressure source for the system consists of three bottles of nitrogen at 2000 psi, whose outputs are combined, the manifold being connected to a pressure-reduction valve. The reduction valve handles a maximum of 3000 psi at the inlet and 1000 psi at the outlet, whereas the useful working range of pressure in this experiment was 150-500 psi. The reduction-valve outlet leads to a 1.5-liter fuel tank, which is connected to the nozzle through an on-off valve.

2.3 Sampling Apparatus

The spray collector is a sampling probe which consists of a tube closed off at one end and rounded to hemispherical shape at the other. A hole is drilled in the rounded nose to admit the spray which strikes it. The collectors used in this experiment are made from 5/16-in. (O.D.) copper tubing with a nose opening of 0.125-in. diameter. A brass plug is fitted and silver-soldered to the other end of the probe, while a hole drilled in this plug accommodates a tapered steel pin to which it is also silver-soldered. This not only seals the end of the probe but furnishes a method of support in the test section. For special evaporation tests, similar probes with opening diameters of 0.149 in., 0.0875 in., and 0.0615 in. were also used. A hard-rubber cap placed over the nose of the probe prevents evaporation out of the open end.

The collector probes are mounted in a rack which is made up of 0.50-in. steel rod welded together in the form of a "T". The crossbar is 19 in. in length and has tapered holes, drilled every inch, which fit the tapered pins of the probes. These holes are accurately centered about the middle hole and are precision-drilled for depth, so that the open ends of the probes lie on a straight line parallel to the centerline of the crossbar. The forms of the probes, caps, and mounting rack may be seen in Fig. 4.

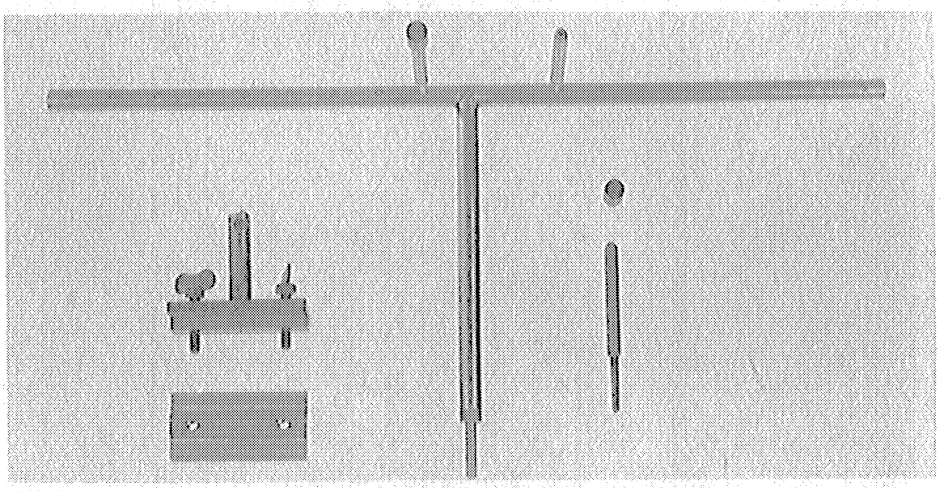

Fig. 4. Collector Tubes and Mounting Apparatus

The collector rack is mounted on a track system by which the probes may be located at any point in the spray. Longitudinal position is determined by two tracks which run parallel to the airstream direction and along the entire length of the test section. A "V" groove cut down the centerline of each track on its top surface acts as a guide for the cross-stream member. Fig. 5 shows track and sampling apparatus in use. The amount of liquid collected by

Fig. 5. Sampling Apparatus Mounted in Test Section

a probe is determined by weighing on an analytical balance accurate to within 0.1 milligram.

2.4 Hot-Wire Anemometer

Except for minor details in construction, the turbulence-measuring equipment is the same as the Bureau of Standards Model 1940.[20] The frequency response of the present amplifier is flat to within 1 db from 20 to 7000 cycles per second. A general view of the equipment is given in Fig. 6, where the calibrating oscillator and monitoring oscilloscope are shown to the right of the main anemometer unit.

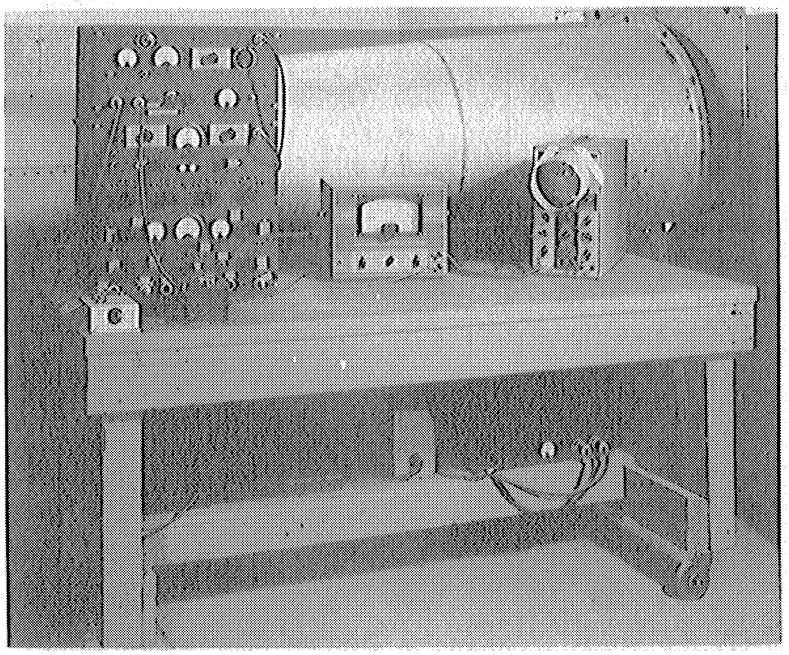

Fig. 6. Hot-Wire Amplifier and Associated Equipment

The hot wires themselves were made up from 0.00035-in. diameter tungsten wire which was copper-plated at the ends by the method of Schubauer and Klebanoff.[21] Wire lengths of about 0.08 in. were soft-soldered in the usual manner to steel supporting needles which had been slightly flattened at the tips. A typical probe is shown disassembled in Fig. 7. The time constant of the wire was determined by mechanically vibrating a sample in a low-turbulence airstream at a number of known frequencies and amplitudes, as described for the Bureau of Standards Model 1940.[20]

Velocity correlation measurements were made with two parallel wires, one of which was movable by a lead screw mechanism. The arrangement is shown in Fig. 8.

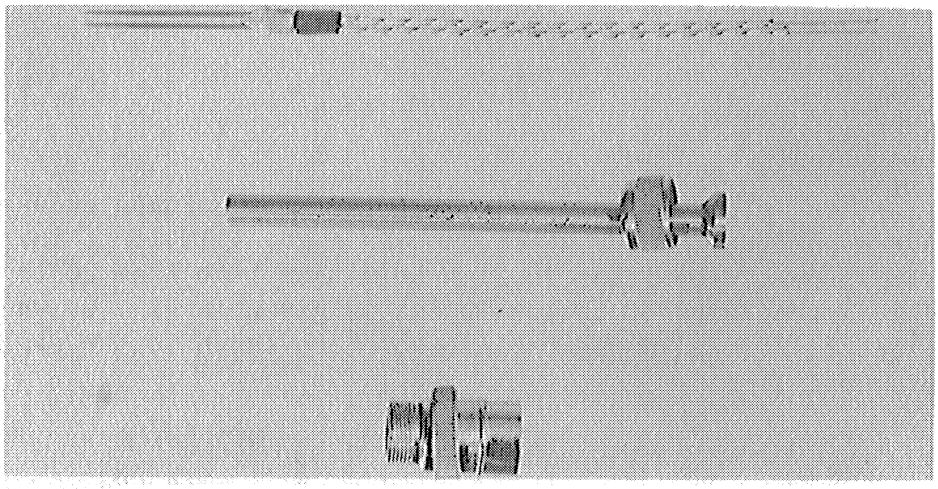

Fig. 7. Hot-Wire Probe

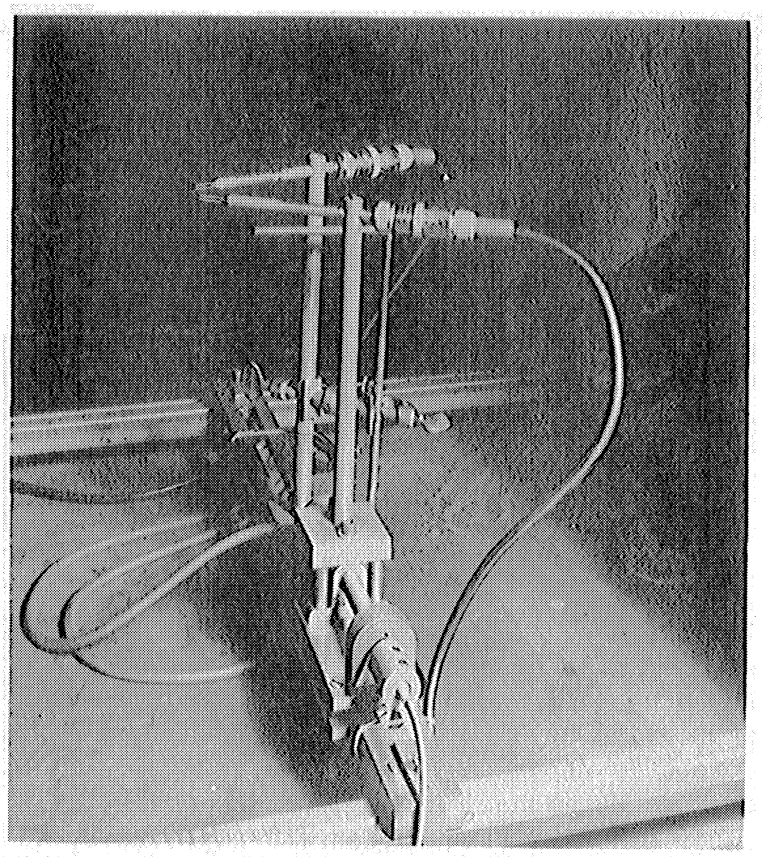

Fig. 8. Hot-Wire Scale Apparatus

2.5 Camera

The camera used for taking photographs of the moving spray is made up of a light-tight box, 8 in. by 11 in. by 10 ft, which is provided with

bellows connections to a 4-in. by 5-in. plate holder at one end and to a lens board at the other. Tracks support the camera at either end to facilitate taking pictures anywhere in the spray. Fig. 9 is a photograph of the camera without the track supports. Further details are to be found in Section 5

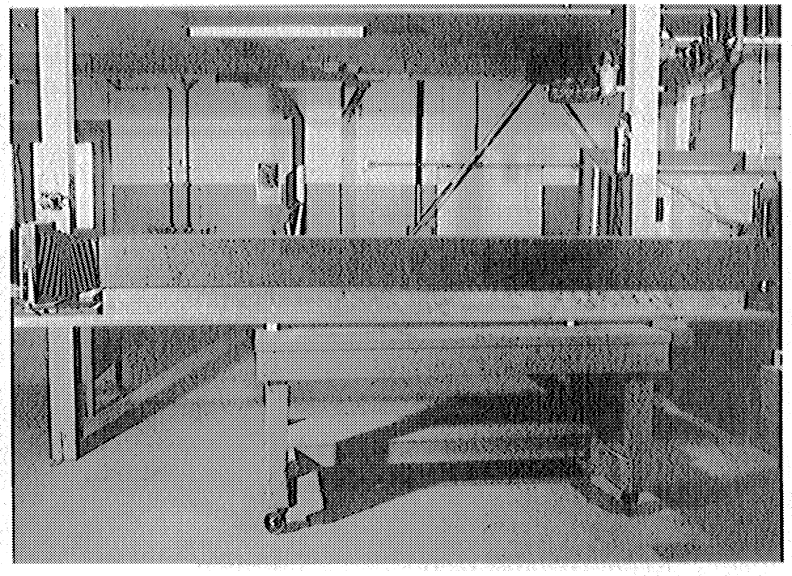

Fig. 9. Spray Camera

3. THEORY OF THE COLLECTOR TUBE

3.1 Drop Trajectories and Spray Collection

Neglecting the force of gravity, the forces acting on a drop moving in an airstream are those of drag and inertia. It is recognized at the outset that the trajectory of the drop will not follow the curved streamlines of the fluid flow. The equations of motion of a drop moving in an airstream are:

$$m \frac{dv_x}{dt} = \frac{\rho}{2} C_D v_r^2 S \ell_1$$
$$m \frac{dv_y}{dt} = -\frac{\rho}{2} C_D v_r^2 S m_1 \quad , \tag{3.1}$$

where m = the mass of the drop
ρ = air density
C_D = drag coefficient for a sphere
S = frontal area of the drop
v_r = relative velocity between air and drop

$$= (v_x - u_x)^2 + (v_y - u_y)^2 \tag{3.2}$$

in which (v_x, v_y) and (u_x, u_y) are, respectively, the x,y components of the drop and air velocities. Drops approaching a body (i.e., a cylinder, sphere, or strip) are assumed to have the velocity U of the airstream up to a distance twice the radius or width of the body.

We further define

$$v_x = -\frac{dx}{dt} \quad , \qquad v_y = \frac{dy}{dt} \tag{3.3}$$

and

$$\ell_1 = \frac{v_x - u_x}{v_r} \quad , \qquad m_1 = \frac{v_y - u_y}{v_r} \quad , \tag{3.4}$$

where ℓ_1 and m_1 are the direction cosines of the resultant drag.

A general solution of Eqs 3.1 is not known due to their complexity and nonlinearity, but a numerical solution is possible using step-by-step integration or a differential analyzer. The particular solutions applicable to the problem of drop collection entail finding trajectories for spherical drops which are moving parallel to the flow with free stream velocity U far upstream of the collector. The u_x, u_y terms are the wind velocity components appropriate to the particular type of collector used.

Complete potential flow solutions for air flow about spheres and cylinders are known, from which u_x, u_y may be determined for every point. Flow of a real fluid about an object does not obey exactly the potential flow equations, due to viscosity. However, measurements show that the pressure coefficients over the region near the leading edges of cylinders, spheres, and streamlined bodies are very close to those for potential flow.[22] The actual velocity field should also be quite close to that produced by potential flow. Drop trajectories, computed using the potential flow solutions for u_x, u_y, can therefore be assumed to have negligible error up to the leading edge of the collecting object.

The drag coefficient C_D of the spherical drop is a function of the drop Reynolds number,

$$\mathrm{Re} = \frac{\delta v_r}{\nu} , \tag{3.5}$$

where ν is the kinematic viscosity and δ is the drop diameter. C_D may be found from experimental results for each Re. Due to the small size of the drop and the small relative velocity of the airborne drop, Re does not approach the critical Reynolds number at which turbulence begins to influence C_D. Accordingly, turbulence need not be considered when calculating C_D.

Langmuir and Blodgett[17] solved Eqs 3.1 by means of a differential analyzer for the cases of flow about spheres, cylinders, and ribbons. They assumed as a boundary condition that the drop moved parallel to U until its distance upstream of the collector was two diameters or widths of the latter. In order to make the trajectories more general, they are found in terms of two dimensionless quantities, ϕ and k, which are dependent on the parameters of the problem. ϕ and k are defined by the relations,

$$\phi = \frac{18\,\rho\, c\, U}{\nu\, \rho_L}$$

$$k = \frac{2\,\rho_L\, a^2\, U}{9\,\rho\,\nu\, c} \tag{3.6}$$

where ρ_L = density of the drop
a = drop radius
c = radius or width of collector.

Fig. 10 shows two trajectories, LP and FJ, of drops in an airstream flowing around a sphere of unit radius. LP is a trajectory along which a drop grazes the sphere, while FJ is the trajectory for collision at some other angle. Any drop of the same size as those which follow LP and FJ will miss the sphere entirely if it starts outside of LP. By examination of the drop trajectories, a number of variables may be defined which are of importance in characterizing drop deposition. These are Θ_M, the maximum deposition angle, β_o, the efficiency of drop collection at the stagnation point, and E_M, the total collection efficiency of the spherical collector.

If there is a uniform distribution of drops in the airstream, they will travel over a family of trajectories, FJ, and the sphere will be wet over the whole surface from D to P. Drops which lie outside of LP will miss the sphere altogether, and the surface from P upward will not be wet. θ_M is defined as the angle beyond which no spray is collected by the sphere. It is measured from the x-axis (parallel to U) and is given by the angle DOP in Fig. 10.

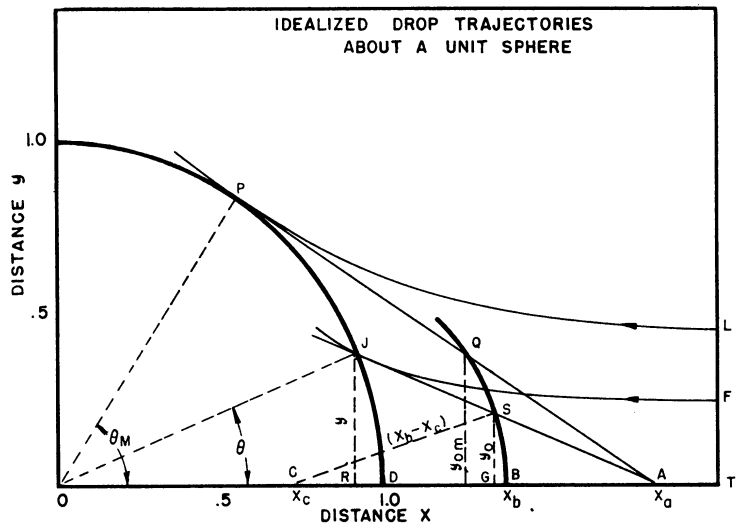

FIG. 10

Total collection efficiency E_M is defined as the ratio of the mass collected by the sphere to the mass which would have been collected had there been no drop deflection. For no deflection the mass collected per second is $\pi c^2 wU$, where w = the liquid mass per unit volume of air. If LP were extended upstream to the point where it is parallel to the x-axis, E_M would be defined by

$$E_M = \frac{\pi y_{o_M}^2}{\pi (1.0)^2} = y_{o_M}^2 , \qquad (3.7)$$

in which y_{o_M} is the ratio of the ordinate of the trajectory where it is parallel to the x-axis to the radius of the sphere.

The deposition efficiency β is defined as the ratio of the mass collected by a given surface area of the sphere (circularly symmetric with the x-axis) to the mass which would have been collected had there been no drop deflection. It is defined by an equation analogous to Eq 3.7, namely

$$\beta = \frac{y_o^2}{y^2} . \qquad (3.8)$$

Finally, the deposition efficiency β_o at the stagnation point is

$$\beta_o = \lim_{y \to 0} \beta . \qquad (3.9)$$

Langmuir and Blodgett[17] showed that the tangents drawn to the various drop trajectories at their points of contact with the sphere all intersect at a point x_a on the x-axis. Further, if the various y_o are plotted on their respective tangents, it is found that all these points lie on the segment of a sphere whose center lies on the x-axis at x_c, so that $x_c < 1$. This permits the calculation of β_o from the trajectories as plotted in Fig. 10, since, by similar triangles,

$$\beta = \frac{y_o^2}{y^2} = \frac{\overline{AG}^2}{\overline{AR}^2} .$$

The limit as $y \rightarrow 0$ gives the stagnation-point efficiency, and it can be seen from the figure that this limit is

$$\beta_o = \frac{\overline{AB}^2}{\overline{AD}^2} = \frac{(x_a - x_b)^2}{(x_a - 1)^2} .$$

A similar procedure is followed for cylinders and ribbons.

In this experiment, tubes with their upstream ends rounded to hemispherical shape are used as drop collectors, the drops being collected through a small hole drilled at the stagnation point. The graphs of β_o, E_M, and θ_M for a sphere, as found in the report by Langmuir and Blodgett,[17] will be used for this collector. Flattening of the tube nose, due to the drilled hole, will cause greater trajectory curvature near the nose and less curvature further out in the stream and thus will tend to increase slightly the stagnation-point collection efficiency of the tube with respect to a smooth sphere.

The density of droplets in a spray is not constant; nevertheless, if the volume chosen is made small enough, the concentration gradient may be neglected and the spray assumed to be uniform in such a volume. Since the previous theory assumed a uniform spray distribution, the collecting area of the probe must be small, so that the concentration gradient across it can be neglected. As the collection opening of the probe is usually much smaller than the tube diameter, the collection efficiency, β, of the collection opening in the probe should be used instead of E_M. However, β will vary with the ratio of the area of the collecting hole to the area of the cross section of the tube.

The charts[17] do not give β but rather E_M, θ_M, and β_o. Values of β may be calculated from E_M, θ_M, and β_o by the method given by Langmuir and Blodgett.[17] Table I shows the results of calculations of β for the probes used in the tests. The calculations were made for drop diameters of 0.0002, 0.0006, and 0.0013 inch for the probes which have opening diameters equal to 0.4 of the outside diameter.

The results of Table I show that $\beta \cong \beta_o$ over a range of drop sizes from 0.002 to 0.0013 inch. As the drop size becomes larger, the difference between β_o and E_M approaches zero, so that β, which lies between them, will approach β_o. β_o will henceforth be used for the efficieicy of the 0.4-diameter-ratio probes employed in this experiment.

TABLE I

Drop Diameter (inch)	E_M	θ_M	β_o	β
0.0013	0.818	84.6°	0.890	0.887
0.0006	0.617	78.1°	0.770	0.766
0.0002	0.192	47.0°	0.380	0.378

The values for β_o and E_M in the charts[17] are applicable to a spray whose drops are all of the same diameter and uniformly distributed throughout the spray. Actual sprays are made up of drops covering a large range of drop sizes which can be assumed to be uniformly distributed throughout the volume of spray which is being sampled by the tube. A mean value which is applicable to the actual spray is defined by

$$\bar{E}_M = \int_0^\infty E_M(\delta) \frac{m(\delta)}{M} d\delta \quad , \tag{3.10}$$

where m is the total mass of spray which would pass through the area occupied by the collector during a given time if the collector were not present, and $m(\delta)$ is the mass distribution function of the spray. $\bar{\beta}_o$ may be similarly defined.

The deposition of ice on the various component parts of an airplane passing through a supercooled cloud or fog is of primary importance in aeronautics. Many experiments have been performed to determine the water content of such clouds. The most generally used collector[16,23] for this type of experiment consists of a slowly rotating cylinder which is placed outside of the airplane. An even coating of ice deposits on the cylinder when it passes through the supercooled cloud. The total mass collected is later determined by melting the ice from the cylinder or measuring the thickness of the deposit. Rotating cylinders might be used to sample spray which does not solidify upon contact if the surface of the cylinder is porous, because liquid will tend to be drawn inward by capillary action. However, the large surface area presented to the airstream by the porous cylinder results in a large surface evaporation rate and renders this method useless except for nonvolatile liquids.

Vonnegut, Cunningham, and Katz[16] inserted a porous cup or liner inside of a collector head which was placed parallel with the airstream, thus providing a large internal surface for catching the liquid. The area out of which evaporation takes place was small compared with that of the rotating cylinder. The porous cup was connected to a fine, calibrated capillary tube.

Collected liquid was drawn through the porous material into the calibrated capillary which measures the catch. By bleeding air through the collector tube, the trajectories of the drops are so altered that more of them enter the tube than enter without the bleed. When a pressure equal to static pressure is maintained at the downstream end of the bleed, the velocity of the air moving through the open tube probe is approximately that of the free stream and there will be little if any drop deflection by the probe. Nevertheless, such a collector will have a rather high evaporation rate, since the porous cup extends to the edge of the entrance hole, thus enabling the saturated vapor to diffuse away easily.

Experiments carried out at the University of Texas[24] indicate that high collection efficiencies are obtainable when a probe equipped with a bleed is used on relatively nonvolatile liquids. Such a system, however, would lead to large evaporation loss for highly volatile liquids, due to the vapor carried away by the bleed air, and is therefore not suitable for the present investigation.

The purpose of the experiments reported here requires the use of a spray of a highly volatile liquid. Hexane was chosen because of its volatility and freedom from toxic danger. Loss of collected mass due to evaporation must be minimized in order for the results to have any meaning. The design of the collector finally chosen was a 5/16-inch (O.D.) copper tube. Spray enters the probe through a 1/8-inch diameter hole drilled in the hemispherical nose, the downstream end of the tube being sealed off as described in Section 2.3. The evaporation was minimized by choosing a relatively small entrance hole and then capping the tubes quickly at the end of a run.

3.2 Evaporation Losses

Inevitably there must be some evaporation loss out of the opening in the front of the probe, even though the opening is small and the flow-stagnation point is at the center of the opening.

The static evaporation out of the tube is negligible, being 0.0012 milligram of hexane per second. This gives 0.1 milligram loss for the 86-second run time of the experiment as compared with total collections ranging, for the most part, from 30 to 150 milligrams. This rate was measured by placing a hexane-filled probe on an analytical balance and measuring the weight as a function of time. This gives a lower limit to the actual evaporation during a run.

Evaporation during a collection is rather complex. Initially there is no liquid in the probe, and the rate at which the liquid is collected is the rate at which spray enters minus the rate at which evaporation takes place. Vapor pressure inside the probe gradually builds up from zero to saturation. The temperature of the probe is lowered by the evaporation of hexane from the outside surface of the probe, thus lowering the temperature and the saturation vapor pressure of the liquid within the probe. Eventually, both temperature and vapor pressure will reach equilibrium values. The rate at which the vapor is carried away

from the probe opening can be surmised to be a function of the velocity and the turbulence of the air moving past the opening. No test has been found for evaporation out of the probe which will faithfully follow the conditions of an experimental collection. However, it is possible to approximate the true loss by assuming some simple and plausible law for evaporation.

During collection the probe is held in a horizontal position, and spray collects along the bottom of the tube in a shallow pool. For the small amounts collected, the width of the surface area of the liquid is assumed to vary as the total mass, m, which has collected in the tube; thus, the evaporation rate out of the tube may be taken proportional to the mass in the tube. The rate of change of mass in the tube is given by

$$\frac{dm}{dt} = a_2 - a_1 m \quad , \tag{3.11}$$

where a_2 = the mass rate at which spray enters the collector, and
a_1 = an evaporation coefficient which depends on the velocity and turbulence of the air as well as on the temperature and hole size of the probe.

The solution of Eq 3.11 for the condition m = 0 at t = 0 is

$$m = \frac{a_2}{a_1}(1 - e^{-a_1 t}) \quad . \tag{3.12}$$

The probe was allowed to collect spray for 10 seconds, whereupon it was capped and weighed. When thoroughly dried out, it was put back in the spray and allowed to collect for 20 seconds, and then capped and weighed again. This procedure was repeated for a collection time up to 90 seconds. In this way a plot of m against t may be obtained. It is not feasible to determine a_1 and a_2 from these data alone, as the plots give nearly straight lines and any number of low-curvature exponentials could be fitted to the data. Therefore, another method must be utilized to obtain more accurate values of the constants.

Suppose that at the end of t seconds a mass m has collected in the tube and, with the spray shut off, the tube is allowed to evaporate into the airstream for another t seconds before capping and weighing. For the evaporation after collection, Eq 3.11 becomes:

$$\frac{dm'}{dt'} = - a_1 m'$$

Its solution for the condition m' = m at t' = 0 is

$$m' = m e^{-a_1 t'} \quad . \tag{3.13}$$

Hence, at the end of t seconds

$$m' = m e^{-a_1 t} \quad ,$$

and the mass Δm lost by this secondary evaporation is

$$\Delta m = m - m' = m(1 - e^{-a_1 t})$$

Substitution of Eq 3.12 into the last relation gives

$$\Delta m = \frac{a_1}{a_2} m^2 \quad . \tag{3.14}$$

Δm was determined experimentally for the values of m corresponding to t = 10, 20, ... 90 seconds. The validity of Eq 3.14 was borne out except at low values of t. This discrepancy is probably due to the fact that the probe temperature does not reach equilibrium except at the higher values of t, and for that reason the points for t = 10, 20 seconds do not appear in Fig. 11, which is a plot of Δm vs m^2 for U = 50 ft/sec and turbulence of 0.59 per cent. This graph is generally a straight line except for low values of t. Values of Δm were of the order of 15 to 20 per cent of m, so that the ratio a_1/a_2 could be determined readily. The quantity a_1 can then be found from the m vs t curve by means of Eq 3.12.

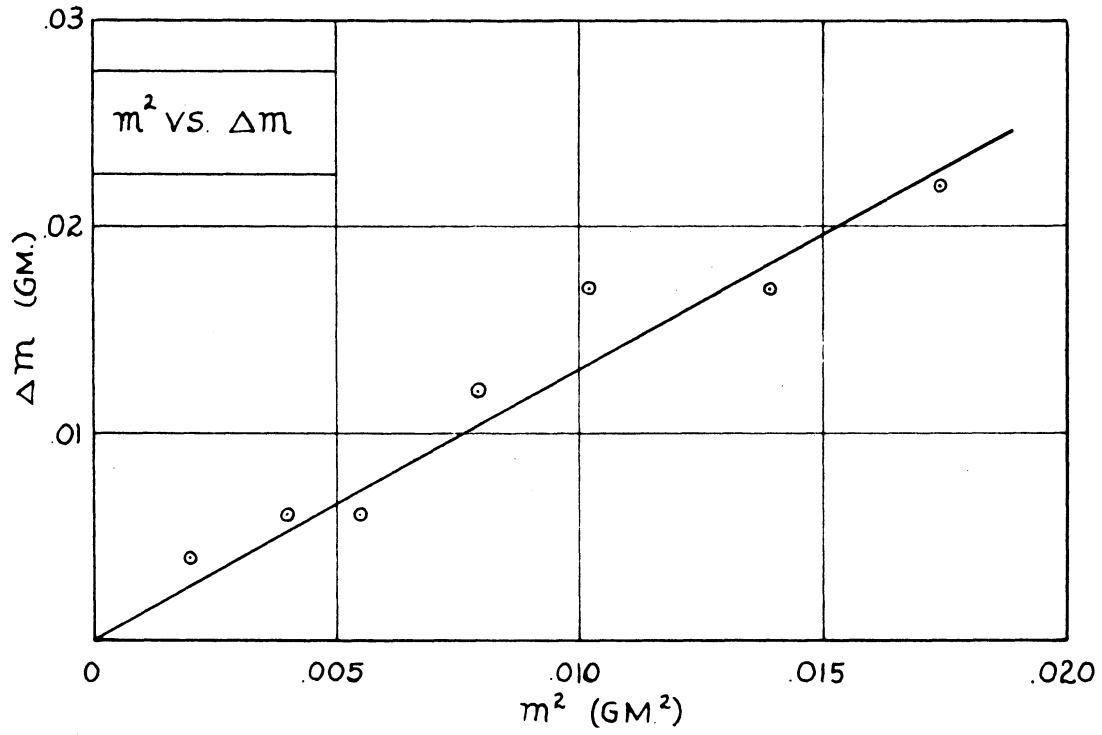

FIG. 11

Eq 3.12 gives the mass left in the tube after collecting for time t. The mass which would have been collected if there had been no evaporation is obviously $a_2 t$. Therefore, the correction factor α, by which the collected mass must be multiplied, is given by the relation

$$\alpha = \frac{a_2 t}{m} = \frac{a_2 t}{(a_2/a_1)(1 - e^{-a_1 t})} , \qquad (3.15)$$

or

$$\alpha = \alpha(a_1, t) .$$

Thus, a_2 drops out and the correction factor for evaporation is found to be not a function of the rate at which mass enters the tube, but only of t and the coefficient a_1. The m and Δm curves were determined experimentally at an ambient temperature of 20°C for turbulence intensities of σ = 0.59, 2.91, and 7.68 per cent at U = 50 ft/sec, σ = 0.52 at U = 60 ft/sec, and σ = 0.57 at U = 75 ft/sec.* There was an initial time lag with regard to the mass collected in the tube due to progressive cooling and build-up of vapor pressure within the tube. The data for m, extrapolated to m = 0, intersect the time axis at values of t from 2 to 4 seconds. Eq 3.12 was fitted to the data, using the appropriate time lag. Figs. 12 and 13 show such a fit for σ = 0.59 and 7.68 per cent at U = 50 ft/sec. This is typical of the data, since there was a high degree of scatter at higher turbulence intensities and velocities, with smaller scatter for the lower values.

FIG. 12

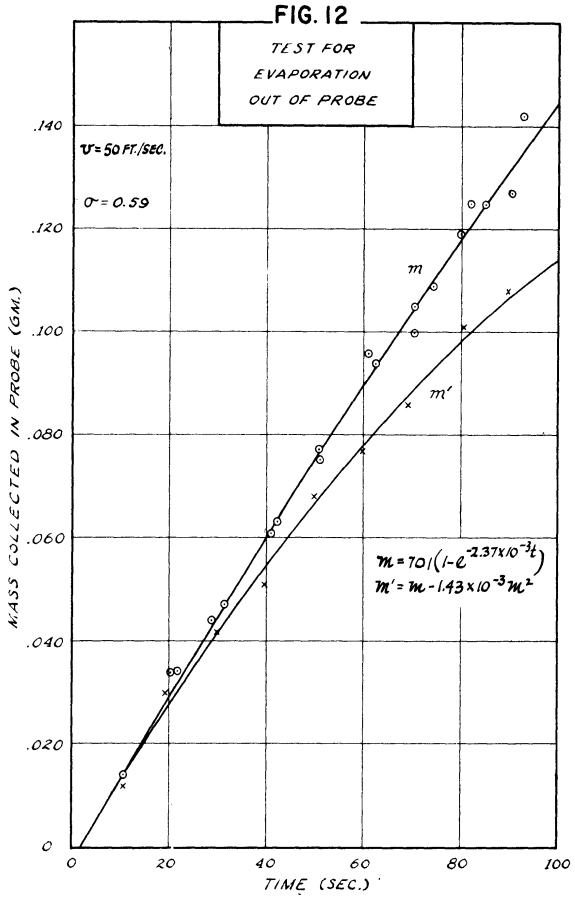

* See Section 6.1 for definition of σ .

FIG. 13

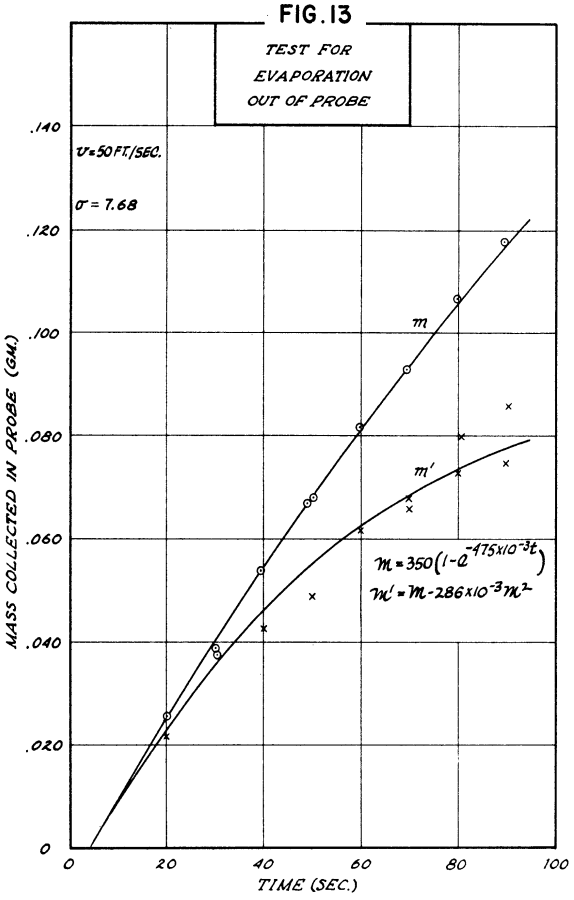

Values of α were calculated for these three cases, with t = 85 seconds, by use of Eq 3.15. Fig. 14 gives the resulting curves of α vs σ.

The values of α determined in this fashion undoubtedly err on the high side, because during the evaporation part of the process the collector was not being cooled by the spray and heat transfer could take place from the air to the probe.

In principle, the evaporation out of the probes can be determined by collecting spray in probes having the same external diameter but different hole diameters. The collection efficiency β_o of these probes is nearly constant up to a hole diameter equal to 0.6 of the external diameter, as was shown in Section 3.1. The total mass m collected by the probes for a run time t, if the evaporation were zero, would be

$$m = \beta_o w U A ,$$

where A is the opening area and w is the mass of spray per unit volume of air. However, the evaporation must be some function of the area, say A^n, where $n > 1$. Then

$$m = \beta_o w U A - k_1 A^n$$

FIG. 14

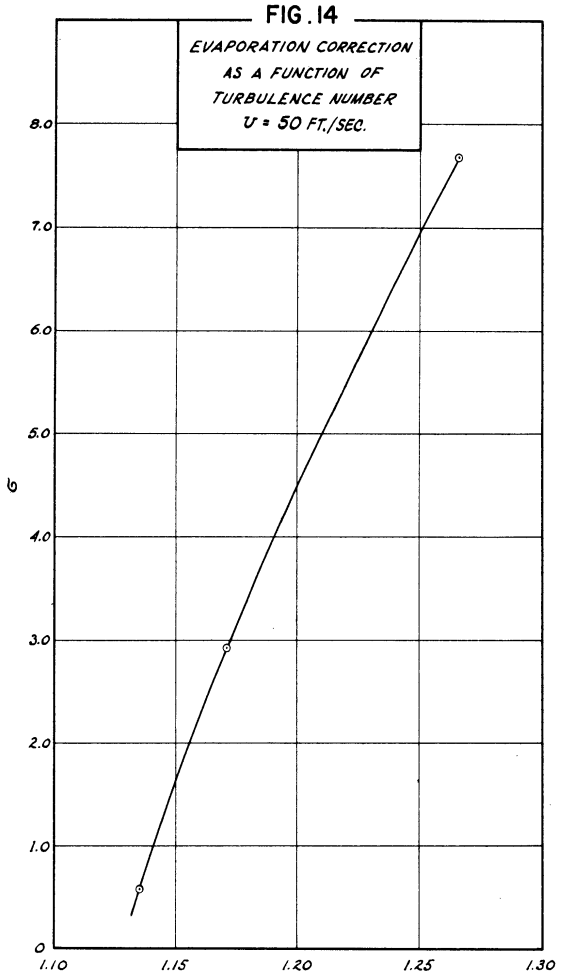

or

$$\frac{m}{A} = \beta_o w U - k_1 A^{n-1} \quad . \tag{3.16}$$

The extrapolation to zero area of curves of m/A vs A would determine the constant $\beta_o wU$, since the second term of Eq 3.16 is zero at A = 0. The value of α for any hole size A may be obtained from the curves by use of

$$\alpha = \frac{\beta_o w U}{m/A} \quad . \tag{3.17}$$

Tests were run over a range of turbulence intensities and velocities using 5/16-inch (O.D.) collector probes having hole areas of 0.00297, 0.00601, 0.01247, and 0.01744 square inches. A very small scatter in mass collected produced a large scatter in m/A at the small values of A, thus making extrapolation to zero area extremely difficult. The values of α would be questionable, as small changes in the extrapolated values cause large changes in α. Nevertheless, the values arrived at in this way may be used to check roughly the accuracy of the previous

method. Fig. 15 shows plots of four sets of data taken by this method. Table II gives the values of α obtained by the hole-size method from the data of Fig. 15, and values previously obtained by the time-lag method.

The agreement is qualitatively good considering the scatter of the hole-size data. The values of α from the time-lag method are used in this report for correcting the collection data.

FIG. 15

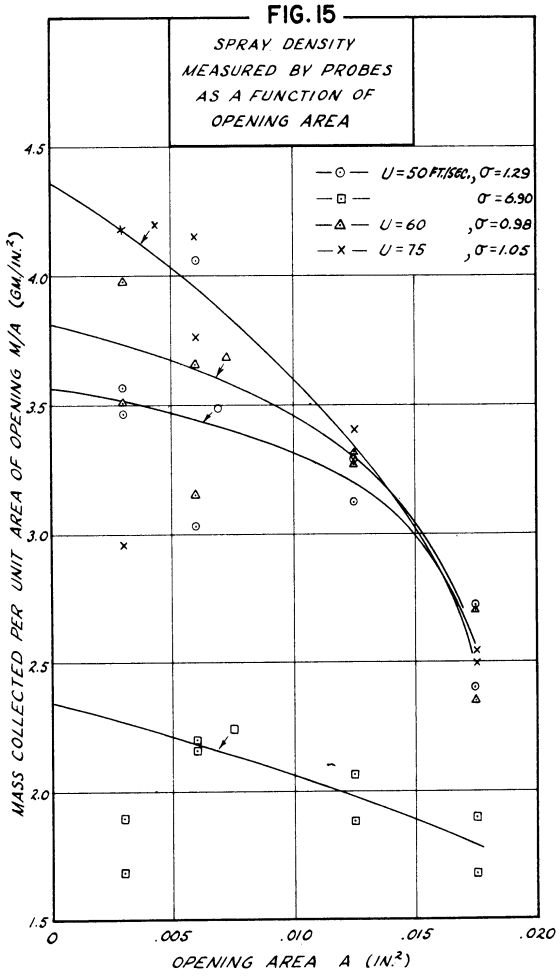

TABLE II

U (ft/sec)	(%)	α (hole-size method)	α (time-lag method)
50	1.29	1.11	1.15
50	6.90	1.19	1.25
60	0.98	1.15	—
75	1.05	1.30	—

3.3 Determination of Mass in Spray

The mass of spray which is carried past a certain station with the airstream may be determined by sampling the spray across the test section. To this end, sampling probes were mounted 2 inches apart in the rack, and a known amount of fuel was fed through the nozzle. The probes were capped and weighed to find the mass of spray collected at each point. The rack was then shifted 1/4 inch cross-stream and the above procedure repeated. For each data point, eight separate samplings were taken in this manner, so that samples of the spray were obtained every 1/4 inch across the spray.

A fictitious spray density, which is useful in computing the total mass, may be defined as the ratio of the mass collected to the hole area of the probe. The spray pattern is reasonably symmetrical, and spray densities for points equidistant from the centerline and lying in the same transverse plane may be averaged to give the mean spray density in the annulus whose center falls on the axis of the spray cone and whose width is 1/8 inch, the diameter of the hole in the probe. Multiplying the annulus area by the mean density gives the mass of spray passing through the annulus during the run time.

FIG. 16

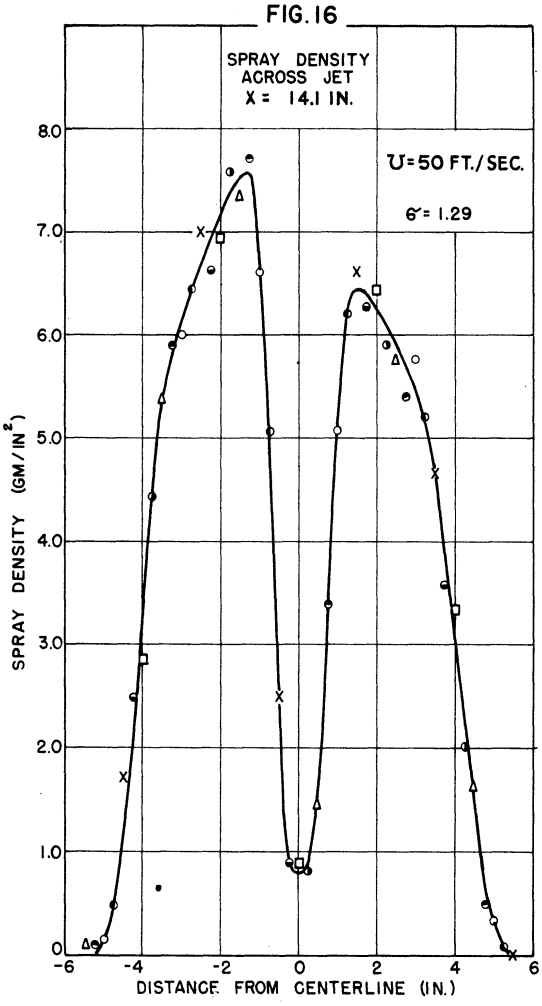

The masses passing through a sequence of 1/8-inch annuli were determined every 1/4 inch across the spray. Masses at the 1/8-inch intermediate positions were found by interpolation of the data. Summing up the masses passing through these annuli will give the total mass of spray passing through a particular cross section when this integrated mass is corrected for evaporation and probe collection efficiency.

Whenever repeat collections of spray were made at the same position in the spray, there was a fair amount of scatter in the collected masses. This is more noticeable at the higher velocities and turbulence intensities. In order to obtain the mass at any station, eight separate mass collections were made, and, while some of the individual points are in error due to scatter, the curves determined by these points are probably fairly accurate because of the large number of points used in their determination. Figs. 16 and 17 show examples of the curves obtained. The crosses, squares, etc., represent the eight different collection runs used in determining the curves. Both sets of data were taken at U = 50 ft/sec and T_a = 20°C, with a low turbulence intensity of 1.29 per cent for Fig. 16 and a high intensity value of 6.33 per cent for Fig. 17. The root-mean-square error based on the total mass collected is 0.1 per cent for the data of Fig. 16 and 0.18 per cent for the data of Fig. 17.

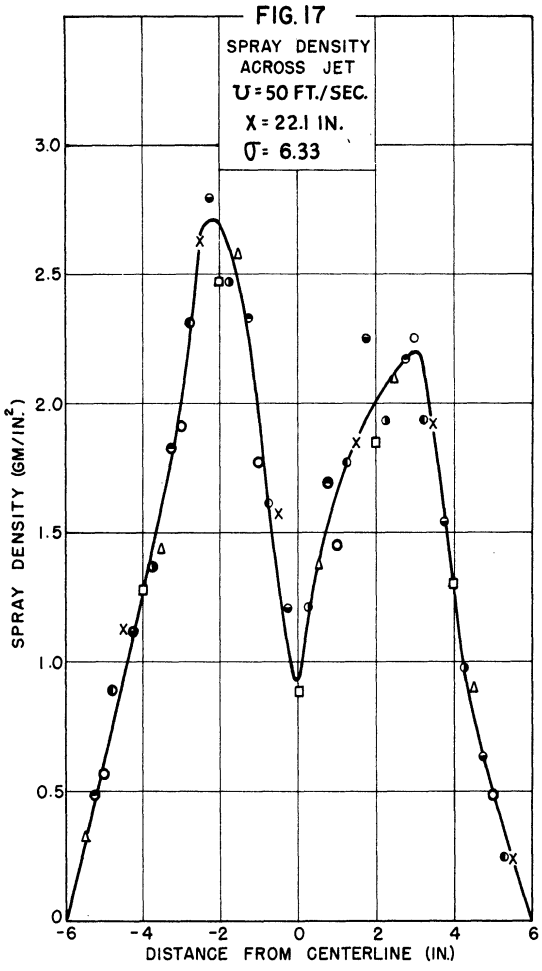

The above analysis shows that the correction for evaporation is dependent not on the rate at which the spray enters the probe but only on the turbulence, velocity, and temperature of the airstream. The temperature is very nearly the same throughout the test section. If it is assumed that all the injected spray is evaporated and that the total heat of vaporization comes from the airstream, its temperature would be reduced by only 0.3°C. As will be shown in Section 6.2, velocity and turbulence intensity are approximately constant across the test section except at the center and near the jet boundary where there is a mixing region.

3.4 Collector Efficiency

The collection efficiency $\bar{\beta}_o$ of the collector tube for the spray used in the experiment may be found from the relation

$$\bar{\beta}_o = \int_0^\infty \beta_o(\delta) \frac{m(\delta)}{M} d\delta \qquad (3.10)$$

if $m(\delta)$ is known. $\beta_o(\delta)$ is found from the charts of Langmuir and Blodgett,[17] as discussed in Section 3.1. The distribution function can in principle be found at every point of the spray for all conditions of velocity, turbulence, and air temperature. However, this involves considerable labor due to the large number of distributions which must be found for an accurate determination of $\bar{\beta}_o$. A simpler method involves an assumption as to the change of drop size with evaporation. Suppose that $m(\delta)$ is determined from photographs taken at a given point in the spray where the mass collected is m_o. Then $\bar{\beta}_o$ may be found from Eq 3.10. The mean drop diameter $\bar{\delta}_o$, corresponding to $\bar{\beta}_o$, may be read from the charts. This is the mean drop diameter of the spray which would give the same collection efficiency as the spray as a whole. Assuming that the spray is uniformly composed of drops of size $\bar{\delta}_o$, the change of mass in the spray from one station to another is due to a change from $\bar{\delta}_o$ to $\bar{\delta}$ by evaporation according to the equation

$$\bar{\delta} = \bar{\delta}_o \left(\frac{M}{M_o}\right)^{1/3} . \qquad (3.18)$$

From the mean diameter found in this way, $\bar{\beta}_o$ can be found for all stations at which a total mass M of spray has been determined. The average collection efficiency is then given by

$$\bar{\beta}_o = \sum \beta_o(\delta_1)\, m'(\delta_1) .$$

The collection efficiency $\bar{\beta}_o$ for the measured distribution (see Section 4) shown on Fig. 18 corresponds to $\bar{\delta}_o$ = 0.003 inch. Eq 3.18 was solved for $\bar{\delta}$ using the values of collected mass corrected for evaporation. The values of $\bar{\beta}_o$ ranged from 0.92 to 0.96. Dividing the masses, which had previously been

corrected for evaporation, by the applicable values of $\bar{\beta}_o$ gave the final corrected mass as collected by the tubes.

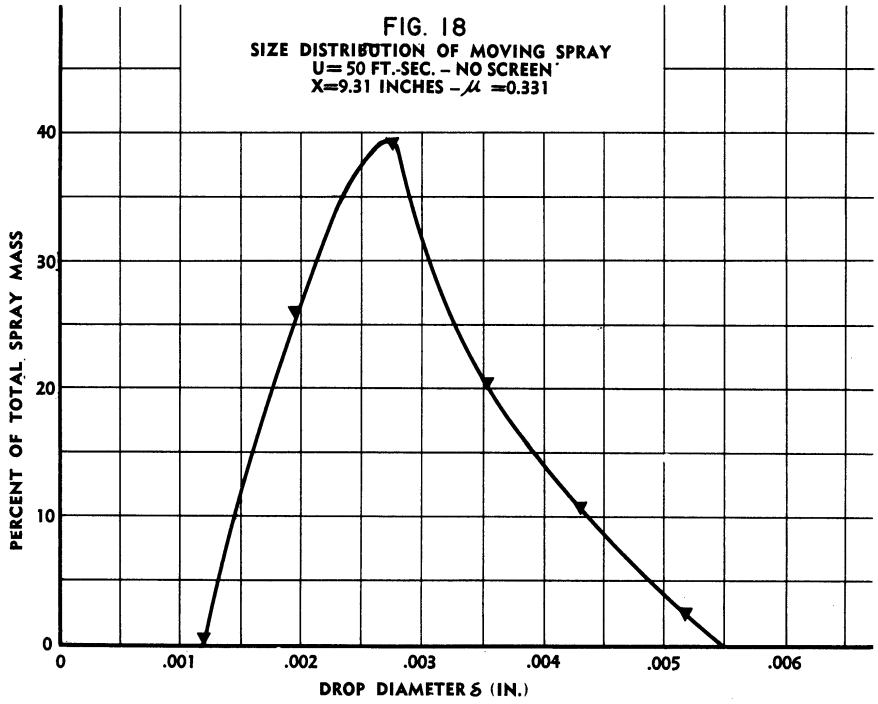

The fact that the values of $\bar{\beta}_o$, the average collection efficiency, are quite close to unity is believed to justify the earlier assumption that the drops approach the collector with the free-stream velocity U to within two tube diameters of the leading edge. Actually, the drop velocities are probably less than U, as will be brought out in Section 6, but this discrepancy appears to have no significant effect upon the action of the collector tube.

4. SPRAY PHOTOGRAPHY

4.1 Description of Method

a) General. -- The photographic method of drop-size measurement has been employed by a number of investigators. Two procedures have usually been used: (1) the drops are first collected by some suitable sampling device which is then photographed with photomicrography equipment, or (2) the drops are photographed in motion, using a high-speed flash lamp of great intensity. The first procedure has been used by Houghton and Radford[5], Rupe[14], and others. York[25,26], Lee and Spencer[27], and Scheubel[28] have used the second procedure.

In the first procedure the optical problems, which will be discussed later, are less troublesome because the standard techniques of photomicrography may be employed. On the other hand, this procedure has the disadvantage that the sampling or collecting device will be more or less selective in its action in capturing drops. Moreover, when the drops are collected, they will change size due to their impact upon the sampling device, necessitating the determination of a "flattening coefficient". Rupe[14] has found, however, that by exercising much care, it is possible to reduce impact distortion to the point where it may be neglected.

The second procedure, sometimes called "open-flash" photography, has drawbacks of its own. First, there is the motion of drops to be considered. Suppose that the drops are carried by an airstream moving 50 ft/sec and that the light source has a flash time of 1 microsecond. Then, during the time of the flash the drops would move 0.0006 inch, a significant distance when referred to a drop of, say, 0.001-inch diameter. Second, the optical problems are aggravated in the following way: A spray injected into the airstream of a wind tunnel demands the use of photographic objective lenses in the second procedure. The lower resolution of photographic objectives as contrasted to microscope objectives limits the accuracy with which small drops can be reproduced.

b) Apparatus Used in Present Work. -- It was decided that, as a matter of convenience, drops would be photographed at 10X magnification. The closed working section of the wind tunnel limited the camera lens to a minimum distance of about 12 inches from the region of spray to be photographed. These factors led to the construction of a special camera with a 10-foot bellows extension, as shown in Fig. 9, page 15. The leather bellows themselves were taken from an 8 x 10-inch view camera which was cut in half, one part being used for the lens board and the other for the 4 x 5-inch film holder. Both lens board and film holder were movable by means of a rack and pinion arrangement. The entire camera was mounted on four wheels which ran along two parallel and level tracks fixed to two wooden supports. This installation, shown in Fig. 19, allows the camera to be moved parallel to the axis of the spray cone.

A number of high-quality lenses were tried, the one finally adopted being a Bausch and Lomb, f/6.3 Tessar of 12-inch focal length. On the recommendation of the manufacturer, this lens was turned end for end, so that the glass

surface which normally faced the object then faced the film holder. This procedure results in sharper images when photographing close objects. All pictures taken with the Bausch and Lomb Tessar were at an indicated aperture of f/11.

Fig. 19. Spray Camera in Operation

Lighting proved to be a rather difficult problem, which required considerable experimentation. York[25,26] found that placing the light source off the optical axis of the camera results in twinned drop images and that it is necessary to point the light directly into the camera to produce single silhouette images. Special care had to be taken to obtain uniform illumination over the region imaged on the 4 x 5-inch film. The light from the flash source is nonuniform in intensity across the beam, and there is a tendency for the camera to form a pinhole image of the electrodes, which aggravates the unevenness of the illumination. Best results were finally obtained using a plano-convex condenser lens of 10-inch diameter, as shown in Fig. 20, to form a conical beam of light converging on the spray region. In addition, an adjustable iris was located directly in front of the flash lamp but above center, as shown in Fig. 21, so as to mask the electrodes and the large gradients in light intensity near them. The general layout is shown schematically in Fig. 20.

The light source used is a G.E. Photolight, Type 936468861. Any light which is turned on and off has an intensity curve which rises to a maximum and then falls to zero more or less gradually. In the present instance, the initial rise time is about 0.5 microsecond, while the decay is approximately exponential. It is customary to define flash time as the width of the curve at 1/e of the maximum intensity. From the manufacturer's curve, reproduced in Fig. 22, it is evident that such a definition leads to a flash time of about 1 microsecond. The effective flash time will depend on the threshold level of film sensitivity, a

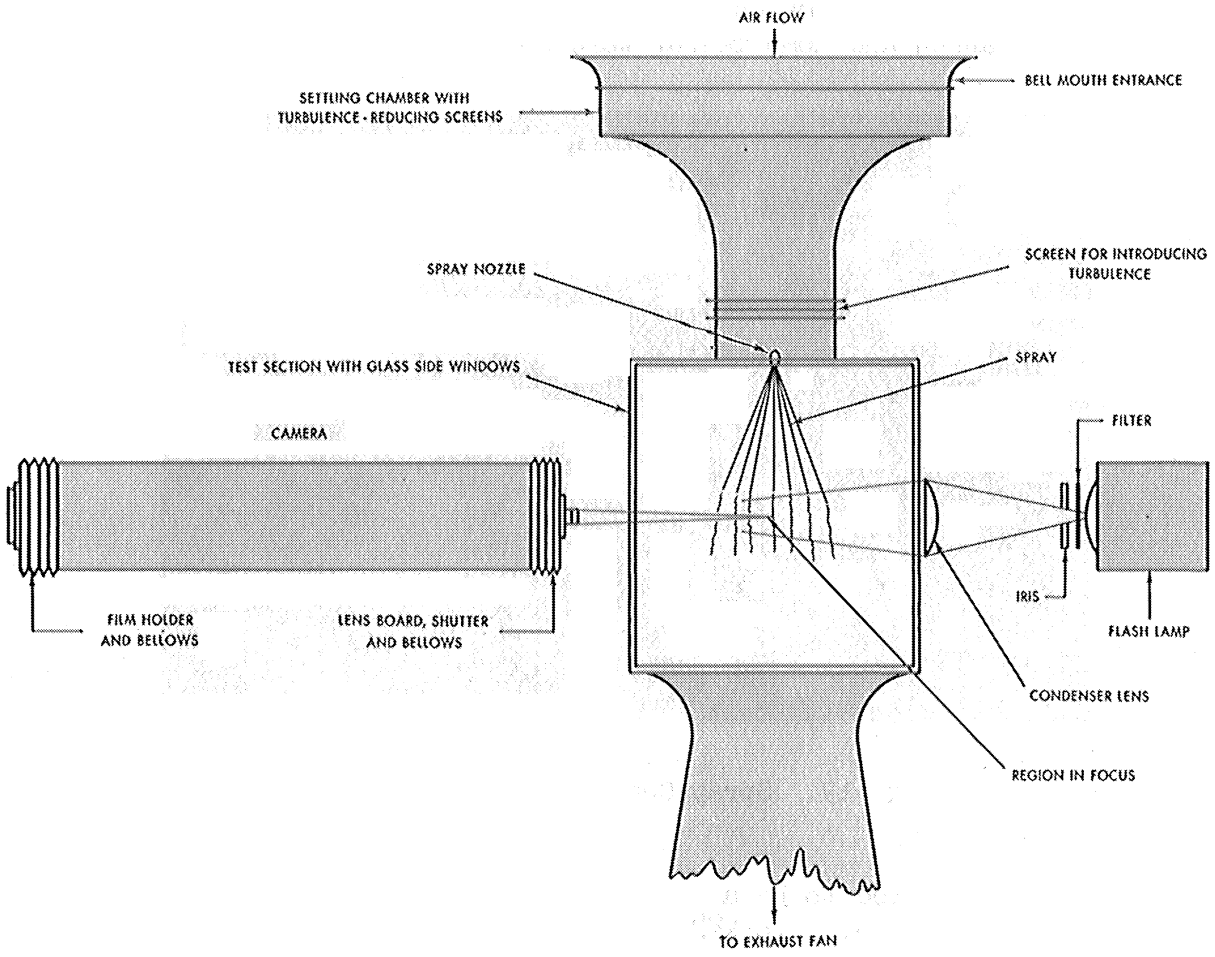

Fig. 20. Arrangement of Photographic Equipment

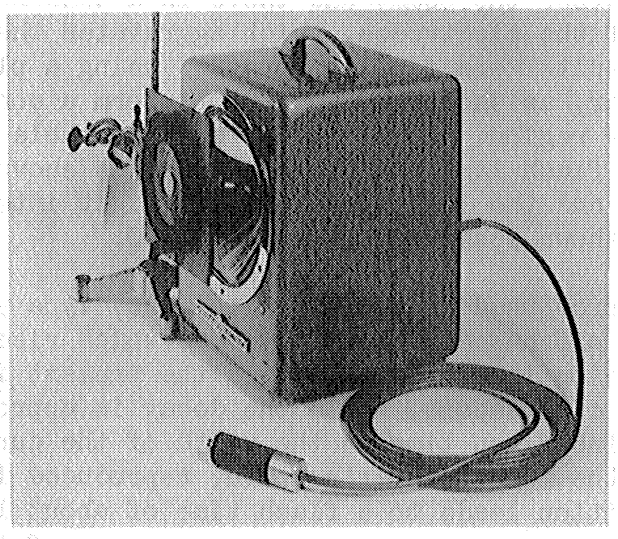

Fig. 21. Flash Lamp and Masking Iris

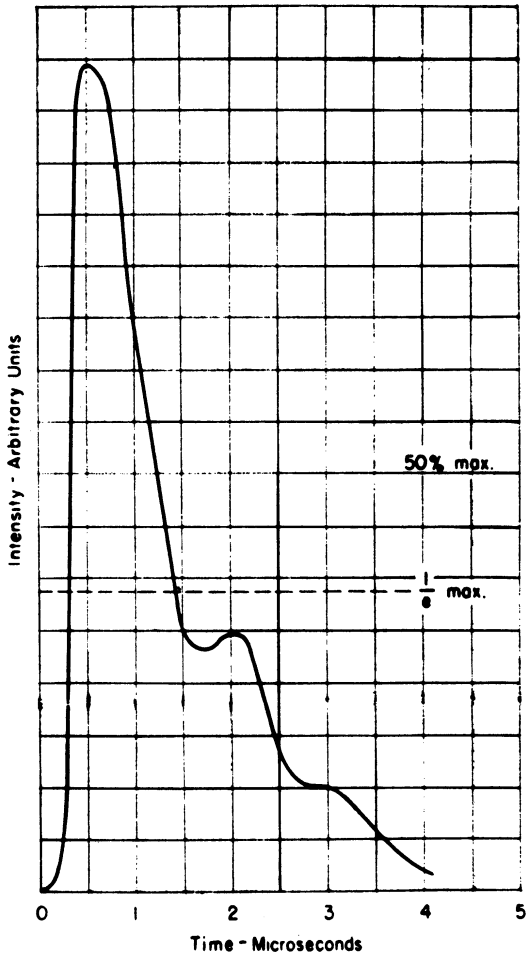

Typical time-intensity curve for photolight

fact which makes it difficult to specify flash time precisely. Photographs of moving drops showed "tails", indicating that the effective flash time was probably greater than 1 microsecond.

4.2 Errors

a) Lens Errors. -- The subject of lens errors has been treated extensively.[29-31] The present discussion will not consider the various lens aberrations such as astigmatism, chromatism, coma, spherical aberration, etc. These aberrations can be corrected to such a degree that they do not limit the perfection of the image. However, even a lens which is perfectly corrected for aberration will be subject to a diffraction error. Diffraction occurs whenever a wave front is confined or limited in extent, e.g., when light is passed through a lens. As a result of diffraction, a point source of light will be imaged as a bright, central disc of finite size surrounded by alternate light and dark diffraction rings. About 84 per cent of the light transmitted by the lens is in the central disc. As this is the major portion of the transmitted light, it has become customary[31] to assess the magnitude of the diffraction effects by

considering only the diameter or radius of this central disc. The intensity is a maximum at the center of the disc and falls off symmetrically and rather sharply to zero on either side. The radius of the central disc[32] is given by the relation

$$z' = \frac{0.61\,\lambda}{\tan\theta'} \quad , \tag{4.1}$$

where λ is the wavelength of light and θ' is the angle between the axis of the lens and a peripheral ray brought to focus at the center of the disc. The value of $\tan\theta'$ is found from the relation

$$\tan\theta' = \frac{\rho'}{p'} \quad , \tag{4.2}$$

where ρ' is the radius of the exit pupil of the lens and p' is the image distance. In the case of a photographic objective it is approximately correct[31] to compute ρ' from the formula

$$\rho' = \frac{F}{2(\text{f/-number})} \quad , \tag{4.3}$$

where F is the focal length of the lens and f/-number is the indicated aperture setting. Eqs 4.1 and 4.3 may be combined to give

$$z' = \frac{1.22\,\lambda\,p'\,(\text{f/-number})}{F} \quad . \tag{4.4}$$

Taking λ = 480 millimicrons, a wavelength around the middle of the blue region of the spectrum which is approximately 460-500 millimicrons, F = 12 inches, and p' = 140 inches, Eq 4.4 leads to

z' = 0.0307 mm = 30.7 microns for f/4.5

and

z' = 0.0752 mm = 75.2 microns for f/11 .

These values of z' are the radii of the central diffraction discs in the image space, i.e., on the film. Because of the 10X magnification of the lens, the corresponding values in the object space are

z' = 0.00307 mm = 3.07 microns for f/4.5

and

z' = 0.00752 mm = 7.52 microns for f/11 .

It is noteworthy that a circular source of light of radius δ microns will, due to diffraction, be imaged as a diffraction disc of radius $z' = 10\delta + 75.2$ microns when the lens aperture is set at f/11. A similar interpretation applies to the values of z' at the f/4.5 setting. Therefore, it is evident that a value of z = 7.5 microns is about the lower limit set by diffraction when the lens is used at f/11 as in the present work. Eq 4.4 shows that the f/-number should be as small as possible to reduce the values of z and z'. However, in practice a

compromise value must be chosen because the depth of field of the lens decreases with increasing aperture. Thus, the points at the periphery of a silhouetted drop will be imaged as discs of approximately the radii given above, resulting in a decrease* in the radius of the drop image by roughly these same values. Inasmuch as the light intensity does not drop sharply to zero at the edge of the central disc, diffraction tends to blur the edge of the drop image. This blurring will, of course, make it difficult to locate a precise "edge" when measuring the size of a drop image on a photographic negative.

In the case of a microscope[31] used under ideal conditions of illumination, the finest detail that can be resolved is

$$z = \frac{\lambda}{2(N.A.)} .$$

The "numerical aperture", N.A., is defined as (N.A.) = n sin θ, where n is the index of refraction of the object space and θ is the half-angle of peripheral rays from the object. For air, n = 1; but with oil immersion, n is approximately 1.5, thus increasing the numerical aperture and the resolution. Here z is the smallest separation of points in the object that can be resolved. High-quality apochromats have values of N.A. around 0.5.[31] Using this value and λ = 500 millimicrons leads to z = 0.5 micron. This value of z may be compared directly with the values of p calculated previously, showing the superiority of microscope objective lenses for short working distances. For photographic work with substantially monochromatic light of 400-millimicron wavelength, the limit of resolution is about 0.13 micron.[33]

b) Film Errors. -- In order to discuss the errors inherent in films, it is necessary to review some of the more important factors and effects involved in the photographic process.[34,35]

The light-sensitive part of photographic films and plates is the emulsion, which is in the form of a thin layer of approximately 0.001-inch thickness attached to one surface of a plastic or glass base. The emulsion itself is composed mainly of a gelatin and silver halide (usually AgBr) crystals or gains which are imbedded in it.** These silver halide crystals vary in size with different types of emulsions and have a distribution in size within a given emulsion. Those crystals which are exposed to light become

---

*This follows from the fact that the drop image is a dark silhouette against a bright field. The diffraction disc of a peripheral point will extend into the geometrical drop image as well as into the surrounding field. This latter extension will not perceptibly change the already bright field, while the former will shrink the drop image.

**Sensitizing dyes, which determine the spectral wavelengths to which the emulsion is sensitive, are also important ingredients. However, details of their action are not important in the present discussion. For further information, see Mees, Theory of the Photographic Process.[34]

sensitized and are subsequently reduced to metallic silver by chemical action of the developer. A developed silver grain is approximately the same size as the halide crystal from which it was derived, although usually there are some changes in both the shape and size of the grain during the process of reduction to metallic silver.[34] The Contrast Process Ortho type of emulsion used in the present work has developed grains ranging in size approximately from 0.3 to 1.5 microns in the largest dimension. The grains were measured with an oil immersion microscope objective having a focal length of 1.8 mm and a numerical aperture of 1.25 which, with the 10X eyepiece, gave a total magnification of about 1000. The microscope was calibrated with a stage micrometer. Film development was in D-11 for 10 minutes at 68°F.

The density of a photographic silver deposit depends upon numerous factors, among which may be mentioned the light intensity, exposure time, color of light, developer, temperature, and the kind of film. In the present usage the word "density" refers to the optical density defined by the relation

$$D = \log_{10} 1/T \quad ,$$

where T is the "transmission" which equals the ratio of the intensity of the transmitted light to that of the incident light. More concisely,

$$D = D\,(I, t, a, b, c, d, \ldots) \quad , \tag{4.5}$$

where D is the density, I the light intensity, t the exposure time, and a,b,c, d,... are parameters corresponding to the other factors mentioned.[35] Exposure is defined as E = It, and, as a first approximation,* sufficient for the present discussion, the density depends only upon E when the other parameters are held constant. With these restrictions, Eq 4.5 can be written D = D(E).

If a film is given a series of exposures over a range of values and the corresponding densities are measured, it will be found that the plot of D vs log E will be as shown in Fig. 23. This curve is known as the "characteristic curve" or "H and D" Curve after Hurter and Driffield, who first plotted the variables in this manner. Its exact shape will depend on the type of film, development, and other factors. The region AB is called the "toe", the region CD the "shoulder", while BC is an approximately straight-line section of the curve. For most purposes the useful range is from P to Q, and this exposure interval is called the "latitude" of the film. There is no simple expression for the entire characteristic curve, but it is a useful and common practice to represent the straight-line portion of the curve by the equation[34]

$$D = A + \gamma \log_{10} E \quad , \tag{4.6}$$

---

*Actually, the density depends upon the magnitude of the light intensity, I, as well as the product, It. This phenomenon is referred to as "reciprocity law failure". See Mees.[34]

where A is a constant and γ is a parameter called the "contrast" or "gamma" of the film. By definition

$$\gamma = \left[\frac{dD}{d(\log_{10}E)}\right]_{max.} . \qquad (4.7)$$

The contrast increases with development time t in accordance with the relation[34]

$$\gamma = \gamma_{\infty}(1 - e^{-kt}) , \qquad (4.8)$$

where k is a parameter measuring the velocity of the development reaction and γ_{∞} is the maximum contrast as $t \rightarrow \infty$.

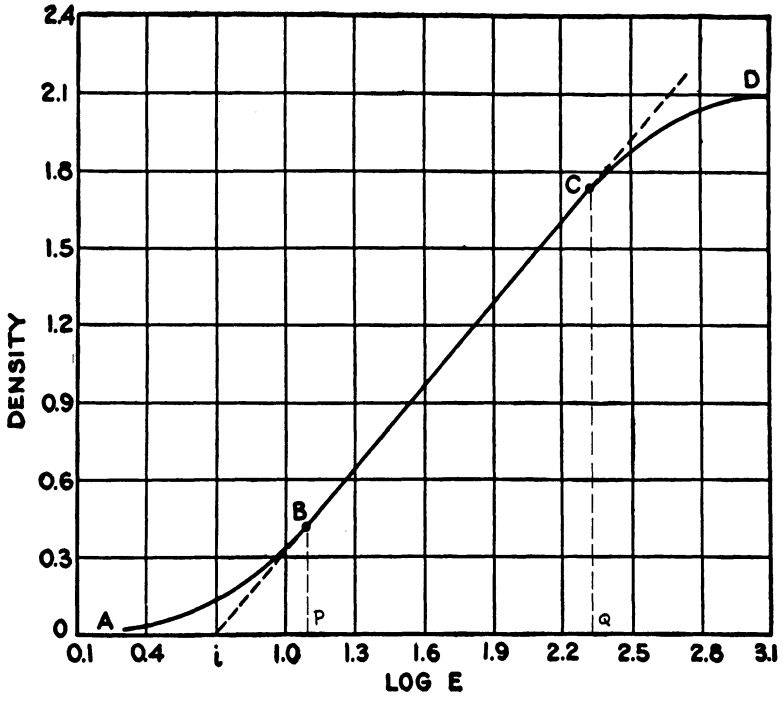

Fig. 23. Typical Characteristic Curve of Photographic Emulsion

Of the several definitions of emulsion speed in use, the one chosen seems to depend mainly on the application to which the film is put. In one definition A is sometimes set equal to $\log_{10}i$, where i is called the "inertia" of the emulsion and is used in defining the "H and D speed", which equals $34/i$. Another definition of speed specifies the exposure required to reach a given density under specified conditions of development.

The photographic emulsion is a turbid medium and, although applied to the film base in a very thin layer, has appreciable depth when measured in terms of the size of a silver halide grain. Light will initially penetrate

normal to the surface and then be diffused parallel to it. Size, shape, and optical properties of the silver halide grains, properties of the gelatin, and the wavelength of the light are among the factors which govern this normal penetration and lateral diffusion of light. Multiple reflection, refraction, and diffraction of the image-forming light by the grains in the emulsion cause even a perfectly sharp image to increase in size with exposure. This spreading or growth of an image with increasing exposure is known as the "turbidity effect". Image spreading may also be caused by reflection from the rear surface of the film or plate, although this source is made negligible by the so-called "antihalation" backings present on most modern films. Ross[35] states that the light intensity falls off exponentially in accordance with the relation

$$I = I_o e^{-\kappa(x+y)} , \tag{4.9}$$

where x is measured parallel to the surface, y is measured into the emulsion normal to the surface, I_o is the incident light intensity, and κ is a constant. Further, Ross derives a relation between the size of a star image and the exposure which produced it. He finds that

$$\text{Diameter} = B + \Gamma \log_{10} E , \tag{4.10}$$

where B is a constant and Γ is called the "astrogamma", a term which is suggestive of "gamma" (γ) in Eq 4.6. It may be mentioned here that the property of image spreading due to turbidity is the basis of photographic photometry methods and that Eq 4.10, or a modification of it, is used in determining stellar magnitudes in astronomy.

The same lateral diffusion of light which gives rise to image growth also produces a gradation of density from the maximum value in the central part of the exposed region to the fog level* of the clear film. This renders an otherwise sharp edge more or less indistinct. The "sharpness" of an image is defined as

$$S = \left(-\frac{dD}{dx}\right)_{max.} , \tag{4.11}$$

that is, the negative slope of the steepest part of the density-gradient curve.

If it is assumed that the parameters a,b,c,d,... are not functions of x, then, as a consequence of Eqs 4.5 and 4.9,

$$\frac{dD}{dx} = \frac{dD}{dI} \cdot \frac{dI}{dx} = \frac{dD}{d(\log_{10} I)} \cdot \frac{d(\log_{10} I)}{dx}$$

$$= \gamma\kappa = \gamma/\sigma , \tag{4.12}$$

---

*The term "fog" is applied to the background density produced by development. Thus, it refers to the silver deposit which is not due to exposure to light.

where γ is the contrast and σ, the turbidity, is equal to $1/\kappa$ by definition. Thus from Eqs 4.11 and 4.12,

$$S = (-\gamma/\sigma)_{max.} \quad . \tag{4.13}$$

Since the higher S, the sharper the image, it follows that large values of γ and small values of σ are necessary for sharp images. It is also desirable to use an emulsion having a minimum amount of toe in its characteristic curve.[35] Finally, it should be noted that sharpness depends on the wavelength and the intensity of the light as well as the exposure time.[35]

Resolving power is another important property of emulsion. It is usually defined with reference to parallel line images.[34,35] Consider two such images of equal width separated by a space ℓ equal to the common width of the lines. Then by definition the resolving power R is the number of lines per millimeter just separated. That is,

$$R = \frac{1000}{2\ell} \quad ,$$

where ℓ is in microns. While resolving power depends upon the wavelength of the light, exposure, type of developer, development time, and other variables, it can be shown that the important parameters are contrast and turbidity.[35] Values of R range approximately from 90 lines per millimeter for fast roll film emulsions to 1000 lines per millimeter for special spectroscopic plates. The latter type of emulsion is ruled out of the present work because of its extremely slow speed. A compromise was therefore necessary between speed and resolution. The Contrast Process Ortho emulsion was finally selected. It has a resolving power of 150 lines per millimeter, which corresponds to the value ℓ = 3.3 microns. Tests with Contrast Process Panchromatic, which has somewhat higher speed but a resolving power of only 105 lines per millimeter, showed it to be inferior to Contrast Process Ortho in the present application.

Lastly, mention should be made of certain characteristics of films and plates which result in movements and distortions of the image.[34] Such effects are sometimes due to drying conditions, which may produce a general expansion of the gelatin layer. Another factor is the Ross effect, i.e., a shrinkage and shifting of the image resulting from the tanning action on the gelatin by chemical reaction products formed during development. Tests were made on the influence of drying by giving a number of pieces of film identical exposures and developments and then drying the individual pieces under widely different conditions. No measurable effect on image size was found.

c) Reading or Personal Errors. -- Photographic images have edges which are more or less diffuse, depending on sharpness of the resultant developed image in the film. Magnifying an image will be of value up to a certain point, but beyond that the increased diffuseness and raggedness of the edge renders further magnification useless. It is desirable, therefore, to obtain as much of the total magnification on the negative as is consistent with film size and the field to be covered. In measuring images visually, an observer

will set up his own criterion as to the location of the "edge" of the image. The disparity between measurements by different observers on a given image will naturally decrease with increasing edge sharpness.

When negatives are projected through a photographic enlarger, it is necessary to consider the resulting optical distortions. Fortunately, these are not severe when working at enlargement factors of about 5X, as in the present investigation. Nonuniformity of magnification can be detected by scratching accurate reference marks at several positions on the negative and measuring the corresponding distances in the plane of the enlarged image. If the negative is projected onto a ground-glass screen, as it was in the present work, the diffuse, fine structure of the glass will contribute to the fuzziness of the edges of the images. Obviously, a ground glass with fine grain texture is desirable.

4.3 Experimental Results

a) Calibration Procedure. -- In view of the complicated lens and film errors, it is evident that one must have recourse to a method of calibration which will check the overall accuracy of reproduction. This requirement can be met partially by photographing objects of known dimensions comparable to the expected drop sizes, namely in the range 0.0005 to 0.010 inch. In the present work a number of test objects were used, among which may be mentioned fine tungsten wires of 0.0003-inch nominal diameter, a 0-80 metal tap whose pitch of 0.0125 inch was accurately known, and an engraver's screen with 140 lines to the inch. These objects may be criticized as calibration test objects on the grounds that they do not produce circular silhouette images as do the drops. To meet this objection, a test object was prepared by spraying ink into a glass slide.* The ink drops dried to form opaque discs which ranged in diameter from about 0.0001 to 0.15 inch, as measured by calibrated comparators or microscopes equipped with micrometer oculars. It seems reasonable to assume that these ink spots will approximate transparent liquid drops in their action on a light beam.[9] When the edges of these ink discs were examined microscopically at 200X magnification, they were observed to be extremely sharp. The general character and size range of the ink drops are shown in Fig. 24, where the total magnification is about 20X. Some of the drops are not truly circular, and in such cases where the departure from a circle is significant the "diameter" was measured in some specified direction. In use the test slide was located in the wind tunnel at the position where spray photographs were to be taken later. For such calibration pictures there was no airflow in the tunnel. As was the case for spray-drop photographs, the test slide was illuminated from behind and in this arrangement produced silhouette images which simulated well those produced by actual spray drops.

---

*A small amount of black, negative-marking ink was brushed on a piece of 70-mesh screen made of monel wire of 0.007-inch diameter. The screen was then held a few inches above a glass slide and a short blast of compressed air blown on the screen with the result that ink was detached from the screen and deposited as drops on the slide.

The negatives were projected at 5X magnification upon a ground-glass screen, where they were measured visually with a straight-edge scale. The camera magnification was 10X, making the total magnification 50X. The precise total magnification was determined carefully, so that from it the "actual" diameters of the drops could be determined. Since certain selected ink drops were measured accurately, it was possible to check their true sizes against the corresponding values determined from the projected photographic negatives. The effects of exposure, development, type of emulsion, etc., could be examined in this manner.

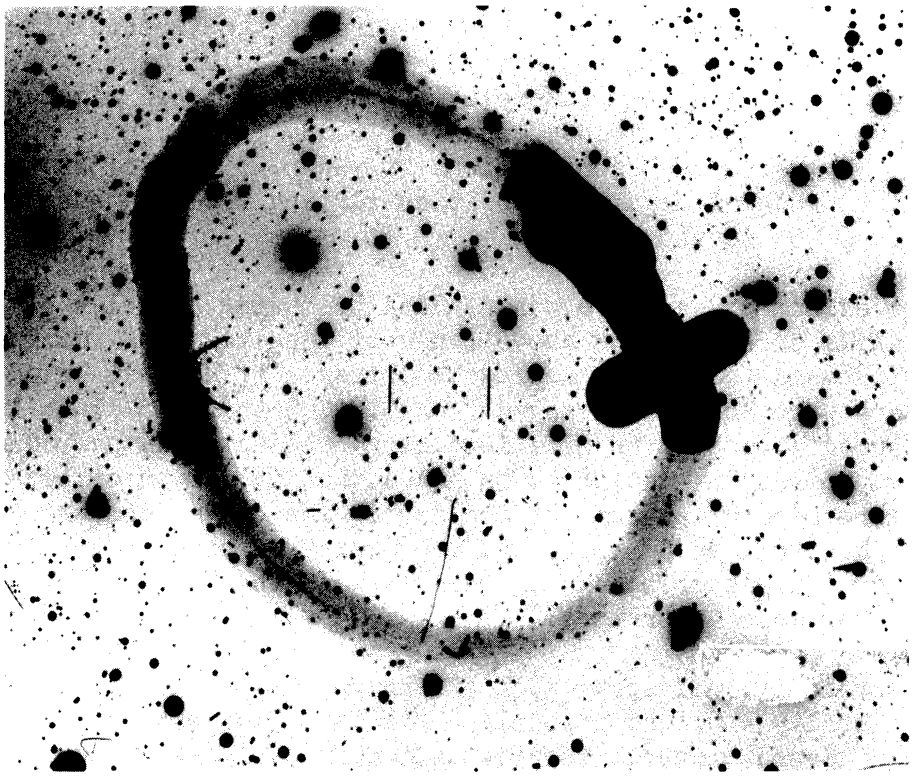

Fig. 24. Typical Photograph of Test Slide

A check on the depth of field of the lens at f/11 was made by clamping the test object to a screw-drive mechanism whereby the slide could be moved along the optical axis of the camera by a fraction of a turn, where one turn equalled 0.025 inch. The position of best focus was determined, and then a series of photographs taken at multiples of 0.025 inch up to 0.125 inch on the near and far sides of the central position. The point at which an object is said to be just in or out of focus is arbitrary and subjective to some extent. However, the above series of negatives was examined by several observers who

agreed that the total depth of field was about 0.075 ± 0.015 inch. Theoretical values of the depth of field of the lens seem to have little practical meaning in the present situation, for the reason that an allowable circle of confusion on the negative must be assumed and there appears to be no way of knowing what value should be chosen. However, if one assumes a circle of confusion of radius z' = 75 microns and uses the standard formula[31], one finds the depth of field to be 0.014 inch. The agreement with the measured value is obviously poor and indicates that the observers unconsciously accepted a larger circle of confusion in judging when an image became out of focus. It is also possible that part of the discrepancy is due to the lens being less highly corrected than was supposed.

b) Effect of Exposure and Development. -- It is convenient to hold constant the development parameters, such as time of development and temperature of the solution. This leaves the exposure as the important free variable. In the present work exposure was varied by placing colored filters in front of the flash lamp to cut down the intensity of the transmitted light. Yellow and magenta filters from a set of Ansco color-printing filter foils were used for this purpose. By using such combinations it was possible to obtain a range of exposures which produced negative densities varying from the barely visible (approximately 0.20) to about 3.0.

The effect of exposure was studied by making a series of photographs of the test slide such that the above range of densities was realized. Drop sizes were then measured from the projected images of certain selected drops whose diameters were known and ranged from 0.00065 to 0.0054 inch. When the ratio of measured size to true size is plotted against negative density, the curves of Fig. 25 result. It is to be noted that variation of size with density is the more severe the smaller the drop. The curves converge approximately in the neighborhood of D = 1.9, and the region of convergence is near the size ratio 1.0. This corresponds in general with the results obtained by the Eastman Kodak Research Laboratory.*

Accordingly, all spray photographs were exposed so as to give a density as close to 1.9 ± 0.1 as possible. All densities were measured with an Eastman Model 1 densitometer. Considerable difficulty was encountered in holding the density within even the range $1.8 \leq D \leq 2.1$. The effect of varying line voltage upon the output of the flash lamp was found to be too small to account for the density variations present under conditions of exposure and development which were as nearly constant and identical as the equipment would permit. Variations in spray density with time and differences in the sensitivities of different emulsion batches may account for some of these erratic density fluctuations.

When the characteristic curve for the emulsion is given, the values of density can be converted to relative values of $\log_{10}E$. Fig. 26 is a copy of the manufacturer's curves for the Contrast Process Ortho type of film. A number of approximations are involved in the present use of these curves: (1) they are merely average characteristics for a number of film samples and therefore apply

---

*Private communication.

only approximately to a given piece of film; (2) they are for exposure to tungsten light, whereas the light used in the present work was predominantly blue in color; and (3) they are for development in the D-8 formula rather than D-11, which was used.* A development time of 10 minutes gives a gamma of about 4.7, as can be seen from the time-gamma curves for D-11. To reach the same gamma using D-8 would require roughly a 3-minute development time. On this basis the 3-minute curve AB was used to convert densities to relative values of $\log_{10}E$.

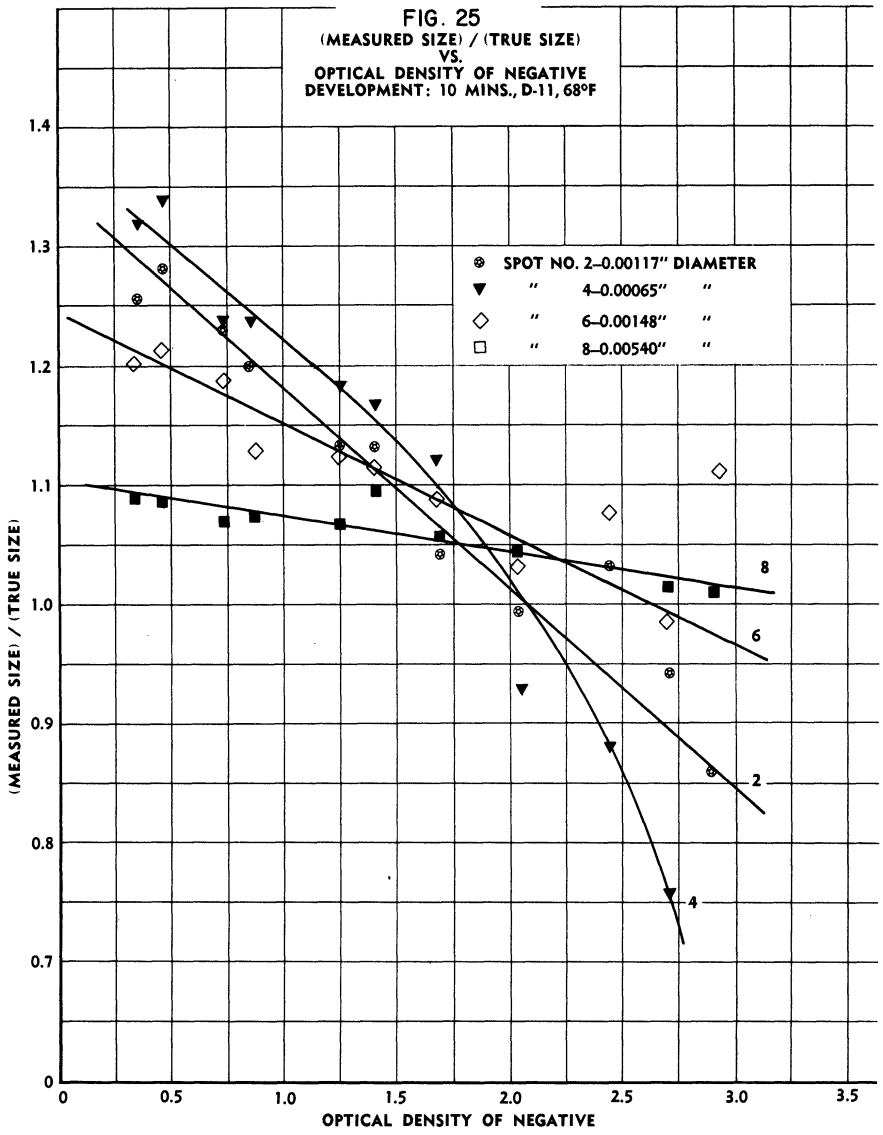

Implicit in this procedure is the assumption that development to a given gamma in D-11 will give a characteristic curve of the same shape as that obtained with development to the same value of gamma in D-8. It is also assumed that the two curves would not be vertically displaced relative to one another by a significant amount, although horizontal displacement would not affect the desired relative values. Using the curve AB, the data of Fig. 26 were replotted in terms of

---

*The keeping qualities of D-8 developer are rather poor, and for this reason it was not used.

(measured size)/(true size) vs $\log_{10}E$. The results are shown in Fig. 27. There is considerable scatter in the points, but in general they confirm the linear relationship of Eq 3.10. The data for the 0.00065-inch diameter spot seem to fit best two straight-line segments; however these points are in doubt, since a drop of this size is near the limit of resolution of the lens.

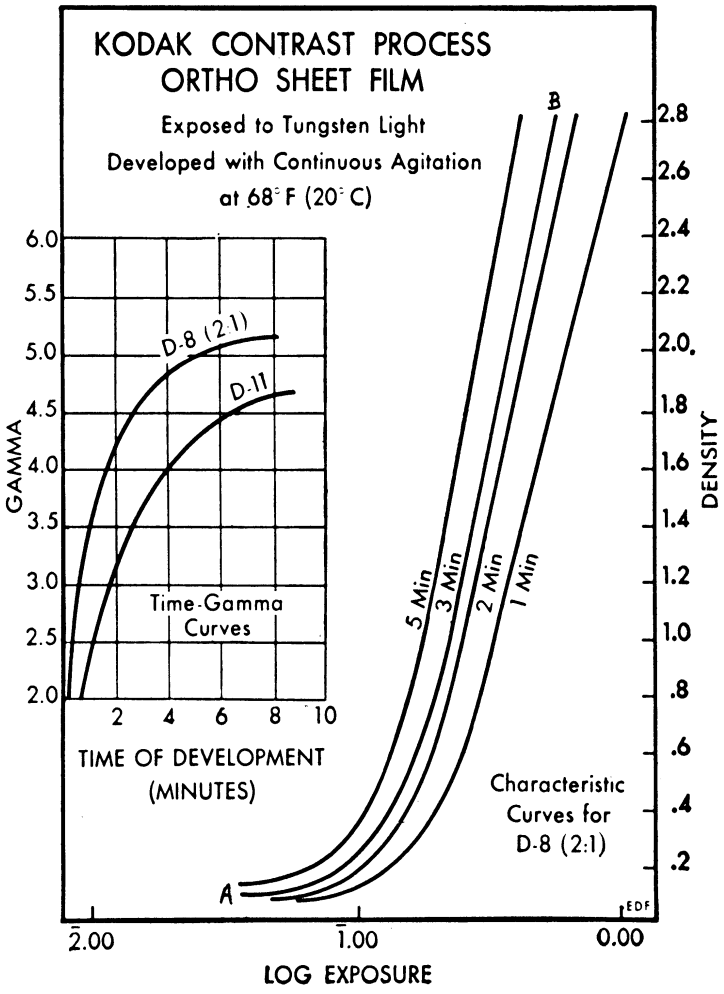

It was found that changing the development time had only a slight effect on the size vs density curves, shorter development times tending to steepen the curves. Fig. 28 is for 6-minute development and is to be compared with Fig. 25, which is for 10-minute development. From the time-gamma curve for D-11 given in Fig. 26, one sees that 10-minute development brings the contrast practically to γ_∞, where the curve is almost flat. For this reason development times somewhat greater than 10 minutes would not be expected to have a large effect on size vs density curves. These considerations lead to the conclusion that small deviations of $\pm$ 0.5 minute, or even $\pm$ 1.0 minute, from 10 minutes in D-11 are of no consequence in the present work. It may be added that there is usually a slow increase in fog density with increasing development time.[34]

c) Spray Results. -- In order to obtain a reasonably accurate mass distribution curve, it was necessary to measure 150 to 200 drops. The spray density and depth of field of the camera jointly restrict the number of drops which appear in focus to about 10 to 20 per negative. This required 10 to 15 photographs to be taken for a single distribution curve. Two such sets of

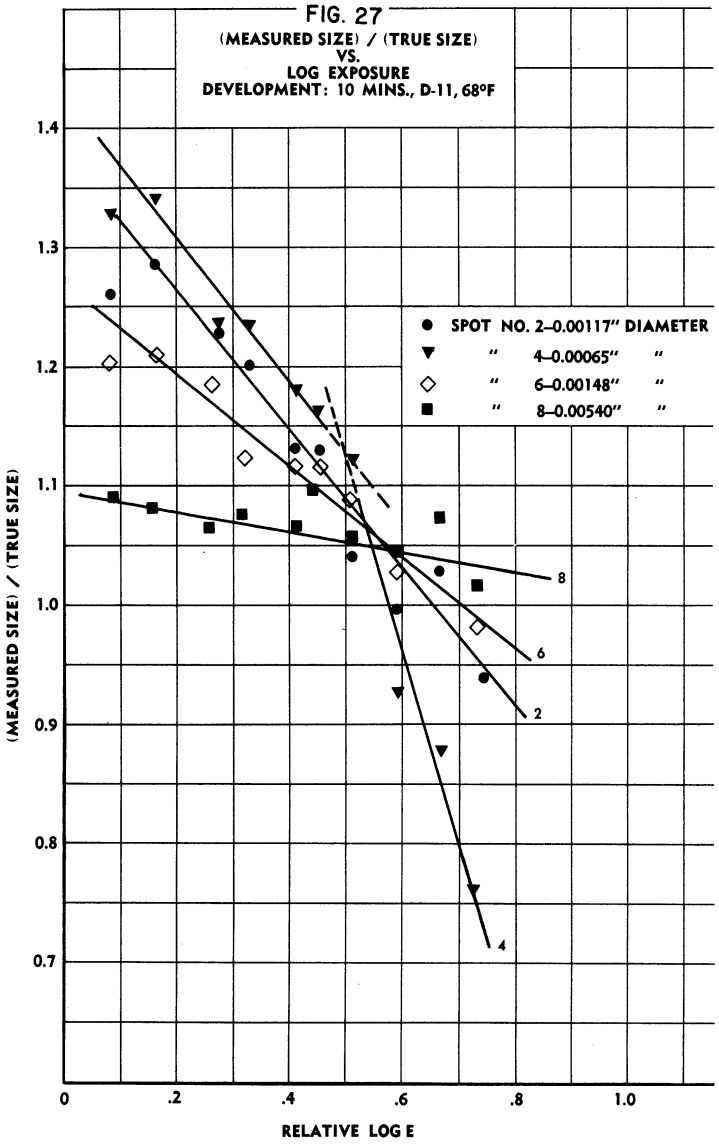

photographs were taken and measured, one at the highest turbulence value of σ = 7.2 per cent, and the other at the lowest value of σ = 0.90 per cent. The photographs and turbulence measurements were made at a point* 12 inches from the tip of the nozzle and 2 inches from the axis of the spray in a

*Strictly speaking, the photographs cover a field volume element 0.4 by 0.5 inch whose thickness is approximately the depth of field of the camera. The "point" of observation is arbitrarily taken to be the center of this volume element.

horizontal plane. Fig. 29 shows the two graphs of mass fraction* plotted against drop diameter δ . These curves show clearly a decrease in diameter of the larger drops for the higher level of turbulence. Fig. 30 is derived from the curves of Fig. 29 and gives curves which show size frequency as a function of drop diameter.

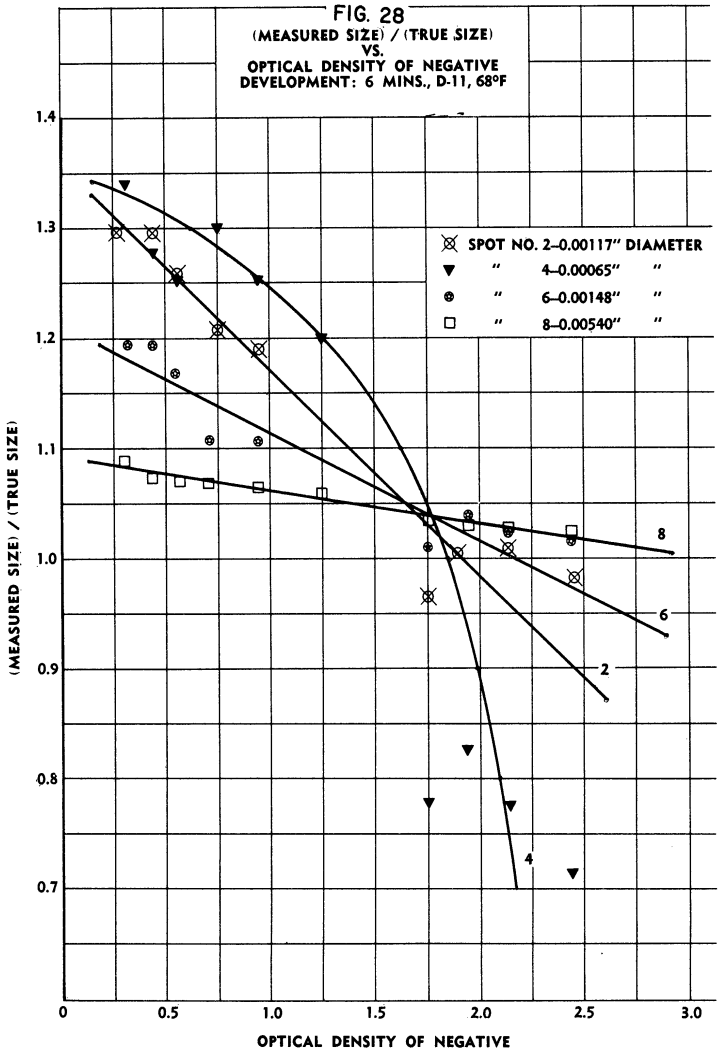

The data of Fig. 29 may be analyzed in the following way to give mean drop diameter, $\overline{\delta}$, and relative mass of the spray. Let $n(\delta)$ denote the number of drops with diameters between δ and $\delta + d\delta$, $m(\delta)$ the mass of drops with diameters between δ and $\delta + d\delta$, N the total number of drops in the spray, and M the total mass of liquid in the spray. For these quantities it holds that

$$N = \int_0^\infty n(\delta)\, d\delta \qquad (4.15)$$

*By definition, R equals the fraction of the total mass contained in drops of diameters above any value δ .

and

$$M = \int_0^{\infty} m(\delta)\, d\delta \quad . \tag{4.16}$$

There is also the relation between R and $m(\delta)$ given by the equation

$$R = 1 - \int_0^{\delta} \frac{m(\delta_1)}{M}\, d\delta_1 \quad , \tag{4.17}$$

where δ_1 is a variable of integration, and the integral itself equals the fraction of the total mass of the spray contained in drops having diameters less than δ. From Eq 4.17 it follows that

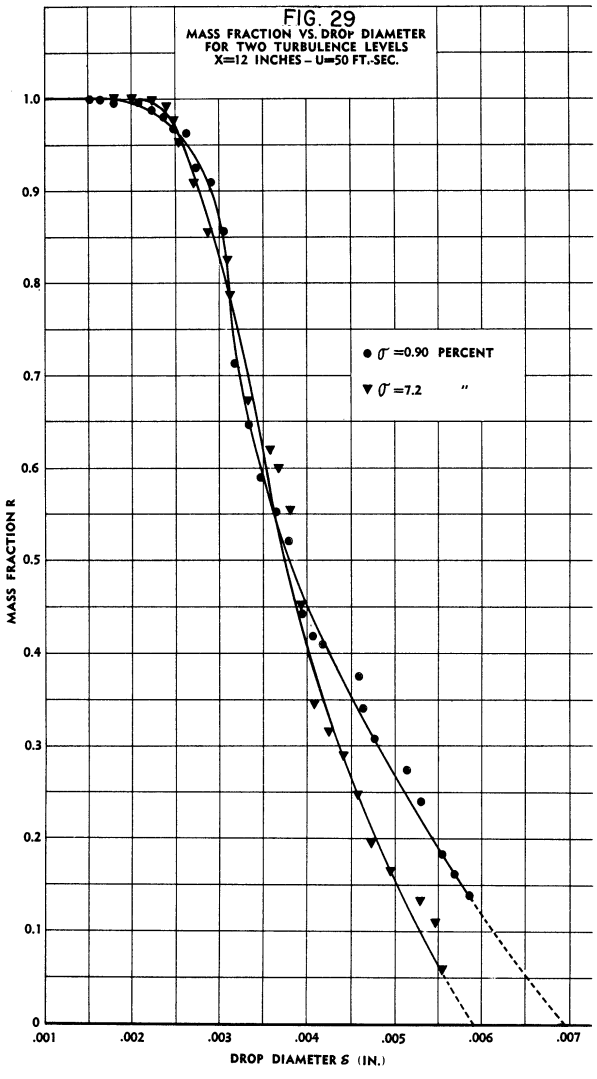

$$m(\delta) = -M \frac{dR}{d\delta} \quad . \tag{4.18}$$

By definition, the mean drop diameter is found from the relation

$$\rho_L \frac{\pi}{6} \bar{\delta}^3 = \frac{M}{N} \quad , \tag{4.19}$$

where ρ_L is the density of the liquid. Moreover,

$$n(\delta) = \frac{m(\delta)}{\rho_L (\pi/6) \delta^3} \quad . \tag{4.20}$$

Substituting Eq 4.20 into Eq 4.15 gives

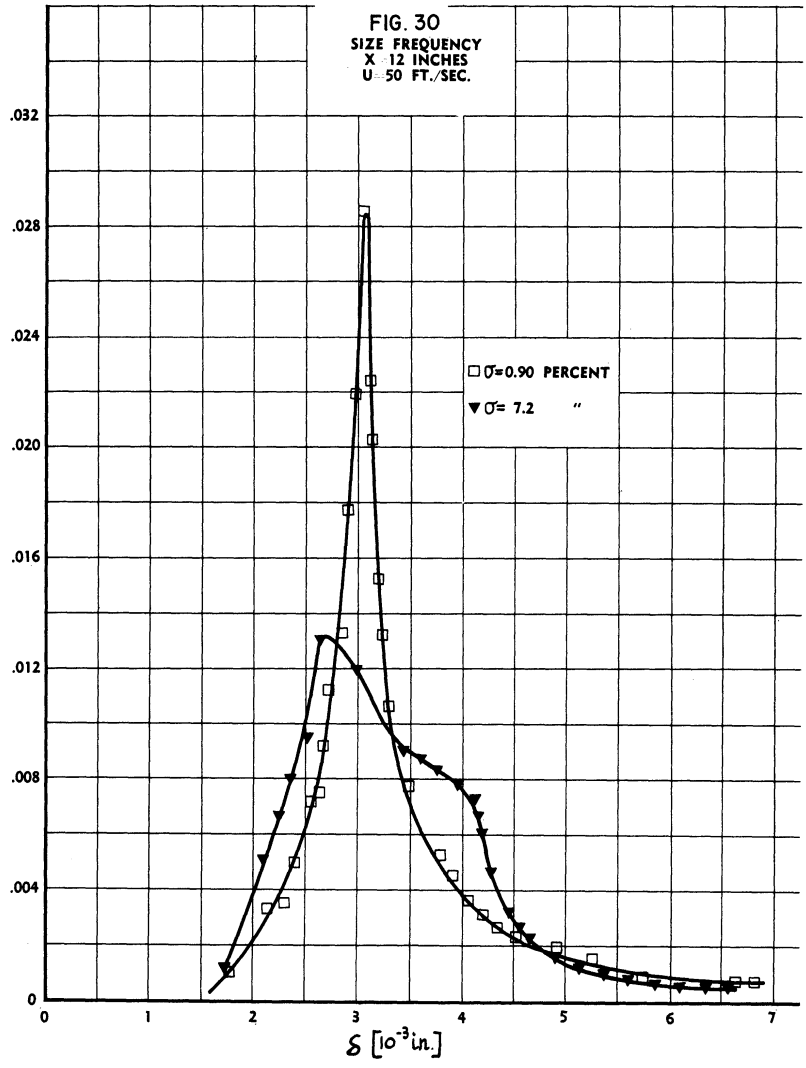

$$N = \int_0^\infty \frac{m(\delta)}{\rho_L (\pi/6) \delta^3} \, d\delta$$

which, by virtue of Eq 4.18, can be written

$$N = \frac{M}{\rho_L(\pi/6)} \int_0^\infty \frac{-dR/d\delta}{\delta^3} \, d\delta \quad . \tag{4.21}$$

Solving Eq 4.21 for M/N and making use of Eq 4.19, we get

$$\bar{\delta}^3 = \left\{ \int_0^\infty \frac{-dR/d\delta}{\delta^3} \, d\delta \right\}^{-1} \quad . \tag{4.22}$$

The derivative $dR/d\delta$ can be found from the experimental curve of R vs δ, and the integral in Eq 4.22 evaluated graphically.

When the procedure given above is used to calculate $\bar{\delta}$ from the data of Fig. 29, the following values are obtained for the two turbulence levels:

$$\begin{aligned} \bar{\delta} &= 0.00341 \text{ inch} \quad \text{for} \quad \sigma = 7.2 \text{ per cent} \\ \bar{\delta} &= 0.00357 \text{ inch} \quad \text{for} \quad \sigma = 0.90 \text{ per cent} \quad . \end{aligned} \tag{4.23}$$

The data on size ratio as a function of exposure show that if exposure and development are controlled to give a negative density between 1.8 and 2.0, an accuracy of about 5 per cent can be expected for $0.002 < \delta < 0.010$ inch. For drops in the range $0.0005 < \delta < 0.002$ inch, the error will be 10 per cent or higher, however. It was found to be difficult to control the negative density within the above limits. The result was that many pictures had to be taken, and only those selected which fell in the optimum density range of 1.8 to 2.0.

5. THEORY OF EVAPORATION

5.1 General

The process of evaporation or mass convection is essentially that of mechanical diffusion of one gas into another.[36] Let c denote the concentration of the vaporized liquid in the gas phase. Then the equation which describes c for evaporation from a liquid surface at rest in a surrounding air flow is

$$\frac{\partial c}{\partial t} = \frac{\partial}{\partial x}\left(D\frac{\partial c}{\partial x}\right) + \frac{\partial}{\partial y}\left(D\frac{\partial c}{\partial y}\right) + \frac{\partial}{\partial z}\left(D\frac{\partial c}{\partial z}\right) , \qquad (5.1)$$

where D is the coefficient of diffusion, and

$$\frac{\mathcal{D}c}{\mathcal{D}t} \equiv \frac{\partial c}{\partial t} + u\frac{\partial c}{\partial x} + v\frac{\partial c}{\partial y} + w\frac{\partial c}{\partial z}$$

when u, v, and w are the velocity components of the air. The problem is subject to two boundary conditions: (1) the air in contact with the evaporating surface is assumed to be saturated, whereby $c = c_m$; and (2) at large distances from the surface c approaches a constant value which can be taken as c = 0. When D = constant, Eq 5.1 becomes

$$\frac{\mathcal{D}c}{\mathcal{D}t} = D\nabla^2 c ,$$

where ∇^2 stands for the Laplacian operator.

For the analogous problem of heat convection, the equation determining the temperature field is

$$\rho C_p\frac{\mathcal{D}T}{\mathcal{D}t} = \frac{\partial}{\partial x}\left(k\frac{\partial T}{\partial x}\right) + \frac{\partial}{\partial y}\left(k\frac{\partial T}{\partial y}\right) + \frac{\partial}{\partial z}\left(k\frac{\partial T}{\partial z}\right) , \qquad (5.2)$$

where ρ, C_p, and k are, respectively, the density, specific heat, and thermal conductivity of the air. When k = constant, Eq 5.2 becomes

$$\frac{\mathcal{D}T}{\mathcal{D}t} \equiv \alpha\nabla^2 T ,$$

and $\alpha = k/\rho C_p$ is called the (thermal) diffusivity.

5.2 Single Drops

The theory of evaporation of drops has undergone considerable development and has been checked experimentally for the case of a single drop. There

appears to be no theory and little experiment for convective evaporation of ensembles of drops, although Probert[37] has discussed the case of a spray moving with the same velocity as the ambient airstream. This section will review the theory of single-drop evaporation for the two cases of stationary and moving single drops.

a) Stationary Drop. -- The evaporation of a single drop at rest with respect to the surrounding air has been studied theoretically by Maxwell[38] and Langmuir[39], who find, for the steady state, the relation

$$\frac{dm}{dt} = -2\pi D \frac{\hat{M}p}{RT}\delta \quad , \tag{5.3}$$

where m, δ, and $\hat{M}$ are, respectively, the mass, diameter, and molecular weight of the drop, while p, R, and T refer, respectively, to the vapor pressure, gas constant, and absolute temperature of the saturated vapor-air mixture at the surface of the drop. Eq 5.3 has been tested experimentally by Morse[40], Houghton[41], Namekawa and Takahashi[42], and others, who verified its correctness.

b) Moving Drop. -- The most complete theoretical and experimental investigation of evaporation from a drop moving with respect to the surrounding air is apparently that of Frössling.[43] Actually, he considered the equivalent case of a drop held fixed in a wind tunnel. Noting that a relative velocity, U, between drop and airstream increases the evaporation, Frössling takes as a starting point the relation

$$\frac{dm}{dt} = -2\pi D \frac{\hat{M}p}{RT}\delta \cdot f \quad , \tag{5.4}$$

where f is called the "wind factor" and specifies the increase due to U. Fick's law[44] states that the rate of diffusion from an element of surface dS equals $-D(\partial c/\partial n)_S \cdot dS$, where $(\partial c/\partial n)_S$ is the concentration gradient normal to the surface. Therefore, the following relation is used by Frössling

$$\frac{dm}{dt} = -D \iint_S \left(\frac{\partial c}{\partial n}\right)_S dS \quad . \tag{5.5}$$

The variables which determine f can be found by putting Eqs 5.1 and 5.5 in nondimensional form. This is accomplished by the following transformations:

$$\left.\begin{aligned} x &= \delta x' \\ y &= \delta y' \\ z &= \delta z' \\ n &= \delta n' \end{aligned}\right\} \qquad \left.\begin{aligned} u &= Uu' \\ v &= Uv' \\ w &= Uw' \end{aligned}\right\} \qquad \left.\begin{aligned} P &= (\rho U^2)P' \\ c &= c_m c' \\ S &= \delta^2 S' \end{aligned}\right\} \tag{5.6}$$

where c_m is the vapor concentration at the surface of the sphere and P is the

total pressure. When Eq 5.6 is applied to Eq 5.1 for the steady state the result is the relation,

$$u' \frac{\partial c'}{\partial x'} + v' \frac{\partial c'}{\partial y'} + w' \frac{\partial c'}{\partial z'} = \frac{D}{U\delta} \left(\frac{\partial^2 c'}{\partial x'^2} + \frac{\partial^2 c'}{\partial y'^2} + \frac{\partial^2 c'}{\partial z'^2} \right) ,$$

which can be written

$$u' \frac{\partial c'}{\partial x'} + v' \frac{\partial c'}{\partial y'} + w' \frac{\partial c'}{\partial z'} = \frac{1}{(Re)(Sc)} \left(\frac{\partial^2 c'}{\partial x'^2} + \frac{\partial^2 c'}{\partial y'^2} + \frac{\partial^2 c'}{\partial z'^2} \right), \quad (5.7)$$

where $Re = U\delta/\nu$ and $Sc = \nu/D \equiv$ Schmidt number. Eqs 5.5 and 5.6 lead to

$$\frac{dm}{dt} = - D c_m \delta \iint_{S'} \left(\frac{\partial c'}{\partial n'} \right)_{S'} dS' . \quad (5.8)$$

Since u', v', w', and P' are functions of x', y', z', and Re, it follows from Eq 5.7 that

$$c' = fn(Re,Sc,x',y',z') . \quad (5.9)$$

Substituting Eq 5.9 into Eq 5.8, noting that $c_m = \hat{M}p/RT^*$, gives

$$\frac{dm}{dt} = - D \frac{\hat{M}p}{RT} \delta \cdot fn(Re,Sc) . \quad (5.10)$$

Frössling next investigates the form of fn(Re,Sc) in Eq 5.10. The boundary-layer equations for a body of revolution are[45]

$$\left.\begin{aligned} u \frac{\partial u}{\partial x} + v \frac{\partial u}{\partial y} &= U_1 \frac{\partial U_1}{\partial x} + \nu \frac{\partial^2 u}{\partial y^2} \\ \frac{\partial (r'u)}{\partial x} + \frac{\partial (r'v)}{\partial y} &= 0 \end{aligned}\right\} , \quad (5.11)$$

where U_1 is the velocity of potential flow at the edge of the boundary layer. Fig. 31 shows the coordinate system with respect to a sphere, where the coordinates of a point Q may be specified in terms of x, measured along a meridian on the surface, and y, measured normal to the surface. u and v are velocity components parallel and perpendicular to the surface S, respectively. The steady-state diffusion equation written in polar coordinates for the case of rotational symmetry is

---

*$p = p_m - p_o$, where p_m = vapor pressure at surface of drop, and p_o = partial pressure of vapor in free stream. Generally, $p_o \ll p_m$ and may be neglected.

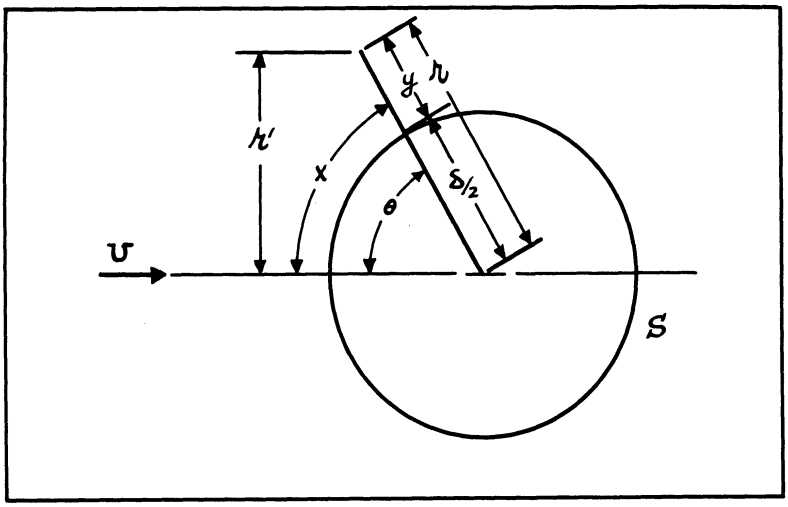

Fig. 31

$$\frac{u}{r}\frac{\partial c}{\partial \theta} + v\frac{\partial c}{\partial r} = D\left[\frac{1}{r^2}\frac{\partial}{\partial r}\left(r^2\frac{\partial c}{\partial r}\right) + \frac{1}{r^2\sin\theta}\frac{\partial}{\partial \theta}\left(\sin\theta\frac{\partial c}{\partial \theta}\right)\right] \quad . \tag{5.12}$$

Noting that, if $\epsilon \ll 1$ and $y \ll \delta$, where ϵ = boundary-layer thickness, and that $r = \delta/2 + y$ and $x = (\delta/2)\theta$, Eq 5.12 comes down to

$$u\frac{\partial c}{\partial x} + v\frac{\partial c}{\partial y} = D\frac{\partial^2 c}{\partial y^2} \quad . \tag{5.13}$$

Eq 5.13 holds for points not too close to the stagnation point, such that the condition $\cot 2x/\delta \ll 1/\epsilon^2$, or $2x/\delta \gg \epsilon^2$. The continuity equation of Eq 5.11 can be written

$$\frac{\partial u}{\partial x} + \frac{\partial v}{\partial y} + \frac{2u}{\delta}\cot\frac{2x}{\delta} = 0 \quad , \tag{5.14}$$

where the term $v/(\delta/2 + y) \cong 2v/\delta$ has been neglected.

Frössling's analysis therefore leads to the following form for the boundary-layer equations:

$$\left.\begin{aligned} u\frac{\partial u}{\partial x} + v\frac{\partial u}{\partial y} &= U_1\frac{\partial U_1}{\partial x} + \nu\frac{\partial^2 u}{\partial y^2} \\ \frac{\partial u}{\partial x} + \frac{\partial v}{\partial y} + \frac{2u}{\delta}\cot\frac{2x}{\delta} &= 0 \\ u\frac{\partial c}{\partial x} + v\frac{\partial c}{\partial y} &= D\frac{\partial^2 c}{\partial y^2} \end{aligned}\right\} \quad , \tag{5.15}$$

subject to the boundary conditions:

$$\left.\begin{aligned} u = v &= 0 \\ c &= c_m \end{aligned}\right\} \quad \text{at } y = 0$$

and

$$\left.\begin{aligned} u &= U_1 \\ c &= 0 \end{aligned}\right\} \quad \text{for } y \longrightarrow \infty \ .$$

By making the substitutions

$$\left.\begin{aligned} x &= \delta x' \\ y &= \frac{\delta}{(Re)^{1/2}} y' \end{aligned}\right\} \qquad \left.\begin{aligned} u &= U u' \\ v &= \frac{U}{(Re)^{1/2}} v' \end{aligned}\right\} \qquad \left.\begin{aligned} c &= c_m c' \\ U_1 &= U U_1' \end{aligned}\right\} \ , \qquad (5.16)$$

Eqs 5.15 transform to

$$\left.\begin{aligned} u' \frac{\partial u'}{\partial x'} + v' \frac{\partial u'}{\partial y'} &= U_1' \frac{\partial U_1'}{\partial x'} + \frac{\partial^2 u'}{\partial y'^2} \\ \frac{\partial u'}{\partial x'} + \frac{\partial v'}{\partial y'} + 2u' \cot 2x' &= 0 \\ u' \frac{\partial c'}{\partial x'} + v' \frac{\partial c'}{\partial y'} &= \frac{1}{(Sc)} \frac{\partial^2 c'}{\partial y'^2} \end{aligned}\right\} \ , \qquad (5.17)$$

where the boundary conditions are now

$$\left.\begin{aligned} u' = v' &= 0 \\ c' &= 1 \end{aligned}\right\} \quad \text{at } y' = 0$$

and

$$\left.\begin{aligned} u' &= U_1' \\ c' &= 0 \end{aligned}\right\} \quad \text{for } y' \longrightarrow \infty \ .$$

Regarding the terms U_1' and $U_1'(\partial U_1'/\partial x')$, Frössling cites certain theoretical and experimental results (Luthander and Rydberg[46], Krell[47]) which prove that for the present range of Re it is approximately true that these terms are functions of x' which are independent of Re. Further, since the first two of Eqs 5.17 are independent of Re, it is known that u' and v' are

functions of x' and y' only. The same is true of the separation points at $(\partial u'/\partial y')_{y'=0} = 0$, which lie along a circle at $\theta=\theta_a \cong 80°$ on the sphere.

It follows from the third (diffusion) equation of Eq 5.17 that c' = fn(x',y',Sc). In terms of the dimensional quantities c, x, and y, this means that

$$c = c_m \Phi\left(\frac{x}{\delta}, \frac{y(Re)^{1/2}}{\delta}, Sc\right) . \tag{5.18}$$

The evaporation through the boundary layer (ahead of the circle of separation) can now be calculated as follows:

$$\frac{dm}{dt} = -D \iint_S \left(\frac{\partial c}{\partial y}\right)_{y=0} dS = -Dc_m \int_0^{\theta_a} \left[\frac{\partial}{\partial y}\Phi\left(\frac{x}{\delta}, \frac{y(Re)^{1/2}}{\delta}, Sc\right)\right]_{y=0} \frac{\pi\delta^2}{2} \sin\theta \, d\theta$$

$$\left[\frac{\partial}{\partial y}\Phi\left(\frac{x}{\delta}, \frac{y(Re)^{1/2}}{\delta}, Sc\right)\right]_{y=0} = \frac{(Re)^{1/2}}{\delta}\left[\frac{\partial}{\partial \zeta}\left(\frac{x}{\delta}, \zeta, Sc\right)\right]_{\zeta=0}$$

$$= \frac{(Re)^{1/2}}{\delta}\Phi_1\left(\frac{x}{\delta}, Sc\right) \quad ; \quad \frac{x}{\delta} = \frac{\theta}{2}$$

$$\frac{dm}{dt} = -D\, c_m\, (Re)^{1/2}\, \delta \int_0^{\theta_a} \frac{\pi}{2}\Phi_1\left(\frac{\theta}{2}, Sc\right) \sin\theta \, d\theta .$$

Since the last integral is a function of Sc only,

$$\frac{dm}{dt} = -2\pi D \frac{\hat{M}p}{RT}\, \delta \cdot \Psi(Sc) \cdot (Re)^{1/2} . \tag{5.19}$$

Frössling shows that most of the evaporation at larger Re occurs ahead of the separation line, so that Eq 5.19 may be expected to hold approximately for the total evaporation.

Comparing Eqs 5.19 and 5.4, it is seen that

$$f = \Psi(Sc) \cdot (Re)^{1/2} .$$

However, it is known that for Re = 0, Eq 5.19 must go over to Eq 5.3; that is, $f = 1$. Hence f must be of the form

$$f = 1 + \Psi(Sc) \cdot (Re)^{1/2} .$$

Frössling evaluates $\Psi(Sc)$ from experimental data and finds that it is quite close to $\Psi(Sc) = 0.276(Sc)^{1/3}$ for the substances he studied. The final expression for the wind factor is, therefore,

$$f = 1 + 0.276(Sc)^{1/3}(Re)^{1/2} \quad . \tag{5.20}$$

This brings Eq 5.19 to the final form

$$\frac{dm}{dt} = -2\pi D \frac{\hat{M}p}{RT}\left[1 + 0.276(Sc)^{1/3}(Re)^{1/2}\right]\delta. \tag{5.21}$$

Eq 5.21 will be used in Section 5.4 in an attempt to treat the evaporation of sprays.

5.3 Effect of Turbulence

Consider first Eq 5.21 from the standpoint of the dependence upon Re only, and how this will be affected by the turbulent fluctuations u_1, u_2, and u_3* present in the airstream. For the case of a moving drop

$$(Re)^{1/2} = \left(\frac{u_r\delta}{\nu}\right)^{1/2} = \left(\frac{\delta}{\nu}\right)^{1/2} u_r^{1/2} \quad , \tag{5.22}$$

where u_r is the relative velocity between drop and airstream. Let u_d denote the drop velocity and assume that it is parallel to U; then

$$\begin{aligned} u_r &= \left[(U + u_1 - u_d)^2 + u_2^2 + u_3^2\right]^{1/2} \\ &= (U + u_1 - u_d)\left[1 + \frac{u_2^2 + u_3^2}{(U + u_1 - u_d)^2}\right]^{1/2} \quad . \end{aligned} \tag{5.23}$$

Suppose that u_1, u_2 and $u_3 = \alpha(U - u_d)$, where $\alpha < 1$. Then

$$\left[1 + \frac{u_2^2 + u_3^2}{(U + u_1 - u_d)^2}\right]^{1/2} = \left[1 + \frac{2\alpha^2}{(1 + \alpha)^2}\right]^{1/2} \quad ,$$

which, if $\alpha < 0.2$, gives

---

* u_1 lies in the direction of U and the x-axis, while u_2 and u_3 lie in the direction of the y- and z-axes, respectively.

$$\left[1 + \frac{2\alpha^2}{(1+\alpha)^2}\right]^{1/2} < (1 + 0.0556)^{1/2} \cong 1.03 \ .$$

Therefore, it is sufficiently accurate for present purposes to let the quantity in brackets equal unity. Then

$$u_r = \bar{u}_r + u_1 \ ,$$

where $\bar{u}_r \equiv U - u_d$. Expanding $u_r^{1/2} = (\bar{u}_r + u_1)^{1/2}$ gives

$$u_r^{1/2} = \bar{u}_r^{1/2}\left[1 + \frac{1}{2}\left(\frac{u_1}{\bar{u}_r}\right) - \frac{1}{8}\left(\frac{u_1}{\bar{u}_r}\right)^2 + \ldots\right] \ ,$$

which, if $u_1 < 0.2\ \bar{u}_r$, gives to the same approximation

$$u_r^{1/2} \cong \bar{u}_r^{1/2} = (U - u_d)^{1/2} \ . \qquad (5.24)$$

The preceding discussion shows that so long as u_1, u_2, and u_3 are small compared with $(U - u_d)$, the effect of turbulence will not affect evaporation through the Reynolds number.

It seems reasonable to expect that turbulence will influence dm/dt through the (mass) diffusion coefficient D. V. Kármán[48] and Schubauer[49] have found that for the transfer of heat the thermal diffusion coefficient D_{heat} in turbulent flow is the sum of the laminar coefficient and a turbulent coefficient $(D_T)_{heat}$ proportional to $u'^2 = (\bar{u}_1^2 + \bar{u}_2^2 + \bar{u}_3^2)$. $(D_T)_{heat}$ is the dominant term, so that $D_{heat} \propto u'^2$ approximately. Assuming similarity between the processes of heat and mass transfer, it will also be true that $D \propto u'^2$.

5.4 Application to Sprays

Eq 5.21 specifies the rate of steady-state evaporation of a single drop. Let the subscript i designate some particular drop of an ensemble of drops; then for such a drop Eq 5.21 is

$$\frac{dm_i}{dt} = -\frac{2\pi\, D\hat{M}p}{RT}\left[1 + 0.276\,(Sc)^{1/3}(Re_i)^{1/2}\right]\delta_i \ , \qquad (5.25)$$

where $Re_i = u_r \delta_i / \nu$, under the assumptions that u_r is the same for all drops at a given x and that each drop evaporates as if it were isolated from the surrounding drops.

If dN_i is the number of drops between δ_i and $\delta_i + d\delta$, then $m_i dN_i$ is the mass of all drops in this size group. Applied to all drops of size δ_i, Eq 5.25 gives

$$\frac{d}{dt}(m_i dN_i) = -A'\left[1 + B'(Re_i)^{1/2}\right]\delta_i \, dN_i \quad , \tag{5.26}$$

where $A' = 2\pi D\hat{M}p/RT$ and $B' = 0.276(Sc)^{1/3}$. Applied to all drop sizes, Eq 5.26 leads to the system of equations

$$\left.\begin{aligned}
\frac{d}{dt}(m_o dN_o) &= -A'\left[1 + B'(Re_o)^{1/2}\right]\delta_o \, dN_o \\
\frac{d}{dt}(m_1 dN_1) &= -A'\left[1 + B'(Re_1)^{1/2}\right]\delta_1 \, dN_1 \\
\frac{d}{dt}(m_2 dN_2) &= -A'\left[1 + B'(Re_2)^{1/2}\right]\delta_2 \, dN_2 \\
&\vdots \qquad\qquad \vdots \\
\frac{d}{dt}(m_i dN_i) &= -A'\left[1 + B'(Re_i)^{1/2}\right]\delta_i \, dN_i \\
&\vdots \qquad\qquad \vdots
\end{aligned}\right\} \tag{5.27}$$

Adding Eqs 5.27 gives

$$\frac{d}{dt}(m_o dN_o + m_1 dN_1 + \ldots + m_i dN_i + \ldots) = -A'\left\{\left[1 + B'(Re_o)^{1/2}\right]\delta_o dN_o + \left[1 + B'(Re_1)^{1/2}\right]\delta_1 dN_1 + \ldots + \left[1 + B'(Re_i)^{1/2}\right]\delta_i dN_i + \ldots\right\},$$

which in the limit becomes

$$\frac{d}{dt}\left\{\int_0^N m \, dN\right\} = -A'\int_0^N \left[1 + B'(Re)^{1/2}\right]\delta \, dN \quad .$$

If M stands for the total mass in the spray at some value of x, the last equation may be written

$$-\frac{dM}{dt} = A' \int_0^N \left[1 + B'(Re)^{1/2}\right] \delta \, dN \ , \qquad (5.28)$$

since $M = \int_0^N m\,dN$.

Eq 5.28 may be written in slightly different form by recalling that $(Re)^{1/2} = (u_r/\nu)^{1/2} \delta^{1/2}$ and splitting up the integral. Thus

$$-\frac{dM}{dt} = A' \int_0^N \delta \, dN + A'B' \left(\frac{u_r}{\nu}\right)^{1/2} \int_0^N \delta^{3/2} \, dN \ ,$$

or

$$-\frac{dM}{dt} = A' \int_0^N \delta \, dN + C' \, u_r^{1/2} \int_0^N \delta^{3/2} \, dN \ , \qquad (5.29)$$

where $C' = A'B'/\nu^{1/2}$ and $u_r = fn(t)$.

As it stands, Eq 5.29 is rather general. However, to bring it down to a form having practical utility requires the use of some specific type of distribution function for drop size. The Nukiyama-Tanasawa relation,

$$dN = a \delta^2 e^{-b\delta^q} d\delta \ , \qquad (1.2)$$

will be used for this purpose.* Substituting Eq 1.2 into Eq 5.29 gives

$$-\frac{dM}{dt} = A'a \int_\infty^0 \delta^3 e^{-b\delta^q} \, d\delta + C' \, u_r^{1/2} \, a \int_\infty^0 \delta^{7/2} e^{-b\delta^q} \, d\delta$$

or

$$-\frac{dM}{dt} = -A'a \int_0^\infty \delta^3 e^{-b\delta^q} d\delta - C' \, a \, u_r^{1/2} \int_0^\infty \delta^{7/2} e^{-b\delta^q} \, d\delta \ .$$

---

* The Rosin-Rammler relation (1.1) could be used equally well here. However, for reasons to be given in Section 6, it is unsuitable to the treatment of the present experimental data.

Both of the above integrals are easily reducible to the standard gamma function form

$$\Gamma(p) = \int_0^\infty \zeta^{p-1} e^{-\zeta} d\zeta ,$$

and give

$$\frac{dM}{dt} = A'a \frac{\Gamma(4/q)}{q\, b^{4/q}} + C'\, a\, u_r^{1/2} \frac{\Gamma(9/2q)}{q\, b^{9/2q}} . \qquad (5.30)$$

The quantity a may be evaluated from the relation

$$N = \int_0^N dN = -a \int_0^\infty \delta^2 e^{-b\delta^q} d\delta = -a \frac{\Gamma(3/q)}{q\, b^{3/q}} ,$$

from which

$$a = - \frac{N\, q\, b^{3/q}}{\Gamma(3/q)} . \qquad (5.31)$$

Combining Eqs 5.30 and 5.31 gives

$$-\frac{dM}{dt} = A'N \frac{\Gamma(4/q)}{b^{1/q}\Gamma(3/q)} + C'Nu_r^{1/2} \frac{\Gamma(9/2q)}{b^{3/2q}\Gamma(3/q)} . \qquad (5.32)$$

The total mass M = fn(t) can, in principle, be found if A', C', and N are assumed constant and u_r, b, and q are known functions of t. There is no theory giving b and q, nor are there sufficient experimental data to determine the time variation of these quantities empirically. Nevertheless, Eq 5.32 can be approximated by a simpler form, involving the mean drop diameter $\bar{\delta}$, as is discussed in Section 6.4b.

6. TURBULENCE AND COLLECTOR TUBE EXPERIMENTS

6.1 Resume of Pertinent Results of Turbulence Theory

The basis of modern turbulence theory is the work of Taylor[50] on isotropic turbulence. His approach was systematized and extended by v. Kármán and Howarth.[51] The discussion here, merely a sketch of the barest essentials of the theory, is needed later to analyze experimental data presented in this report.

Consider the steady flow in a wind tunnel. Let the coordinate system have the axes x_1, x_2, and x_3, of which the x_1 axis is parallel to the mean flow of velocity U in the test section. The total velocity components will then be

$$u = U + u_1$$

$$v = u_2$$

$$w = u_3 \ ,$$

where u_1, u_2, and u_3 are the components of the velocity fluctuations along the x_1, x_2, and x_3 axes, respectively. Taking average values defined by

$$\bar{u} = \frac{1}{T}\int_0^T u \, dt \ ,$$

it is found that

$$\bar{u} = U$$

$$\bar{v} = 0$$

$$\bar{w} = 0 \ ,$$

because $\bar{u}_1 = \bar{u}_2 = \bar{u}_3 = 0$.

The turbulence is said to be isotropic if average values of functions of the velocity components and their derivatives are not changed by rotation of the coordinate system or by reflection of the axes in any plane through the origin.

Let P and P' be two points a distance r apart. The velocity components at these points will be designated by u_1, u_2, and u_3 and u_1', u_2', and u_3', respectively. By isotropy $\bar{u}_1^2 = \bar{u}_2^2 = \bar{u}_3^2 = \bar{u}^2$. The correlation coefficients of the velocity components are defined by the relation

$$R_{ij} \equiv \frac{\overline{u_i u_j}}{\bar{u}^2} \ ,$$

where i and j = 1, 2, 3. For the case where i = j = 1 and i = j = 2 or 3, the particular notation

$$f(r,t) = \frac{\overline{u_1 u_1'}}{\overline{u^2}}$$

and

$$g(r,t) = \frac{\overline{u_j u_j'}}{\overline{u^2}} , \qquad j = 2 \text{ or } 3 ,$$

is used.

Isotropy requires that $\overline{u_i u_j'} = 0$ when $i \neq j$. It has been shown by v. Kármán and Howarth[51] that the R_{ij} are components of a second-order tensor which can be written

$$R_{ij} \equiv \frac{\overline{u_i u_j'}}{\overline{u^2}} = \frac{f(r,t) - g(r,t)}{|\vec{r}|^2} \vec{r}\,\vec{r} + g(r,t)\,\delta_{ij} ,$$

where

$$\delta_{ij} = \begin{cases} 1 & \text{when } i = j \\ 0 & \text{when } i \neq j \end{cases} .$$

Fig. 32 is a pictorial representation of the velocity components entering into the functions f(r,t) and g(r,t).

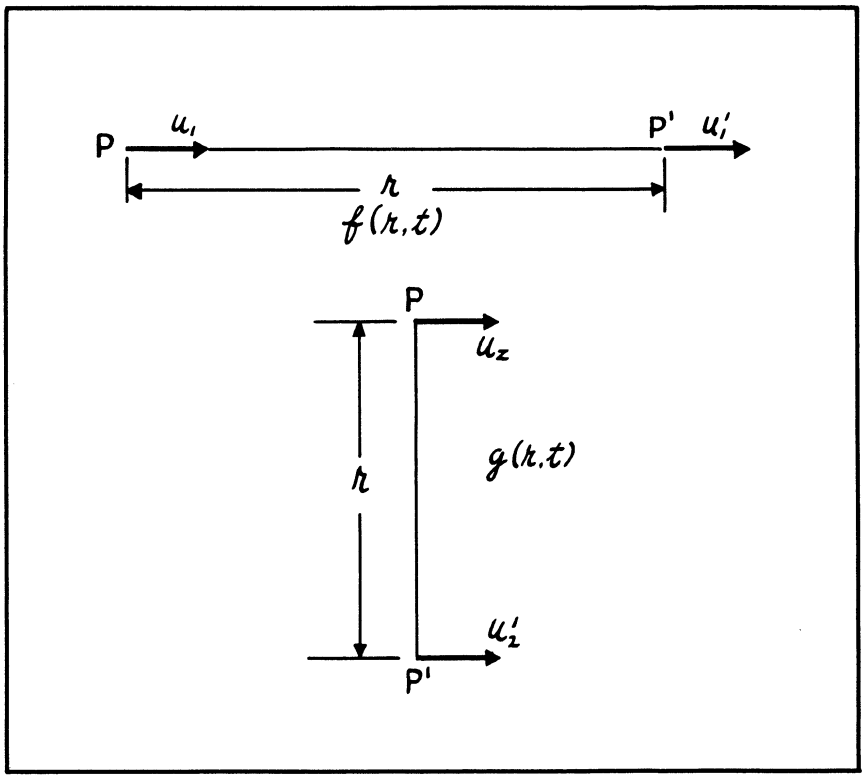

Fig. 32

It is usual practice to adopt the length L, defined by the equation

$$L = \int_0^\infty g(r)\, dr \ ,$$

as a measure of the scale of the turbulence. The function g(r) can be measured by means of two hot wires whose cross-stream separation can be varied. Graphical integration will then give L. Certain corrections[52] for finite wire length are necessary to arrive at the true value of L.

The rate of dissipation of energy in a viscous, incompressible fluid is given by the expression[45]

$$\epsilon = \mu \left\{ 2\overline{\left(\frac{\partial u}{\partial x}\right)^2} + 2\overline{\left(\frac{\partial v}{\partial y}\right)^2} + 2\overline{\left(\frac{\partial w}{\partial z}\right)^2} + \overline{\left(\frac{\partial v}{\partial x} + \frac{\partial u}{\partial y}\right)^2} + \overline{\left(\frac{\partial w}{\partial y} + \frac{\partial v}{\partial z}\right)^2} + \overline{\left(\frac{\partial u}{\partial z} + \frac{\partial w}{\partial x}\right)^2} \right\} .$$

Written in index notation, this equation becomes

$$\epsilon = \mu \overline{\frac{\partial u_i}{\partial x_j}\left(\frac{\partial u_i}{\partial x_j} + \frac{\partial u_j}{\partial x_i}\right)} , \qquad i, j = 1, 2, 3 \ .$$

If isotropy is assumed, the last equation can be shown[50] to come down to

$$\epsilon = \frac{15 \mu \overline{u}^2}{\lambda^2} \ , \tag{6.1}$$

where λ is found from the curvature of the g(r) curve at r = 0. Taylor interprets λ as a measure of the diameters of the smallest eddies through which energy is dissipated.[50]

The kinetic energy of turbulence per unit volume is

$$\frac{1}{2} \rho \left(\overline{u}_1^2 + \overline{u}_2^2 + \overline{u}_3^2\right) \ .$$

For isotropic turbulence this becomes

$$\frac{3}{2} \rho \overline{u}^2 \ .$$

The rate of change of kinetic energy due to decay of the turbulence will then be

$$-\frac{3}{2} \rho \frac{d}{dt} \left(\overline{u}^2\right) \ ,$$

which, if $t = x/U^*$, is the same as

$$-\frac{3}{2}\rho U \frac{d}{dx}(\overline{u}^2)$$

when the turbulence is superimposed on a mean velocity U. Since the dissipated energy is derived from the loss of kinetic energy, the above rate must equal the dissipation ϵ given by Eq 6.1. This reasoning leads to the equation

$$U \frac{d}{dx}(\overline{u}^2) = -10 \frac{\nu \overline{u}^2}{\lambda^2} . \qquad (6.2)$$

Taylor[50] finds that the relation

$$\frac{\lambda}{M} = A\left(\frac{\nu}{M\sqrt{\overline{u}^2}}\right)^{1/2} \qquad (6.3)$$

holds for turbulence behind a square-mesh screen or grid of mesh length M. Eqs 6.2 and 6.3 lead to

$$U \frac{d}{dx}(\overline{u}^2) = -\frac{10(\overline{u}^2)^{3/2}}{A^2 M} ,$$

which integrates to

$$\frac{U}{\sqrt{\overline{u}^2}} = \frac{5x}{A^2 M} + B , \qquad (6.4)$$

where A and B are constants. Eq 6.4 is Taylor's formula[50] for the decay of turbulence behind a square-mesh screen. It assumes that the scale of turbulence is determined by the mesh-length M.

A quantity which is commonly used in wind-tunnel work to specify turbulence intensity is the "turbulence number", σ, defined as

$$\sigma = \frac{\sqrt{(1/3)(\overline{u_i u_i})}}{U} \times 100 \ \% , \qquad i = 1, 2, 3 ,$$

where the repeated index signifies summation over i. In the present treatment of decay behind a screen, it is assumed that the three $\overline{u_i u_i}$ are equal, so that σ can be written

---

* In the remainder of this report, x will be written without a subscript.

$$\sigma = \frac{\sqrt{\overline{u^2}}}{U} \times 100 \ \% \quad .$$

More recently the theory and measurement of decay of isotropic turbulence have been extended by Batchelor and Townsend.[53-56] They divide the decay into initial and final periods which are connected by a transitional period.

For the initial period it is deduced that the decay behind a square-mesh grid obeys the law

$$\overline{u^2} \propto 1/t$$

which, since $t = x/U$, can be written

$$\frac{U^2}{\overline{u^2}} \propto x \quad . \tag{6.5}$$

The equation

$$\frac{U^2}{\overline{u^2}} = \alpha\left(\frac{x}{M} - \frac{x_o}{M}\right) \quad , \tag{6.6}$$

where α and x_o are constants, is found to fit experimental data very well up to $x/M \cong 150$, which is roughly the beginning of the transitional period. The exact extent of the initial period seems to depend somewhat on the grid Reynolds number $R_M = UM/\nu$. The measurements of Batchelor and Townsend[55] were made with grid Reynolds numbers in the range $0.28 \times 10^4 \leq R_M \leq 4.42 \times 10^4$, for which 150 mesh lengths is an approximate limit to the initial period. Measurements[55] of g(r) indicate limited self-preservation; that is, g(r) is found to be self-preserving* for roughly the range $0 < r/\lambda < 1$. Values of $(L/M)^2$ vs x/M fall fairly well on a straight line, although Batchelor and Townsend[55] doubt whether the variation of L with x follows a simple power law, as this would imply complete self-preservation.

The existence of a final period of decay has been confirmed[56] for $x/M > 400$ at a grid Reynolds number of 650. Here the energy decays according to the law

$$\overline{u^2} \propto 1/t^{5/2} \quad . \tag{6.7}$$

In the present work, $x/M < 60$, so that all measurements were made in the initial period. Therefore, the final period will not be discussed further.

---

* The term "self-preserving" applies to correlation functions such as f(r) and g(r) which do not change with time when they are plotted against r/ℓ, where ℓ is any measure of the scale, such as L or λ.

6.2 Turbulent Field in the Test Section

The airflow in the test section is produced by a 12-inch-square jet flowing into a 24-inch-square test chamber. Large vortices are undoubtedly set up between the jet boundary and the walls of the test section. Furthermore, instability at the rear of the test section, where it joins the diffuser, produces a motion or vibration of the entire jet.

The turbulence in the jet as it enters the test section is probably isotropic and obeys the decay laws for the initial period. Within the test section, however, there are superimposed upon the isotropic turbulence additional fluctuating velocities which are induced by the vortices at the boundary and the unstable waving of the jet. These superimposed velocities may be expected to increase with proximity to the jet boundary or the rear of the test section. The downstream variation of turbulence is thus the sum of a decreasing isotropic turbulence and an increasing induced turbulence, the net result depending upon the relative magnitudes of the two. Qualitatively, the isotropic turbulence levels will decrease with downstream distance, while the induced turbulence will increase. Fig. 33 shows this for five turbulence fields, ranging from the residual field to that produced by the 2.5-mesh screen with cloth streamers.

FIG. 33

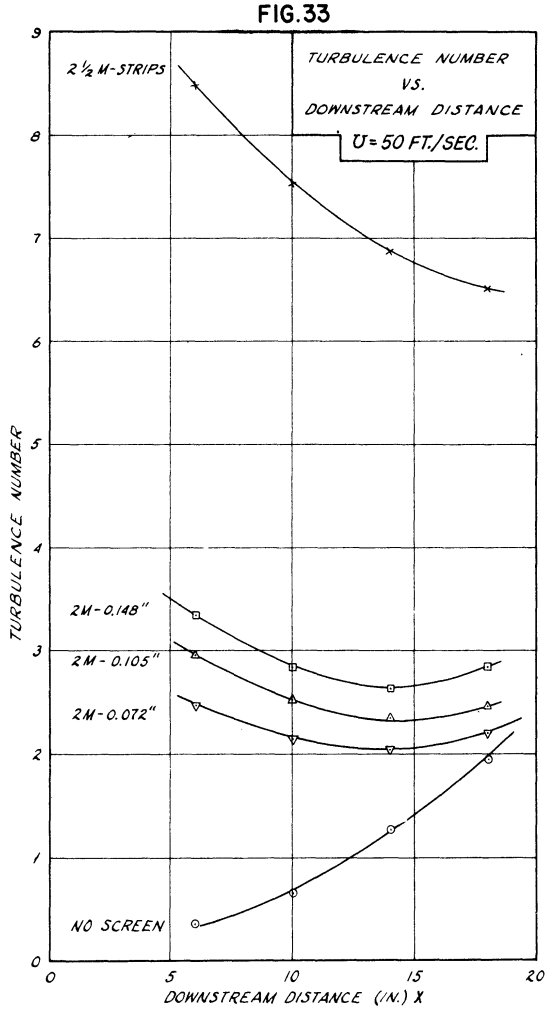

The data of Fig. 33 show that σ is not a monotonic decreasing function of downstream distance as the isotropic theory requires, except for the field of highest intensity. The theory further indicates that $1/\sigma^2$ should increase linearly with distance from the screen. Fig. 34 shows $1/\sigma^2$ vs x for the four fields of highest intensity. As can be seen, the linear relationship does not exist for any of the fields, although that of highest intensity follows the law approximately.

FIG. 34

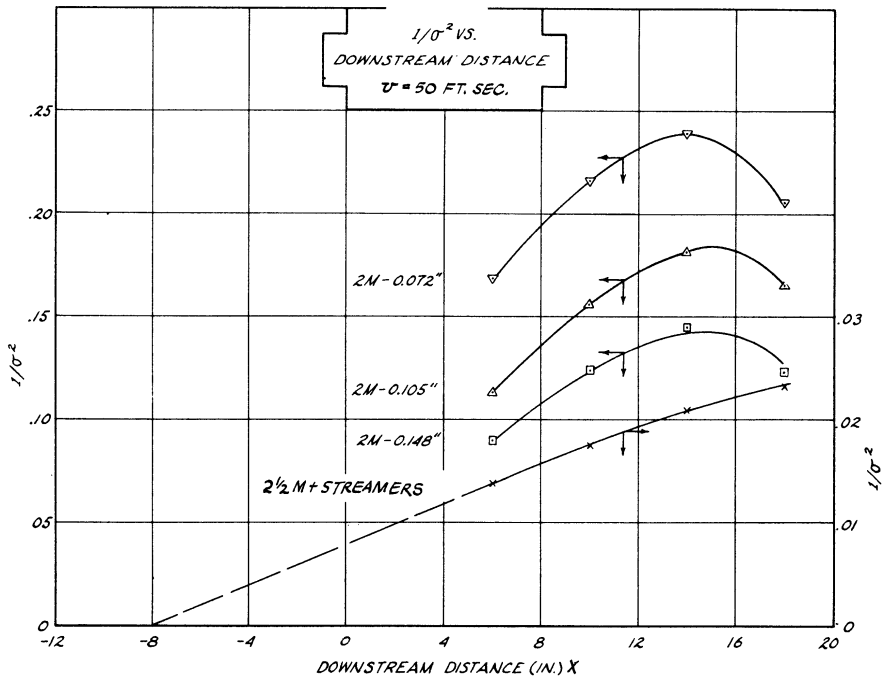

If the isotropic and induced velocities are independent, the isotropic turbulence should follow the linear decay law. The mean square velocity $\overline{u}^2$ is given by

$$\overline{u}^2 = (\overline{u'+a})^2 = \overline{u}'^2 + 2\,\overline{au}' + a^2 ,$$

where u' and a are, respectively, the isotropic and induced velocity fluctuations. If u' and a are independent, $\overline{au}' = 0$, and the above equation reduces to

$$\overline{u}^2 = \overline{u}'^2 + \overline{a}^2 ;$$

$\overline{u}'^2$ may be found from the data for the higher turbulence levels by assuming $\overline{a}^2(x)$ to be an invariant for all the fields and equal to the residual turbulence level. Reciprocals of $\overline{u}'^2$ found in this way are plotted against x in Fig. 35. The decay was linear for the highest turbulence level, but not even approximately so for the others. Presumably the approximation of independence of a and u' is not correct at the lower turbulence levels, where they are of the same order of magnitude. The curve corresponding to the turbulent field of highest intensity is a straight line with intercept at x = -8 inches, which is the position of

the turbulence screen. The curves for the other fields were nonlinear, but could reasonably be extrapolated to x = -8 inches.

FIG. 35

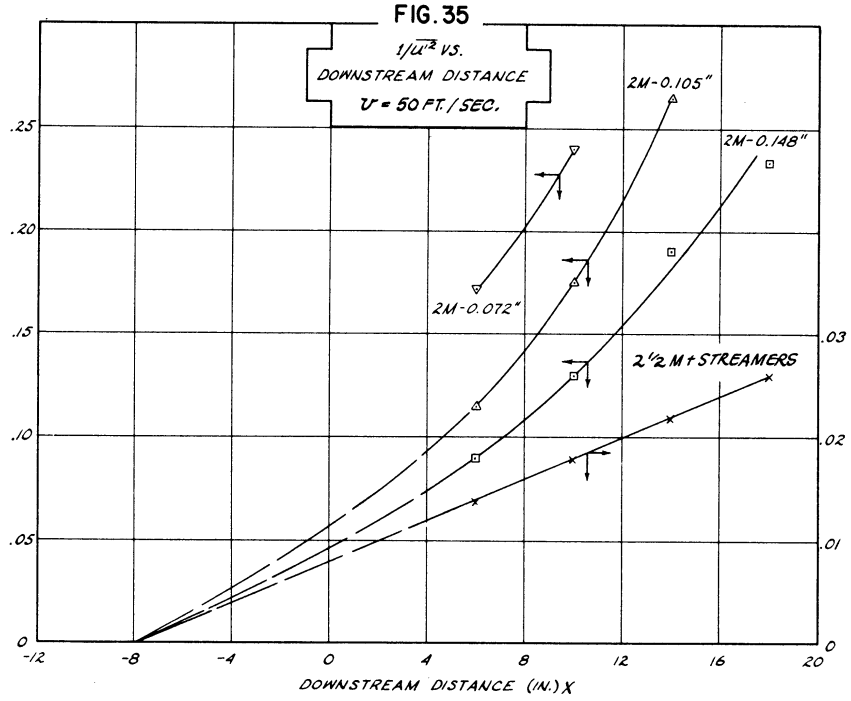

The cross-stream variation of σ for the no-screen condition and a stream velocity of 50 ft/sec is shown in Figs. 36 and 37 at points 6 inches and 18 inches downstream of the test-section entrance, with the nozzle strut

FIG. 36

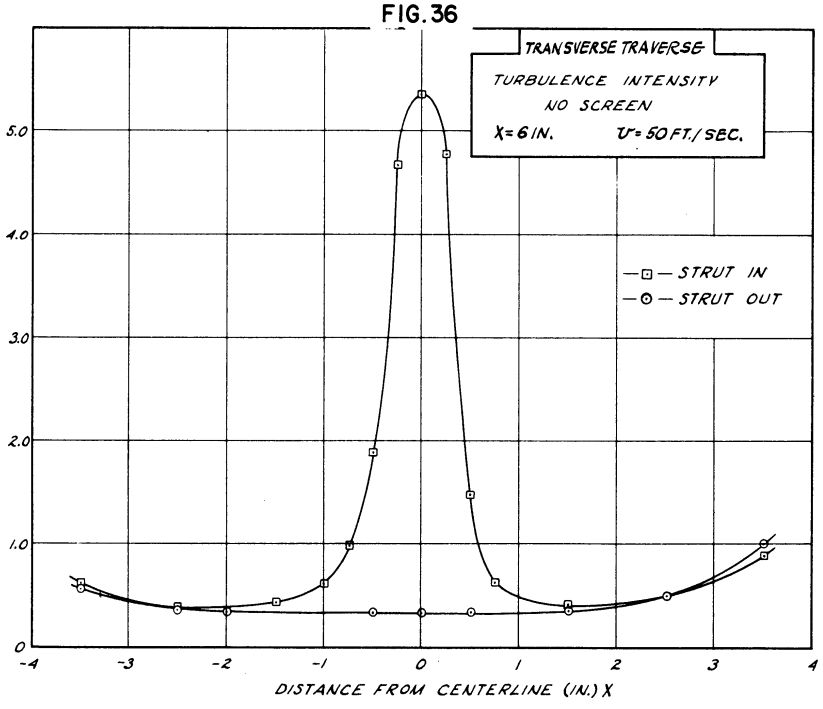

both in and out of the airstream. Fig. 38 is a similar plot for the intensity field at 12 inches with the 2-mesh screen of 0.105-inch rod diameter. The cross-stream data also show that σ increases toward the edge of the jet.

FIG. 37

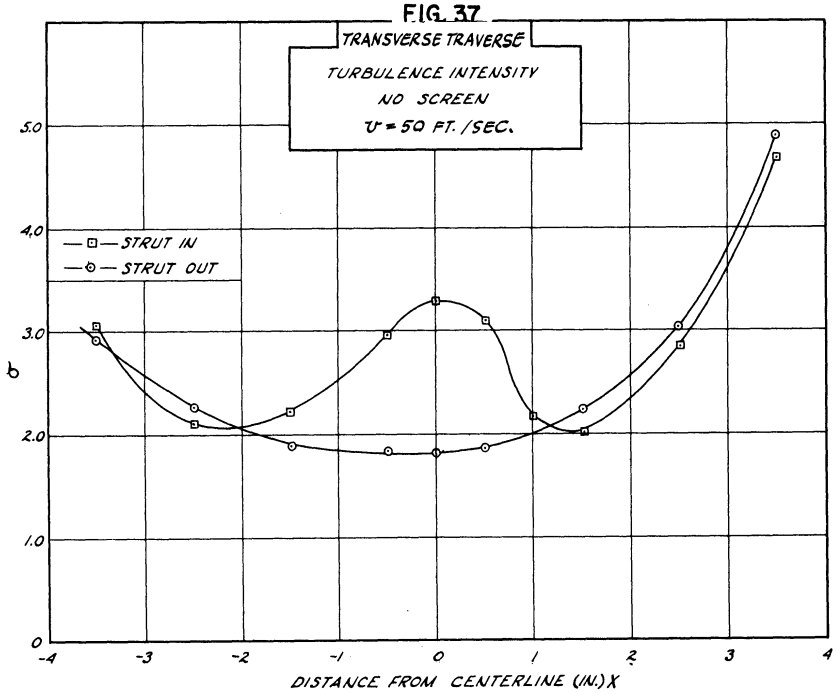

As can be seen from Figs. 36 and 37, the wake of the strut and nozzle body produces a region of higher turbulence along the centerline of the jet. It is also evident that the wake turbulence does not appreciably affect σ away from the centerline.

FIG. 38

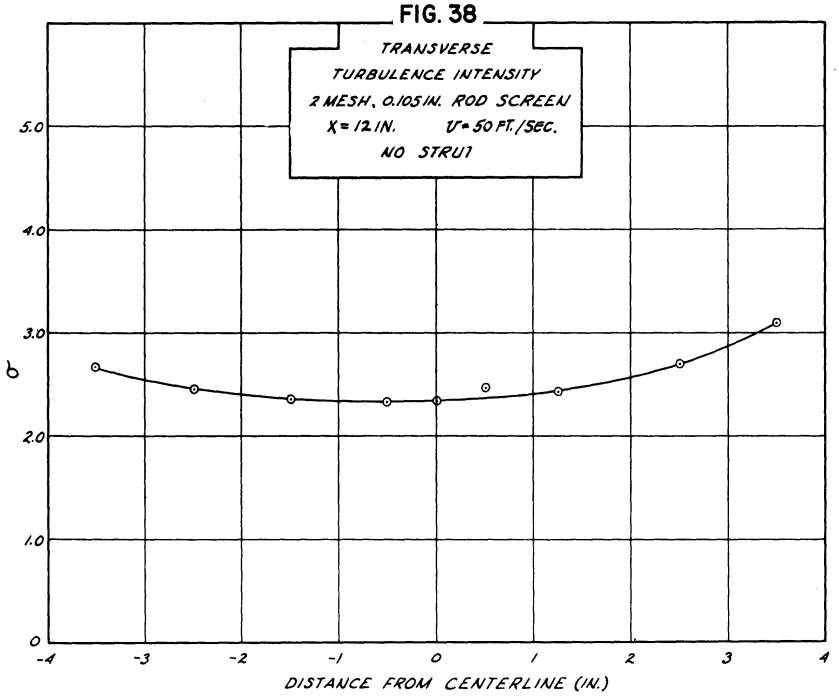

The centerline wake is produced by separation of the flow near the nozzle tip on the central body. To investigate the flow over the body under operating conditions, the body was coated with a lampblack-kerosene mixture. When the airstream was started, flow separation was indicated at a station about two-thirds of the length back from the nose. The spray was then started and the aspirator effect prevented the separation; the lampblack-kerosene solution streamed back along the body and mixed with the spray at the tip. It was therefore concluded that the turbulence measurements with the strut out were indicative of operating conditions.

In isotropic turbulence the correlation coefficient is asymptotic to zero, and the scale has a finite value which increases with downstream distance. Figs. 39 and 40 show the variation of the correlation curves with downstream distance for the residual field and that produced by the 2-mesh, 0.148-inch screen.

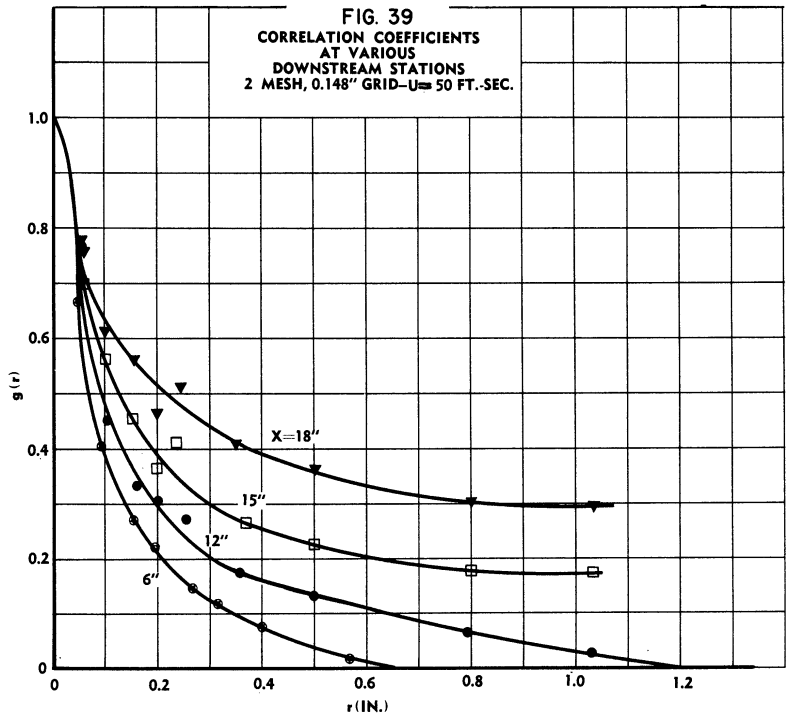

These data show that downstream of the entrance a station is reached where the correlation function is asymptotic, not to zero, but to some finite value. The scale, as defined by Eq 6.1, would be infinite at this station. Fig. 41 shows the variation of scale with downstream distance for the screens used in the present work. No values are plotted for downstream distances greater than 12 inches, as the scale rapidly approached infinity beyond this station. The correlation g(r) between the fluctuating velocities at points P_1 and P_2 is given by

$$g(r) = \frac{\overline{u_1 u_2}}{\overline{u_1}^2} = \frac{\overline{u_1' u_2'}}{\overline{u_1}^2} + \frac{\overline{a_1 a_2}}{\overline{u_1}^2} ,$$

where u_1 and u_2, and a_1 and a_2 are isotropic and induced components, respectively.

FIG. 40

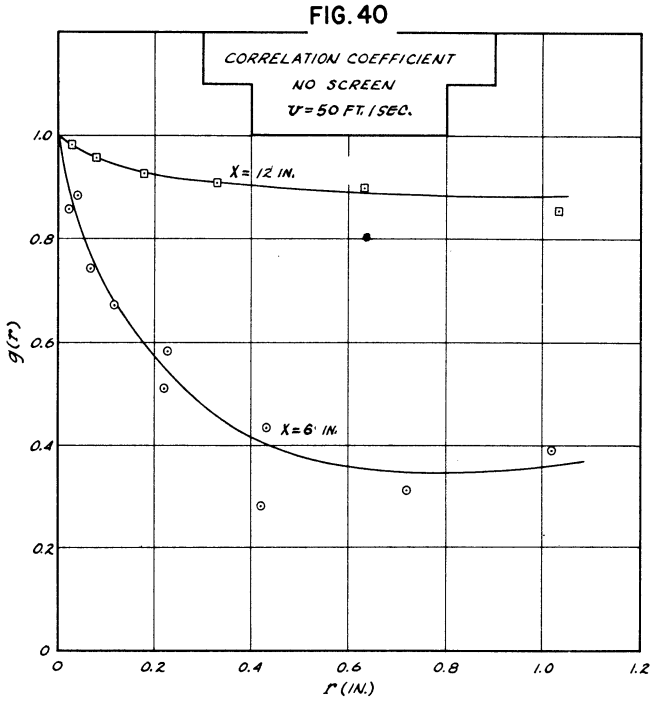

FIG. 41
VARIATION OF SCALE
WITH DOWNSTREAM DISTANCE
U=50 FT./SEC.

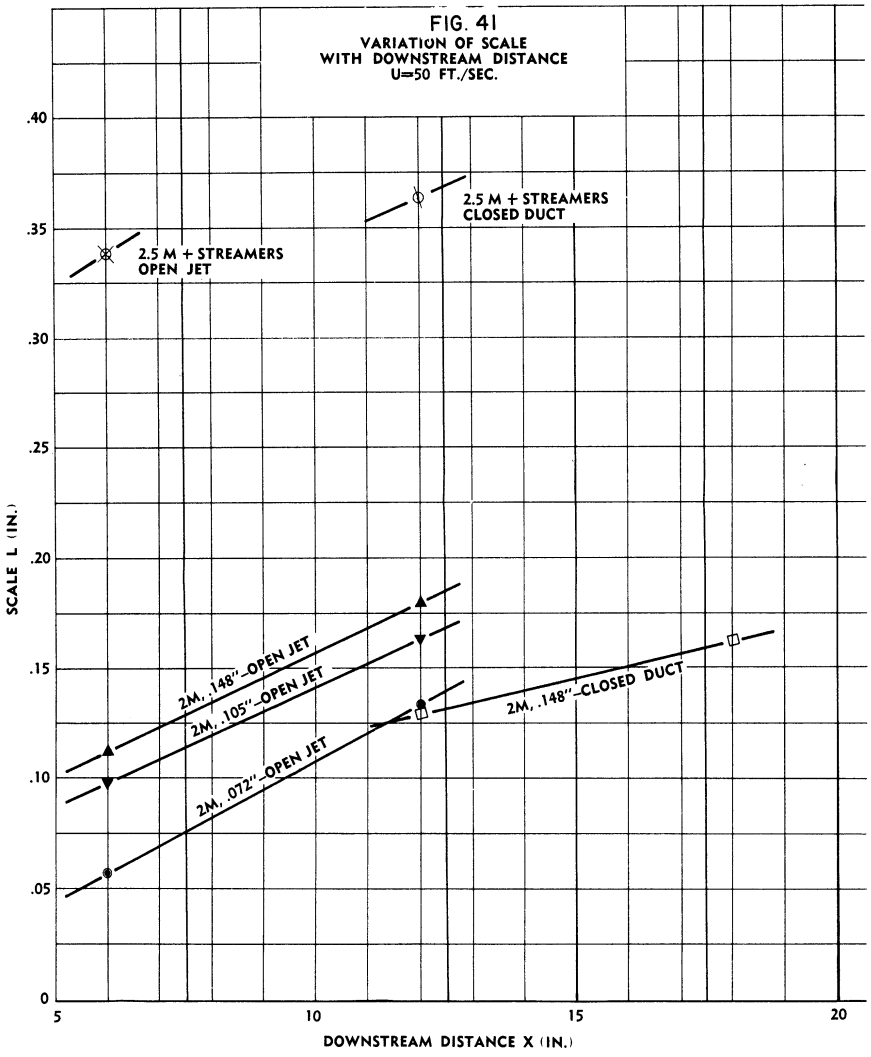

A major part of the fluctuation velocities a_1 and a_2 is probably produced by a random motion of the entire jet. Since the magnitude of the term $\overline{a_1 a_2}$ will be independent of the distance r between P_1 and P_2, g(r) will approach a constant

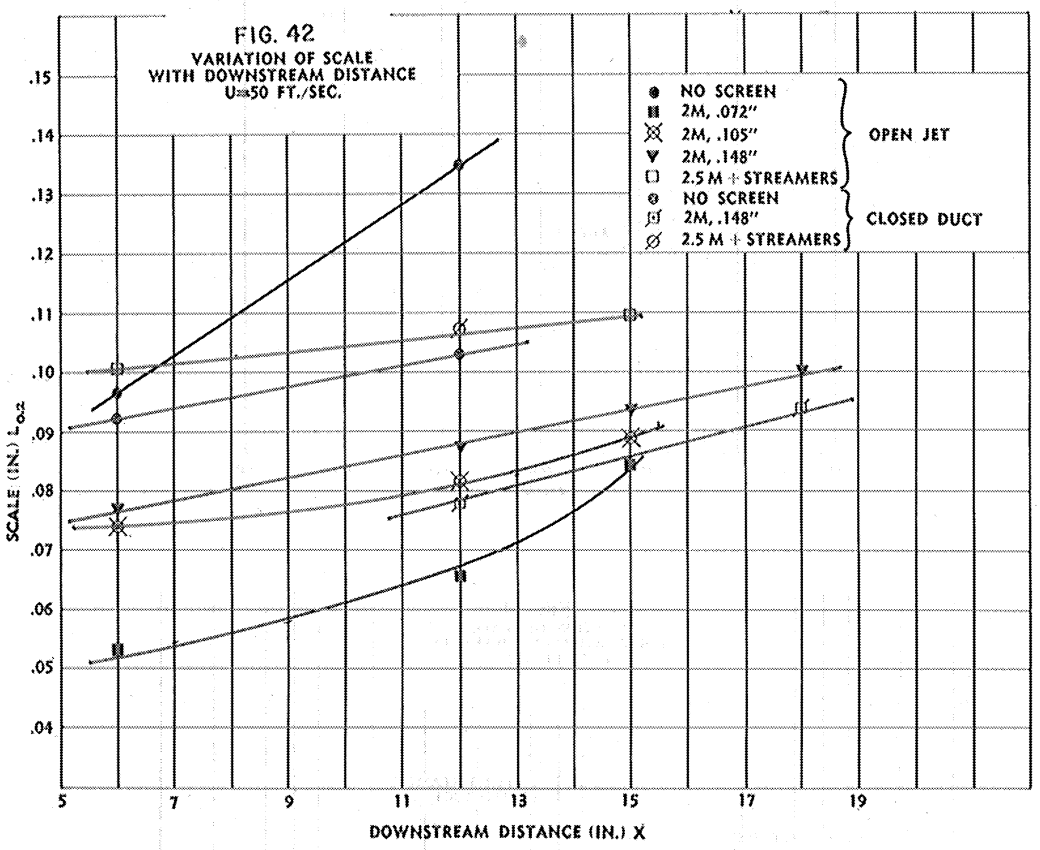

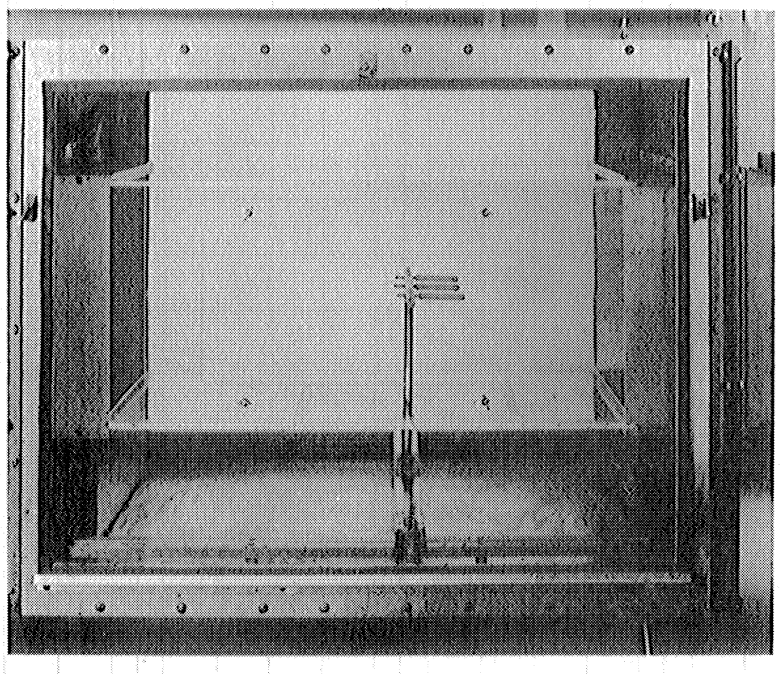

Fig. 43. Closed Duct Test Section with Collector Tubes

$\overline{a_1 a_2}/\overline{u_1}^2$ for large values of r. The scale as computed by Eq 6.1 will be infinite for this case. However, this difficulty can be overcome in an arbitrary fashion by integrating from zero to some finite value of r. For purposes of comparison, the upper limit was set equal to 0.2 inch, with resulting values of L, which are given in Fig. 42 (open jet curves).

The data designated "closed duct" in Figs. 41 and 42 were obtained in the closed section shown in Fig. 43. This section was constructed to avoid the turbulence induced in the main stream by the unsteady flow at the boundaries of the jet. The duct, made of plexiglas, was equipped with an access port on one side and slots on the bottom for introducing collector tubes and hot-wire probes. It may be seen from Fig. 44 that measurements of the decay of turbulence along the centerline show that the variation of $1/\sigma^2$ with x is much closer to linear than in the open jet. It is further noted that the magnitudes of corresponding values of σ are lower in the case of the straight duct. Evidently such a modification of the test section brings the turbulence closer to a state of isotropy, as indicated by the decay law.

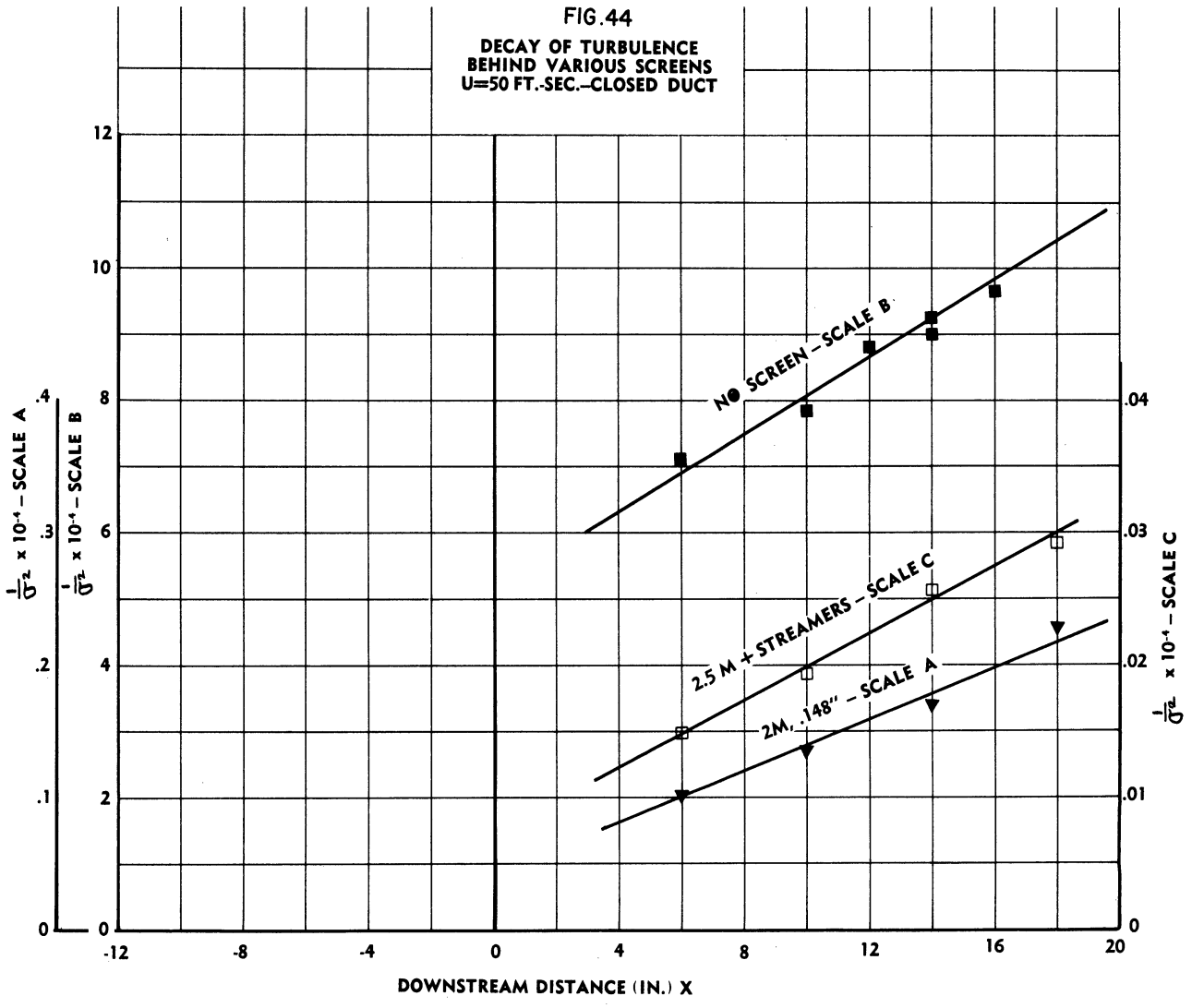

Scale measurements in the modified test section were carried out as before. Figs. 45, 46, and 47 give experimental curves of g(r) vs r for two screens and the no-screen condition. Reference to Fig. 39 shows that, under the same conditions in the open jet, g(r) approaches a positive value with increasing r for roughly x = 12 inches. The curves of Fig. 45, on the other hand, indicate that $g(r) \rightarrow 0$ as $r \rightarrow \infty$ for x = 18 inches. Regarding the no-screen condition, it is seen in Fig. 47 that the correlation curves do not go to zero, indicating that the turbulence is still not truly isotropic. Nevertheless, the curves tend to considerably smaller values of g(r) than do corresponding curves in Fig. 40. Values of

$$L = \int_0^{\infty} g(r)\, dr$$

are plotted for comparison in Fig. 41. When the integration is from r = 0 to r = 0.2 inch, the values of L are as shown in Fig. 42.

The cross-stream variation of velocity in the open test section is shown in Fig. 48 for the no-screen condition with the nozzle strut in place.

FIG.45
CORRELATION COEFFICIENTS
AT TWO DOWNSTREAM STATIONS
U=50 FT.-SEC.—2M, 148" SCREEN
CLOSED DUCT

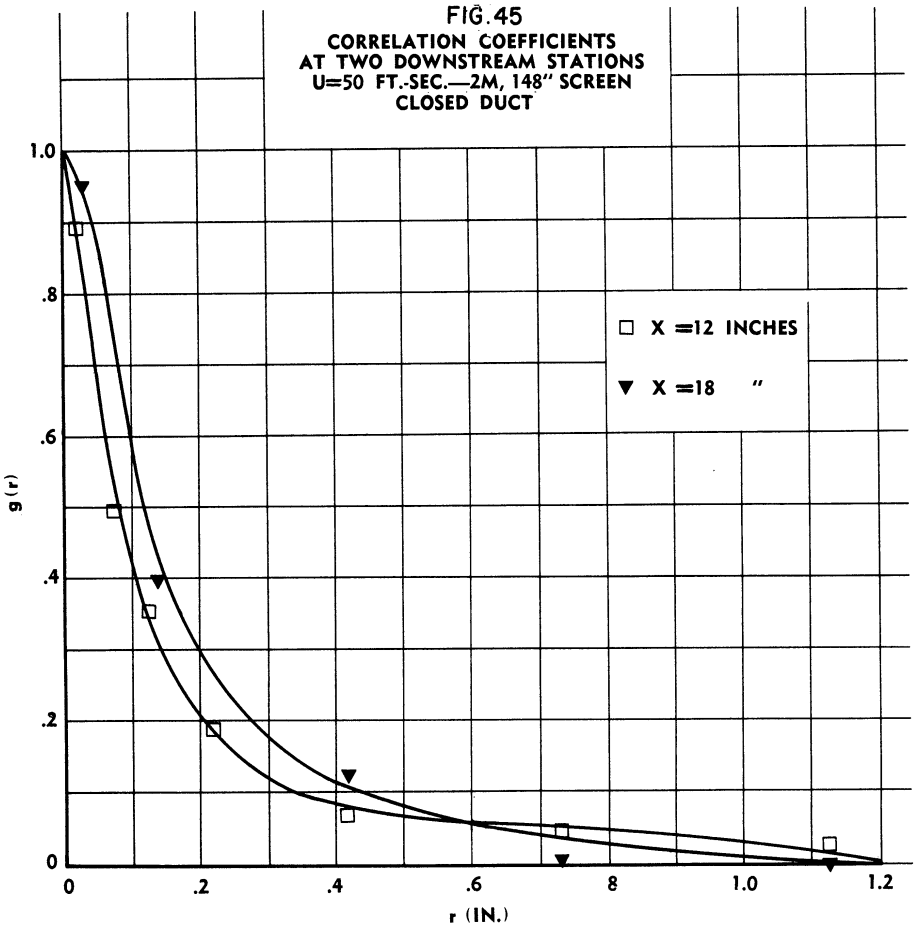

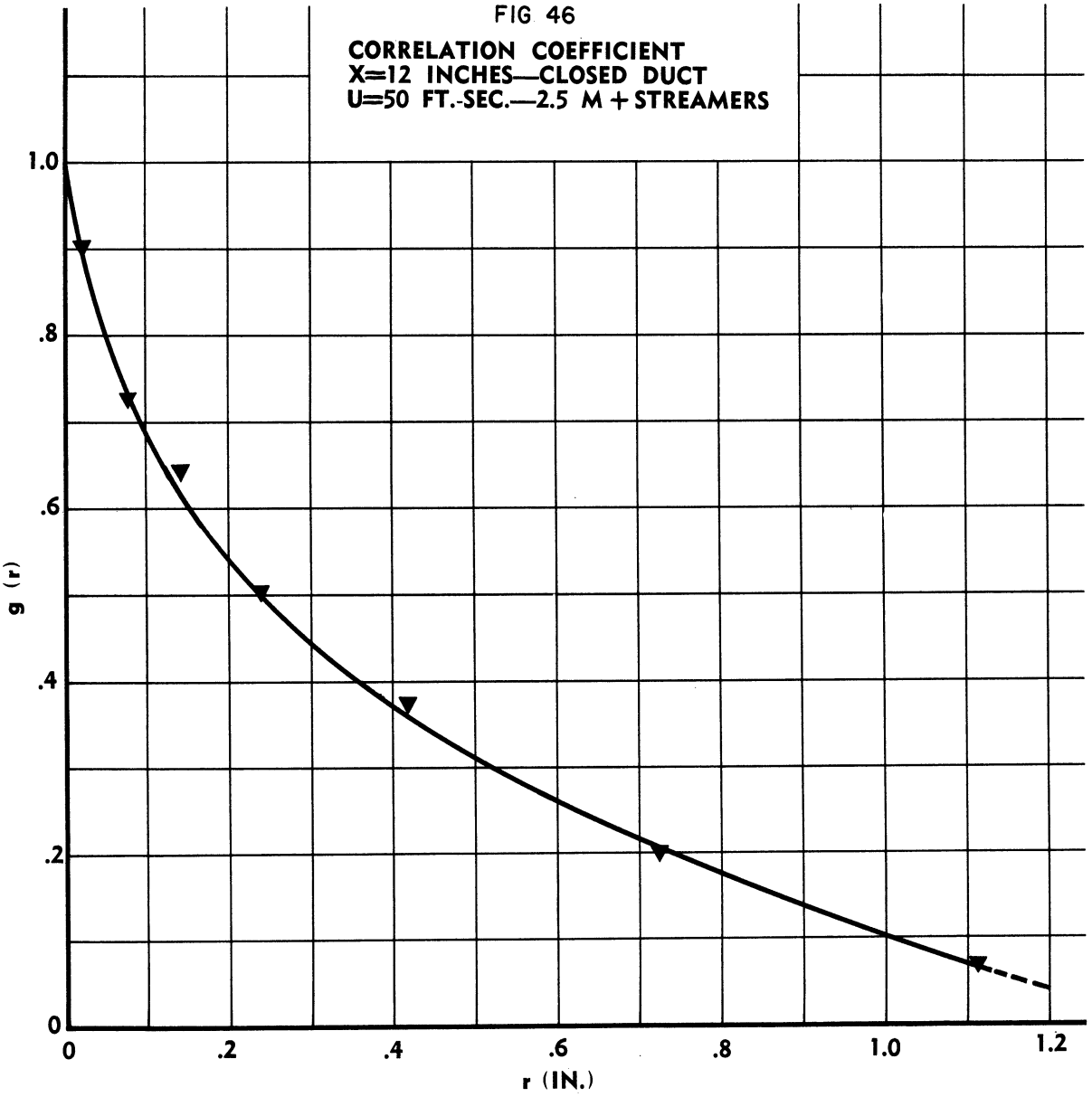

It can be seen that the velocity is uniform over the interval $-4.5 \leqq y \leqq 4.5$, except for a small change near the centerline caused by the strut. Since, as described earlier, the aspirator effect of the spray prevents flow separation on the central body, it probably also prevents the dip in velocity shown in Fig. 48 at the center of the stream.

6.3 Effect of Turbulence upon Evaporation of Spray

Section 6.2 described the characteristics of the five turbulence fields for which spray evaporation tests were run. The evaporation was found in terms of a parameter μ, which is defined as the ratio of spray mass evaporated upstream of the location of the probe to the mass initially injected into the airstream. Fig. 49 shows the variation of μ with downstream distance x for the five turbulence fields. The free airstream velocity U is 50 ft/sec; the temperature of the airstream is 20°C. Since σ varies with x (Fig. 33), it is not possible to assign a particular value of σ to each of

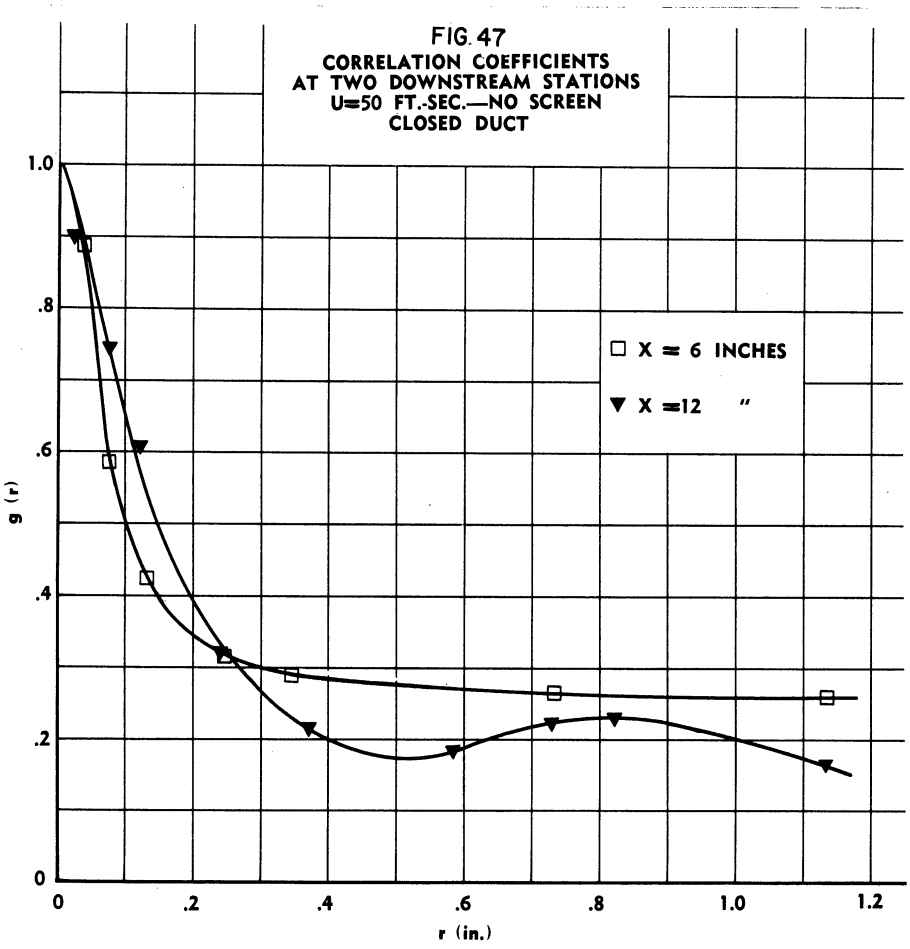
FIG. 47
CORRELATION COEFFICIENTS
AT TWO DOWNSTREAM STATIONS
U=50 FT.-SEC.—NO SCREEN
CLOSED DUCT
□ X = 6 INCHES
▼ X =12 "
g (r)
r (in.)
1.0
.8
.6
.4
.2
0
.2
.4
.6
.8
1.0
1.2

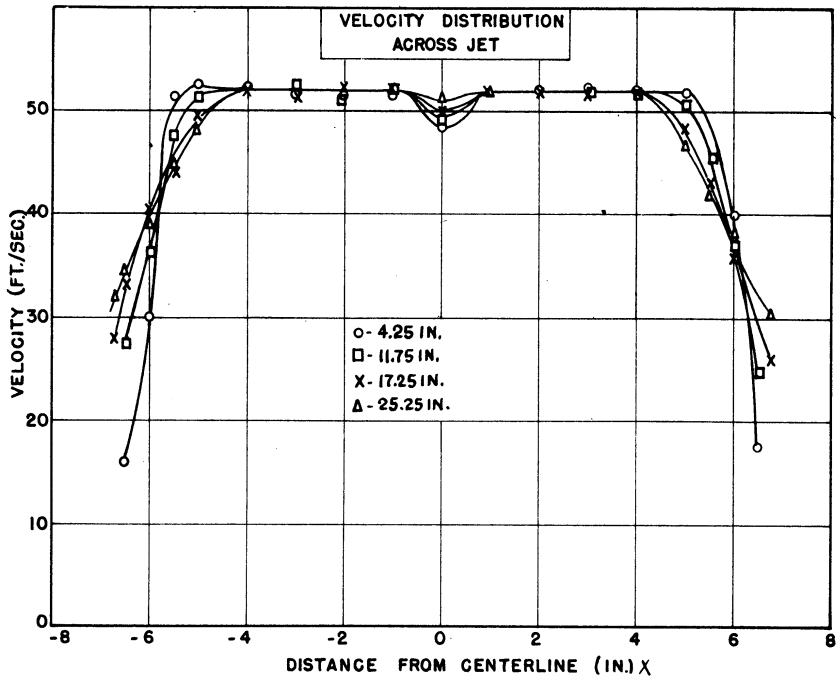
VELOCITY DISTRIBUTION
AGROSS JET
o- 4.25 IN.
□- 11.75 IN.
X- 17.25 IN.
Δ- 25.25 IN.
VELOCITY (FT./SEC.)
DISTANCE FROM CENTERLINE (IN.) X
50
40
30
20
10
0
-8
-6
-4
-2
0
2
4
6
8

Fig. 48

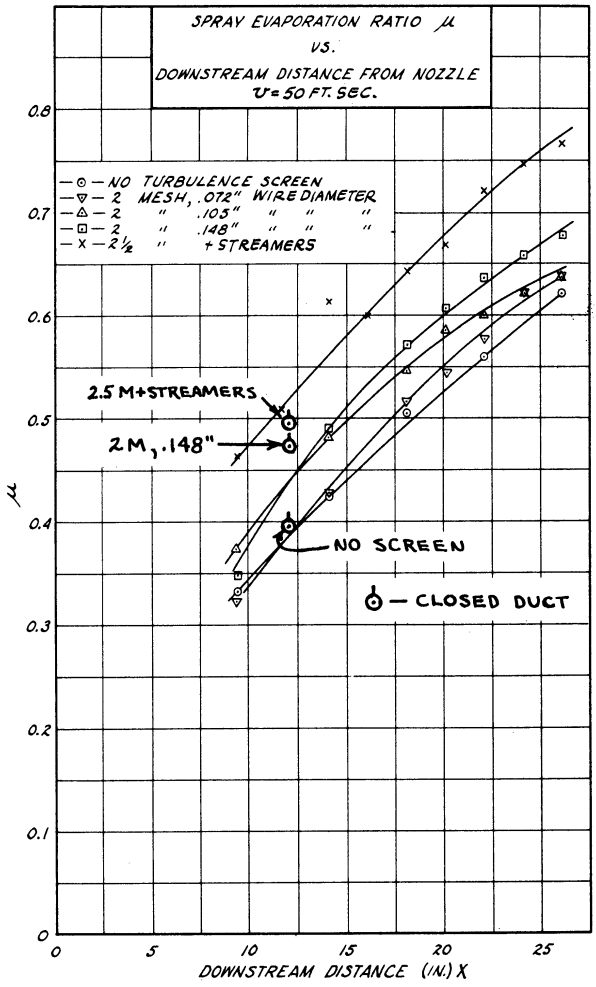

Fig. 49

the curves. The curves are therefore designated according to the device used to generate the turbulence. On this basis Fig. 49 shows that μ increases with increasing σ .

There is always evaporation out of the probe during a collection. The total mass actually collected by the probes is, of course, less than the mass which would have been collected in the absence of evaporation out of the probes. The method described in Section 3.2, by which the total collected mass is corrected for evaporation out of the probes, has been applied to all the data given in Fig. 49. Implicit in this correction is the assumption that cross-stream variations in turbulence number σ and mean velocity are of negligible effect, so that a single value of the correction factor α may be applied to the entire rack of collector tubes at any given station.

Spray collections in the closed duct were made at x = 12 inches for two screens (2-1/2 M + streamers and 2 M, .148) and the no-screen condition. The data points are designated by the symbol ⊙ in Fig. 49. These points indicate the same trend of increasing μ (i.e., increasing evaporation) with increasing σ as do the data for the open jet in Fig. 49. Table III summarizes the comparative data.

TABLE III

Screen	Tunnel Condition	$L_{0.2}$* (inch)	σ (per cent)	μ
2-1/2 M + Streamers	Closed Duct	0.107	6.67	0.496
	Open Jet	0.106	7.18	0.517
2 M, .148	Closed Duct	0.079	2.55	0.474
	Open Jet	0.087	2.71	0.437
None	Closed Duct	0.103	0.34	0.395
	Open Jet	0.135	0.94	0.385

(All data at x = 12 inches)

The data given in the table give some indication that a decrease in scale of the turbulence results in a greater rate of evaporation. However, the experimental scatter shown in Fig. 48 and the fact that the evaporation is an integrated value from the tip of the spray to the point of measurement makes such a conclusion hazardous.

Theoretically it is possible to check the collection data by the spray photography technique described in Section 4. However, a very large number of photographs would be required at cross-stream and downstream positions. Due to the limited data obtained by photographing the spray, it is possible to check the collection data only at x = 12 inches for σ = 7.2 and σ = 0.90 per cent. Under the assumption that N, the total number of drops, remains constant, the total mass varies as the cube of $\bar{\delta}$, the mean drop diameter. Then the masses stand in the ratio

$$\frac{(M)_{\sigma=7.2}}{(M)_{\sigma=.90}} = \frac{(\bar{\delta})^3_{\sigma=7.2}}{(\bar{\delta})^3_{\sigma=.90}} = 0.87 \ ,$$

where $(\bar{\delta})_{\sigma=7.2}$ and $(\bar{\delta})_{\sigma=.90}$ are the values of mean drop size determined from the photographs. Since

$$1 - \mu \equiv 1 - \frac{M_e}{M_o} = \frac{M}{M_o} \ ,$$

where M_o is the initial mass and M_e is the mass evaporated, the mass ratio can

* $L_{0.2} \equiv \int_0^{0.2} g(r)\, dr$.

be found from the values of μ by the relation

$$\frac{(M)_{\sigma=7.2}}{(M)_{\sigma=.90}} = \frac{1 - (\mu)_{\sigma=7.2}}{1 - (\mu)_{\sigma=.90}} \quad . \tag{6.8}$$

The values $(\mu)_{\sigma=7.2} = 0.515$ and $(\mu)_{\sigma=.90} = 0.384$ may be read from the experimental curves in Fig. 49. Substitution into Eq 6.8 gives

$$\frac{(M)_{\sigma=7.2}}{(M)_{\sigma=.90}} = 0.79 \quad .$$

The agreement between this value and 0.87, the value obtained from the photographic method, is fairly good considering the assumptions involved in their direct comparison and the rather limited number of drops photographed.

6.4 Effect of Relative Velocity on Evaporation of Spray

In Section 5.4 an attempt was made to apply Frössling's equation, 5.21, for a single drop to the evaporation of an entire spray, leading to Eq 5.32 under the assumption of a Nukiyama-Tanasawa size distribution. Before Eq 5.32 is applied to the experimental data, the assumptions underlying this equation will be examined for the case of n-hexane, the particular liquid fuel used in the present tests.

a) Drop Temperature. -- Perhaps the most important assumption is that involved in writing

$$A' \cong \frac{2\pi D\hat{M}p}{RT} = \text{constant} \quad , \tag{6.9}$$

where D is the diffusion coefficient for hexane diffusing into air, $\hat{M}$ is the molecular weight of hexane, while p, R, and T denote, respectively, vapor pressure, gas constant, and absolute temperature of the saturated vapor-air mixture at the surface of the drop. A' is a strong function of T through the quantities D and p, which are functions of temperature. In particular, p increases very rapidly with increasing T.[57] The process of forced convection of mass leads to a boundary layer of mass transfer as well as thermal and velocity boundary layers. Since D is a function of temperature, there is some question as to the temperature at which D should be evaluated. In the present instance, the value of D used is that at the surface temperature, since in any case the variation of D is not important compared with the change in p.

A drop of hexane when first formed will be at the bulk liquid temperature, which in this case is the same as the airstream temperature T_a. As soon as the drop has formed, it will begin to evaporate, and its temperature will fall

at a rate which, as the rough calculation below will show, is extremely high. The drop temperature can fall as low as T_w, the dewpoint with respect to the hexane content, after which it will remain at T_w. When $T = T_w$, the quantities D, p, R, and T are all constant, and therefore Eq 6.9 is established. Consequently, the question to be answered now is this: What time is required to reach the temperature T_w after the spray leaves the nozzle? To answer this it is necessary to set up an equation for the instantaneous transfer of heat to a representative drop. Such a formulation applied to an entire spray can at best be only approximate. Nonetheless the results of calculations to be discussed below indicate that the method is adequate for the problem at hand.

The usual manner of handling mass- and heat-transfer problems is through appropriate coefficients based on the area of the surface involved in the transfer. Accordingly, the equation relating the instantaneous rates of heat transfer is

$$k_g(p - p_a)\hat{M}A\lambda = h_g(T_a - T)A + C_p\left(\frac{dT}{dt}\right)m \quad , \tag{6.10}$$

where the symbols are defined as follows:

k_g = mass-transfer coefficient, lb moles/(hr)(ft^2)(atm)

h_g = heat-transfer coefficient, Btu/(hr)(ft^2)(°R)

A = area of drop surface, ft^2

p = vapor pressure of hexane at surface of drop, atm

p_a = vapor pressure of hexane in free airstream, atm

λ = latent heat of vaporization of hexane, Btu/lb

T_a = temperature of free airstream, °R

T = temperature of surface of drop, °R

C_p = specific heat of liquid hexane, Btu/(lb)(°R)

m = mass of drop, lb moles

$\hat{M}$ = molecular weight of pure vapor (i.e., hexane), lbs .

The physical interpretation of the terms of Eq 6.10 is the following: The left-hand term is the rate of transport of heat away from the drop by evaporation; the first term on the right is the rate of transfer of heat from the air to the drop, since $T \neq T_a$; the second term on the right is the rate of change of heat content of the drop due to the unbalance of the other two terms. Since for the present experiment p_a is never more than 1 or 2 per cent of p, even if all the spray were evaporated, it is safe to drop p_a and write

$$k_g \hat{M} \lambda p = h_g(T_a - T) + C_p \left(\frac{dT}{dt}\right) \frac{\rho_L \bar{\delta}}{6} , \qquad (6.11)$$

where both sides of Eq 6.10 have been divided by A. When the steady state has been reached, dT/dt = 0, and Eq 6.11 reduces to

$$k_g \hat{M} \lambda p_w = h_g(T_a - T_w) , \qquad (6.12)$$

which is the standard formula for the wet-bulb temperature T_w at equilibrium.

When a drop first begins to evaporate and cool, $T = T_a$. This fact furnishes the starting point for the numerical integration of Eq 6.11. Thus

$$\left(\frac{dT}{dt}\right)_{t=0} = \frac{6\, k_g\, \hat{M}\, \lambda\, p}{C_p\, \rho_L\, \bar{\delta}} \qquad (6.13)$$

Choosing small increments of time Δt and starting with the initial rate given by Eq 6.13, Eq 6.11 can be integrated by an approximate step-by-step procedure to give drop temperature T as a function of time.

The wet-bulb temperature T_w was calculated from Eq 6.12 by trial and error. A value of $T_w < T_a$ was guessed, the corresponding p_w was calculated from an empirical equation[57] relating T and p, and the pair of values was checked for compatibility in Eq 6.12. The quantity $h_g/k_g\hat{M}\lambda$ is approximately a constant for a given system according to Perry[58], and may be calculated from the relation

$$\frac{h_g}{k_g \hat{M} \lambda} = C_p \left(\frac{\mu/\rho D}{C_p \mu / k_q}\right)^{2/3} \cdot \frac{\hat{M}_a P}{\hat{M} \lambda}$$

$$= C_p \left(\frac{Sc}{Pr}\right)^{2/3} \cdot \frac{\hat{M}_a P}{\hat{M} \lambda} , \qquad (6.14)$$

where $\hat{M}_a$ = molecular weight of air, P = total pressure, and k_q = thermal conductivity of the hexane-air mixture = k_q for air. All the quantities on the right-hand side of Eq 6.14 are either known from experiment or calculable from semi-empirical formulas.[58] The value thus found was T_w = 25.0°F for T_a = 68°F, or a depression of $(T_a - T_w)$ = 43.0°F.

An experimental check on T_w was made in the following manner. Wet- and dry-bulb thermometers were situated in the closed-duct test section in such a fashion that the wick of the wet bulb passed through the bottom of the duct into a bottle of hexane. To insure saturation of the wick surrounding the bulb, a medicine dropper was used to apply additional hexane just before a measurement was to be made. The tunnel was run at U = 50 ft/sec, and the wet-bulb reading taken at its lowest value. As an average of several measurements, it was found

that T_w = 31.1°F for T_a = 73.3°F, or (T_a-T_w) = 42.2°F. Hence the calculated and measured wet-bulb depressions are in good agreement.

The determination of k_g and h_g merits some comment. In Eq 6.12, only the ratio k_g/h_g is needed, and it can be calculated from Eq 6.14. The integration of Eq 6.11, on the other hand, requires that both k_g and h_g be known. Hence one or the other of these coefficients must be determined separately. The methods employed below are those discussed by Perry.[58]

Method 1. -- Frössling's equation, 5.21, may be written in terms of the mass-transfer coefficient k_g as

$$\frac{k_g R T \bar{\delta}}{D} = 2\left[1 + 0.276\ (Sc)^{1/3}(Re)^{1/2}\right], \qquad (6.15)$$

which may be used to calculate k_g. No measured values of D for a hexane-air system could be found in the literature, so the method given by Perry[58] was used to calculate D = 0.259 ft^2/hr. The Schmidt number $Sc \cong \nu/D$ was found using this value of D and ν for air. T was taken as T_a = 68°F. $\bar{\delta}$ was found from the collection curves of μ vs x by the use of Eq 3.18. The value for pure air, R = 0.729 (atm)(ft^3)/(lb mole)(°R), was used. To determine Re, it was necessary to know the initial velocity of the spray. While no really satisfactory method was found for this purpose, an approximate value was found by measuring the sheath thickness of the spray as close as possible to the nozzle (i.e., at x = 0.5 in.). Two procedures were used. In the first, the thickness of the sheath was measured roughly with a sharp-edged ruler placed normal to the conical surface. The interior of the spray cone was laid open to view through the wake of a slender rod or wire inserted opposite the ruler, the entire cone being strongly illuminated from the side. Using the measured thickness of 0.044 in. and the known mass flow, the velocity tangential to the sheath turns out to be 10 in./sec. The x-component of this velocity is about 8 in./sec, since photographs show that the spray has a half-angle of 30°. The second procedure made use of a strain-gauge spray analyzer devised by Dodge and Hagerty[26] and Elabd[59], which showed that, at x = 0.5 in., the velocity varied around the periphery of the spray from a minimum of 1.2 ft/sec to a maximum of 2.0 ft/sec. Both procedures assume that at this relatively small distance from the nozzle the conical sheath is still largely in an unatomized state. With the initial spray velocity known, Re becomes known, and it is possible to calculate k_g from Eq 6.15. The resulting value is k_g = 18.7 (lb moles)/(hr)(ft^2)(atm). From Eq 6.14 the corresponding value of h_g is 2.72 (Btu)/(hr)(ft^2)(°R).

Method 2. -- Perry[58] points out that Eq 6.15, applied to a single drop, will correctly represent heat-transfer data if $k_g R T \bar{\delta}/D$ is replaced by the Nusselt number $Nu \equiv h_g \bar{\delta}/k_q$, and Sc is replaced by the Prandtl number $Pr \equiv \mu C_p/k_q$ thus indicating the similarity of heat- and mass-transfer processes for spheres. The fact that similarity exists means that k_g can also be calculated from the h_g obtained by heat-transfer experiments with spheres. Curves quoted by McAdams lead to h_g = 230 (Btu)/(hr)(ft^2)(°R),[60] from which k_g = 15.8 (lb moles)/(hr)(ft^2)(atm). Kramers[61] gives the empirical equation,

$$Nu = 2.0 + 1.3(Pr)^{0.15} + 0.66(Pr)^{0.31}(Re)^{0.50} , \qquad (6.16)$$

for heat transfer from spheres to flows of air, water, and oil. Eq 6.16 gives, for air, $h_g = 349$ (Btu)/(hr)(ft^2)(°R), from which $k_g = 24.0$ (lb moles)/(hr)(ft^2)(atm).

The results of the foregoing calculations are summarized in Table IV.

TABLE IV

Method	k_g	h_g
1 (Frössling)	18.7	272
2 (McAdams)	15.8	230
(Kramers)	24.0	349

Integration of Eq 6.11 was carried out using the values of k_g and h_g found by Method 1, above. The resulting values of drop temperature as a function of x are shown in Fig. 50.*

There is clearly considerable variation among the above three sets of values for k_g, h_g. In spite of this, it seems evident that all three pairs would lead to essentially the same result when applied to Eqs 6.11 and 6.12. In other words, the drop temperature will most likely have become virtually constant at T_w before the drop has travelled as little as an inch from the nozzle. Therefore, the assumption of Eq 6.9 appears justified for $x \geq 9$ inches, the minimum distance for spray collection.

b) Use of Mean Drop Diameter. -- The reduction of Eq 5.32 to a form which is simple enough to check the limited data obtained from the present tests presents a major obstacle. Since there are neither data nor theory to tell how b and q vary with time, it is necessary to put Eq 5.32 into the form

$$-\frac{dM}{dt} = (\text{const.})\,\bar{\delta} + (\text{const.})\,u_r^{1/2}\,\bar{\delta}^{3/2} . \qquad (6.17)$$

This can, in fact, be done if it is true that

$$\frac{\Gamma(4/q)}{b^{1/q}\,\Gamma(3/q)} = C_o\,\bar{\delta} \qquad (6.18)$$

---

* During the very short time that the drop temperature is falling, the drop velocity is assumed constant at $u_d = 8.0$ in./sec, the initial drop velocity. Therefore, t and x are related by $t \cong x/u_d$.

and

$$\frac{\Gamma(9/2q)}{b^{3/2q}\Gamma(3/q)} = (C_o \bar{\delta})^{3/2} , \tag{6.19}$$

where C_o = constant. From Eq 6.19

$$\frac{1}{b^{1/q}} \left\{ \frac{\Gamma(9/2q)}{\Gamma(3/q)} \right\}^{2/3} = C_o \bar{\delta} . \tag{6.20}$$

Consequently, Eqs 6.18 and 6.20 lead to

$$\frac{\Gamma(4/q)}{\Gamma(3/q)} = \left\{ \frac{\Gamma(9/2q)}{\Gamma(3/q)} \right\}^{2/3} . \tag{6.21}$$

Eq 6.21 cannot be established for arbitrary values of q, but is approximately correct over a wide range of q, as can be seen from Fig. 51.

FIG. 50
THEORETICAL TEMPERATURE OF MEAN DROP VS. DISTANCE FROM NOZZLE

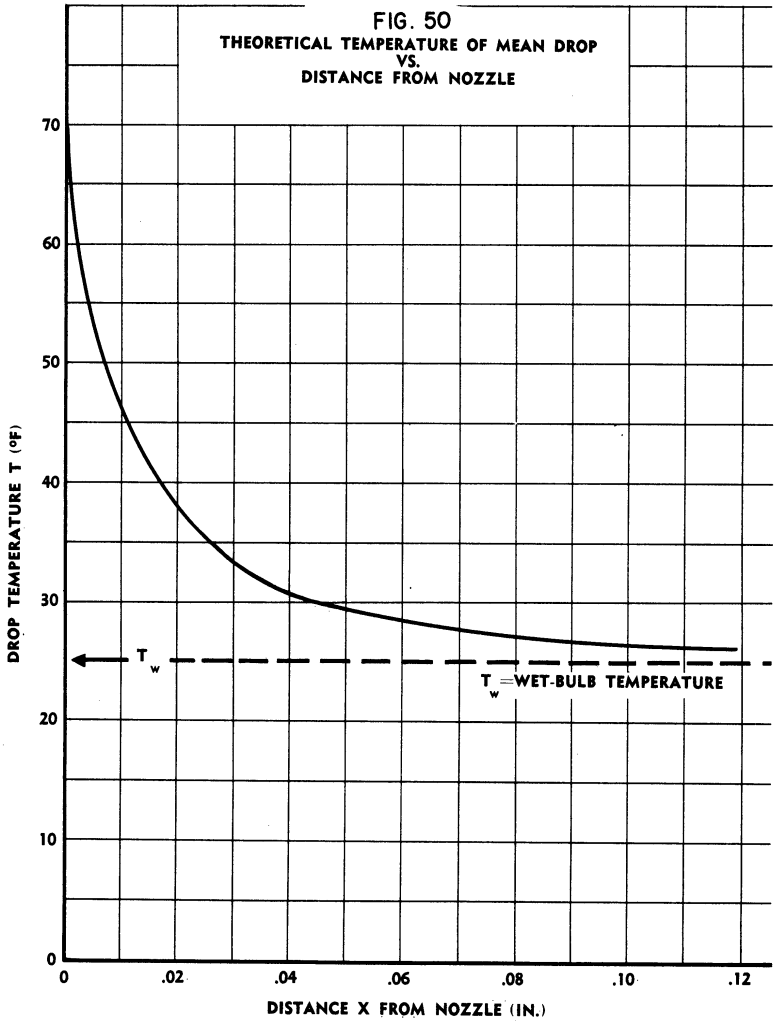

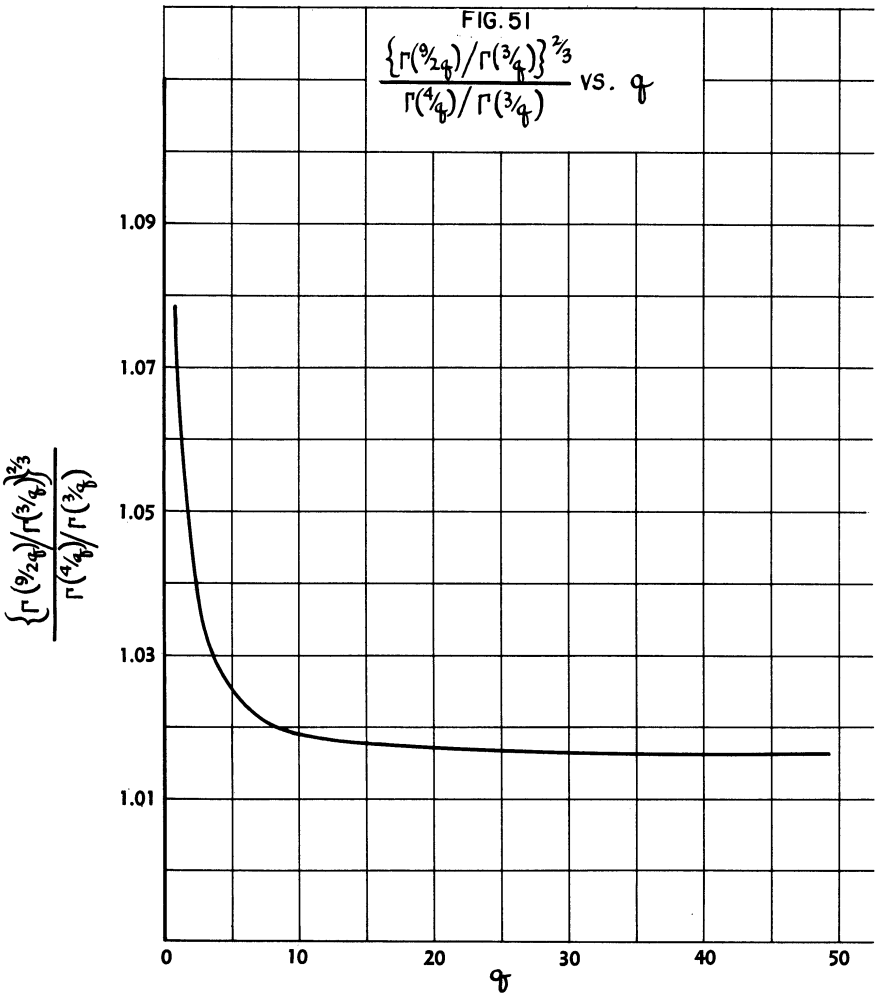

The method of determining q will be taken up at this point. In mass-fraction form the Rosin-Rammler distribution is given by $R = e^{-b\delta^q}$, from which

$$\log (\log 1/R) = \log (b/2.30) + q \log \delta \quad , \qquad (6.22)$$

where log is the base-10 logarithm. Eq 6.22 shows that plotting the data as log(log 1/R) vs logδ should give a straight line shose slope is q. This method was applied to the present data with the result that values of $q < 3$ were obtained. As Bevans[1] points out, the Rosin-Rammler distribution gives a mean diameter $\bar{\delta} = 0$ from Eq 1.5 for $q < 3$. The reason for this is that the Rosin-Rammler formula predicts an infinite number of infinitesimal drops when $q < 3$. This restriction does not apply to the Nukiyama-Tanasawa distribution, where q is found[1] by plotting $\log [(1/\delta^5)(dR/d\delta)]$ against δ^q and choosing q to give the best straight line through the points. This has been done using the two curves of R vs δ discussed in Section 4.3c, and resulting values of q are

$$q \cong 1.0 \quad \text{for} \quad \sigma = 7.2$$

$$q \cong 0.5 \quad \text{for} \quad \sigma = 0.90$$

When these values of q are substituted into Eq 6.21, it is found that

$$\frac{\Gamma(4/q)}{\Gamma(3/q)} = 3.0 \,, \qquad \left\{\frac{\Gamma(9/2q)}{\Gamma(3/q)}\right\}^{2/3} = 3.2 \qquad \text{for} \quad q = 1.0$$

$$\frac{\Gamma(4/q)}{\Gamma(3/q)} = 42 \,, \qquad \left\{\frac{\Gamma(9/2q)}{\Gamma(3/q)}\right\}^{2/3} = 48 \qquad \text{for} \quad q = 0.5$$

The most that can be drawn from the above considerations is that Eq 6.21 is approximately satisfied at the one point for which values of q are available. Therefore, it remains as a special assumption that Eq 6.17 or its equivalent from Eq 5.32,

$$-\frac{dM}{dt} = A'NC_o\bar{\delta} + C'NC_o u_r^{1/2}\bar{\delta}^{3/2} \,, \qquad (6.23)$$

is valid for other values of x in the test section. Making the substitutions $A \equiv A'NC_o$ = constant and $B \equiv C'NC_o$ = constant brings Eq 6.23 to the form

$$-\frac{dM}{dt} = A\bar{\delta} + B u_r^{1/2}\bar{\delta}^{3/2} \,, \qquad (6.24)$$

where $u_r^{1/2} = fn(t)$.

c) Mean Spray Velocity. -- A method of determining the initial spray velocity was described above (on p. 83). The rough value thus obtained is, of course, an average for the entire spray. More than this, it is of interest to know how the spray velocity u_d, and therefore $u_r = U - u_d$, varies with distance downstream from the nozzle. Preferably, this problem should be attacked by direct measurement of the velocities of individual drops, from which an "average" spray velocity might be deduced; but apparatus for such an approach was not available at the time the present data were taken. Frössling's equation seems at present to provide the only analytical way to approach the problem.

Let m denote the mass of the mean drop which is assumed to characterize the spray at any time, and let m_i be the initial mass of this drop when it is formed near the nozzle. Then, from the relations

$$\mu = \frac{m_i - m}{m_i} = 1 - \frac{m}{m_i}$$

$$\frac{d\mu}{dx} = -\frac{1}{m_i}\frac{dm}{dx}$$

$$\frac{dm}{dt} = \frac{dm}{dx}\frac{dx}{dt} = u_d\frac{dm}{dx}$$

it follows that

$$\frac{dm}{dt} = - m_i u_d \frac{d\mu}{dx} .$$

Hence, Frössling's equation for the mean drop may be rewritten:

$$m_i u_d \frac{d\mu}{dx} = \frac{2\pi D \hat{M}p}{R T} \left[1 + 0.276(Sc)^{1/3}(Re)^{1/2}\right] \bar{\delta} . \qquad (6.25)$$

By squaring both sides and noting that $Re = (U-u_d)\bar{\delta}/\nu$, Eq 6.25 can be written in the form

$$A_1 u_d^2 + B_1 u_d + C_1 = 0 , \qquad (6.26)$$

where

$$\left.\begin{aligned} A_1 &\equiv \frac{13.1}{(Sc)^{2/3}} \left[m_i \left(\frac{d\mu}{dx}\right) \frac{R T}{2\pi D \hat{M}p} \left(\frac{1}{\bar{\delta}}\right)\right]^2 , \\ B_1 &\equiv \frac{26.2}{(Sc)^{2/3}} \left[m_i \left(\frac{d\mu}{dx}\right) \frac{R T}{2\pi D \hat{M}p} \left(\frac{1}{\bar{\delta}}\right)\right] - \frac{\bar{\delta}}{\nu} , \end{aligned}\right\} \qquad (6.27)$$

and

$$\left.\begin{aligned} C_1 &\equiv \frac{13.1}{(Sc)^{2/3}} - \frac{U \bar{\delta}}{\nu} . \end{aligned}\right\}$$

$d\mu/dx$ can be found from the curves of Fig. 52, which give μ vs x for U = 50, 60, and 75 ft/sec. $\bar{\delta}$ and m_i can be calculated using the same curves, Eq 3.18, and the value of $\bar{\delta}$ measured photographically. Over the range of $9 \leq x \leq 26$ in. the quantities $(Sc)^{2/3}$, $RT/2\pi D\hat{M}p$, and ν are considered constant, as discussed above. Solving Eq 6.26 for u_d for the three cases U = 50, 60, and 75 ft/sec gave the results shown in Fig. 53.

d) Drag Coefficient. -- It appears, from a survey of the literature, that no theoretical or experimental study has been attempted of the drag force on a drop which is surrounded by a cloud of other drops, the entire system undergoing evaporation. Indeed, even the simpler case, where evaporation is absent, has only been treated for the Stokes-law range of $Re < 0.1$.[62]

The drag force $\mathcal{D}$ on a spherical drop is

$$\mathcal{D} = \frac{\rho_a}{2} C_D S_f (U - u_d)^2 , \qquad (6.28)$$

where ρ_a = density of air, C_D = drag coefficient of drop, and S_f = frontal area of drop. In terms of u_d, Eq 6.28 becomes

FIG. 52
EVAPORATION AS A FUNCTION OF DOWNSTREAM DISTANCE FOR VARIOUS VALUES OF U NO SCREEN

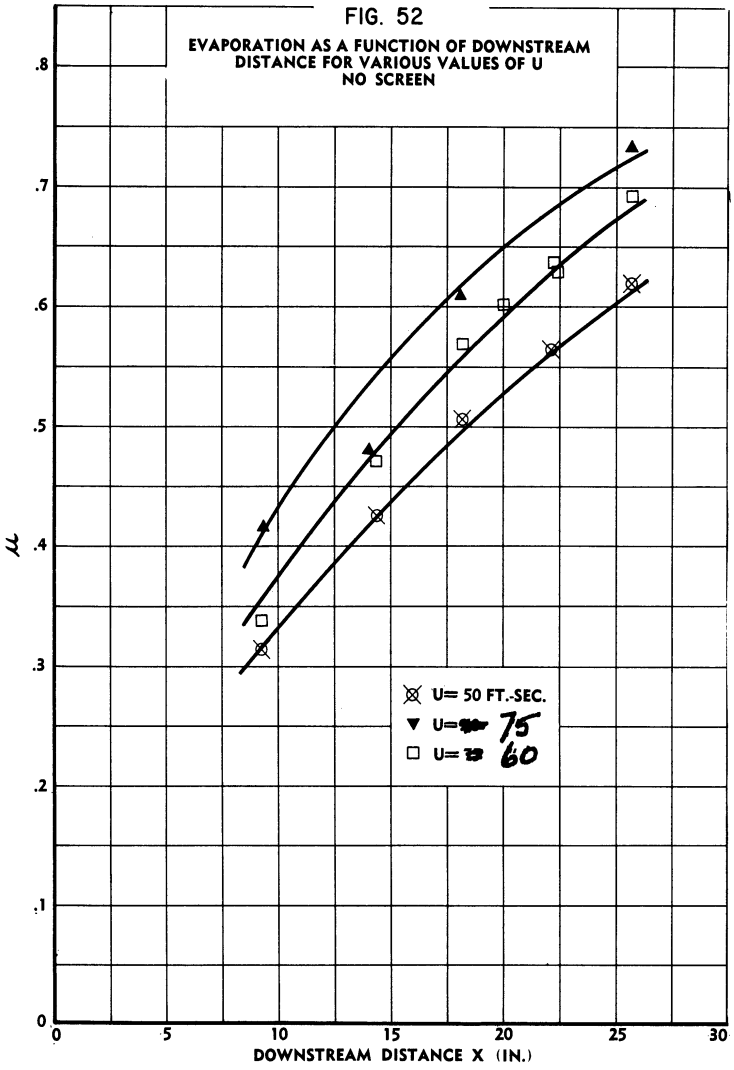

$$m \frac{du_d}{dt} = \frac{\rho_a}{2} C_D S_f (U - u_d)^2 \quad .$$

This last relation becomes

$$\frac{du_d}{dt} = 1.36 \times 10^{-3} \frac{C_D}{\bar{\delta}} (U - u_d)^2 \qquad (6.29)$$

when it is noted that $m = \rho_L \pi \bar{\delta}^3/6$, $S_f = \pi \bar{\delta}^2/4$, and $\rho_L = 42.4$ lbs/ft^3. The derivative $du_d/dt \cong u_d(\Delta u_d/\Delta x)$, so that from Eq 6.29

$$C_D \cong \frac{\bar{\delta} (\Delta u_d/\Delta x) u_d}{1.36 \times 10^{-3} (U - u_d)^2} \quad . \qquad (6.30)$$

Since $\bar{\delta}$ is known as a function of x, and u_d and $(\Delta u_d/\Delta x)$ can be obtained roughly from the curves of Fig. 51, it is possible to calculate the way in which C_D varies with x and Re. The results are given in Figs. 54 and 55.

FIG. 53

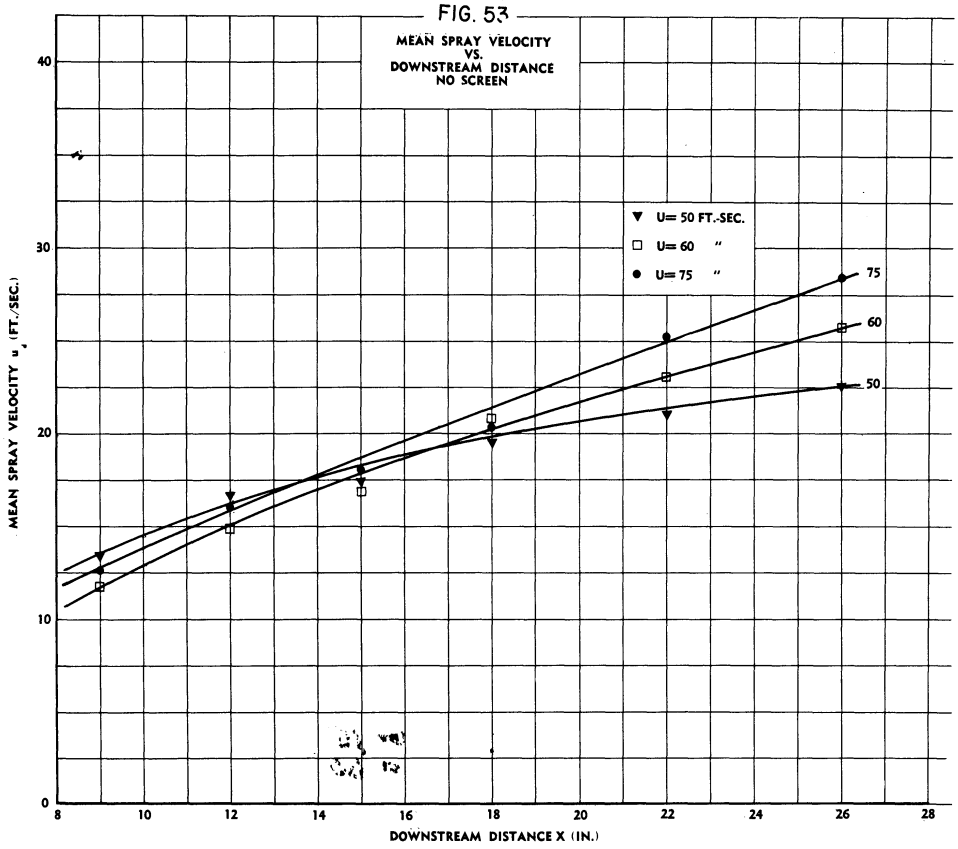

The curves of Fig. 55 would be expected to coincide if the Reynolds number were the only significant variable. The curves are in fact rather widely separated and, moreover, the magnitude of the indicated drag coefficients is quite low compared with drag measurements on solid spheres.[63]

These anomalies are not necessarily due to defects in the present theory. In fact, an evaporating drop may be compared roughly with a sphere through the surface of which a gas is flowing. Also, in this case the density and viscosity used in calculating the Reynolds number should probably correspond to some mixture of air and hexane at some temperature between the drop temperature and the air temperature. No suitable test values of C_D are available for this case.

The magnitude of the velocity v_n of the hexane vapor as it diffuses away along a normal to the drop surface can be calculated from the data obtained. At any instant the mass flow of hexane must satisfy the relation

$$-\frac{dm}{dt} = \rho_v v_n S = \rho_v v_n \pi \bar{\delta}^2 ,$$

from which

$$v_n = \frac{-dm/dt}{\pi \rho_v \bar{\delta}^2} .$$

Since $dm/dt = -m_1 u_d (d\mu/dx)$, the last equation can be written

FIG. 54
DRAG COEFFICIENT
vs.
DOWNSTREAM DISTANCE
NO SCREEN

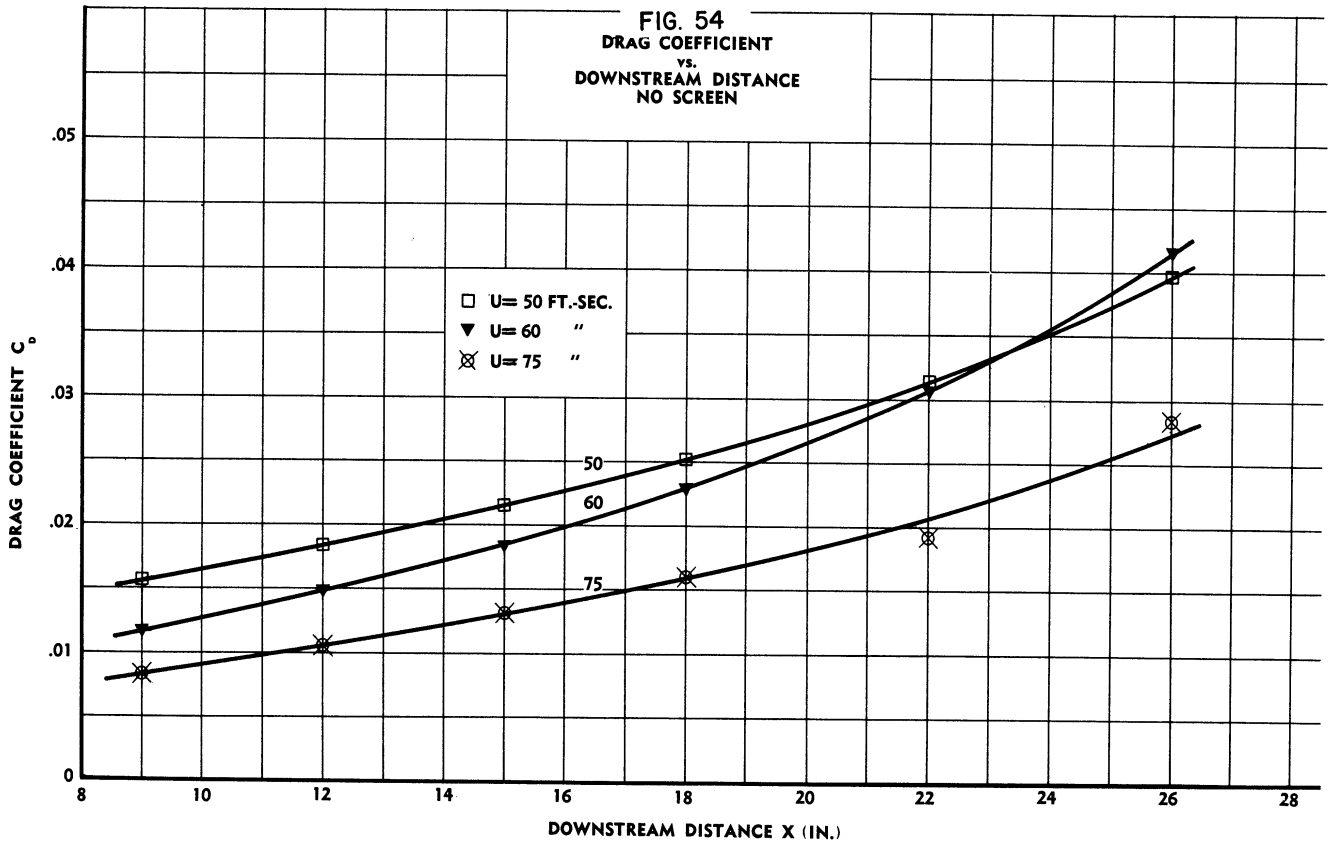

FIG. 55
DRAG COEFFICIENT
VS.
REYNOLDS NUMBER
NO SCREEN

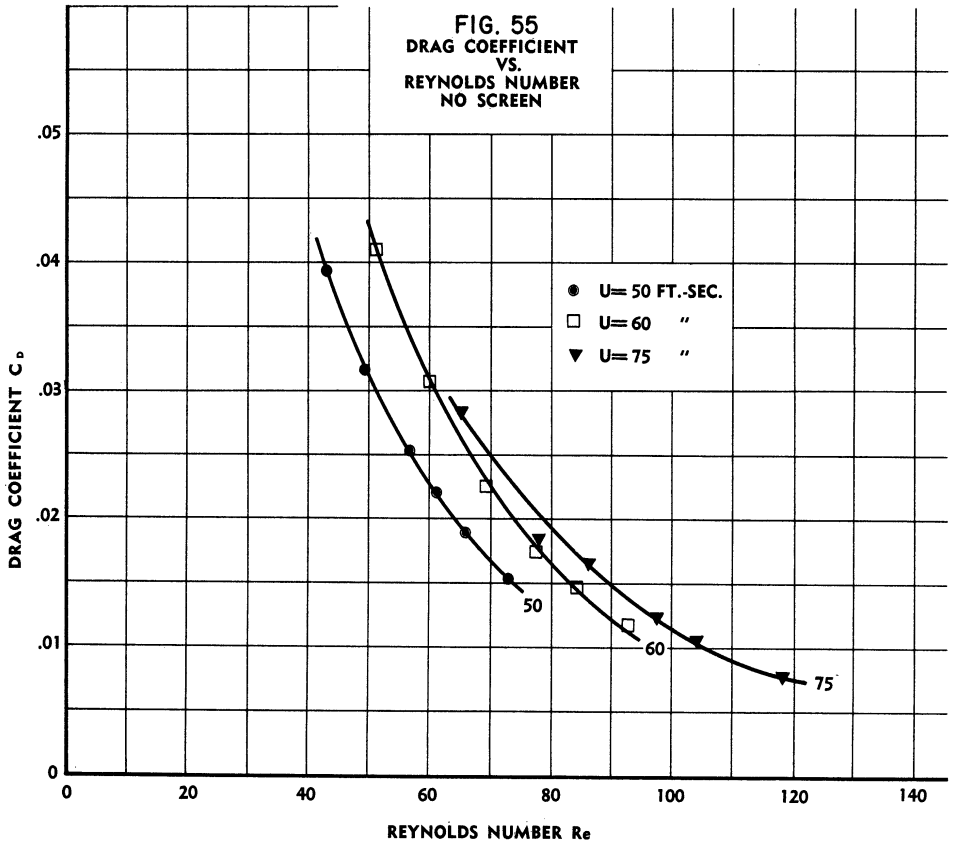

$$v_n = \frac{m_i u_d \, (d\mu/dx)}{\pi \rho_v \bar{\delta}^2} \qquad (6.31)$$

The vapor density ρ_v is calculated from the known temperature and vapor pressure by using the gas law. The other quantities are found as already discussed. For a typical case at x = 12 inches and U = 50 ft/sec, it is found from Eq 6.31 that v_n = 0.42 ft/sec. While the ratio v_n/U is only 0.008, the effect of v_n on a flow as complicated as that past a sphere could still be significant.

Finally, it should be recalled here that the application of Frössling's equation to the spray required the assumption that all the drops travelled with the same velocity, so that u_r could be treated as a constant in Eq 5.32. The fact that there exists a distribution of drop velocities in the spray[2] could modify the results considerably.

e) Effect of U on Spray Formation. -- There remains the question of what effect varying the stream velocity U has on the atomization process itself. In an effort to pick up any gross effects of wind speed, a series of photographs at various values of U was taken of the portion of the spray near the nozzle. Fig. 54 reproduces these pictures for U = 0, 25, 50, 75, and 87.5 ft/sec. The area covered by the individual photographs is 0.4 by 0.5 inch. There is no measurable difference in spray angle in pictures 1 to 5 of Fig. 56, though some narrowing of the spray with increasing wind speed is noticed farther downstream. Although the resolution is clearly inadequate to detect fine changes in the structure of the spray, there does not appear to be any gross effect of U. Pictures 1-5 of Fig. 56 show a wavelike formation on the surface of the spray sheath. Picture 6 illustrates the effect of removing the swirl insert.

FIG. 56

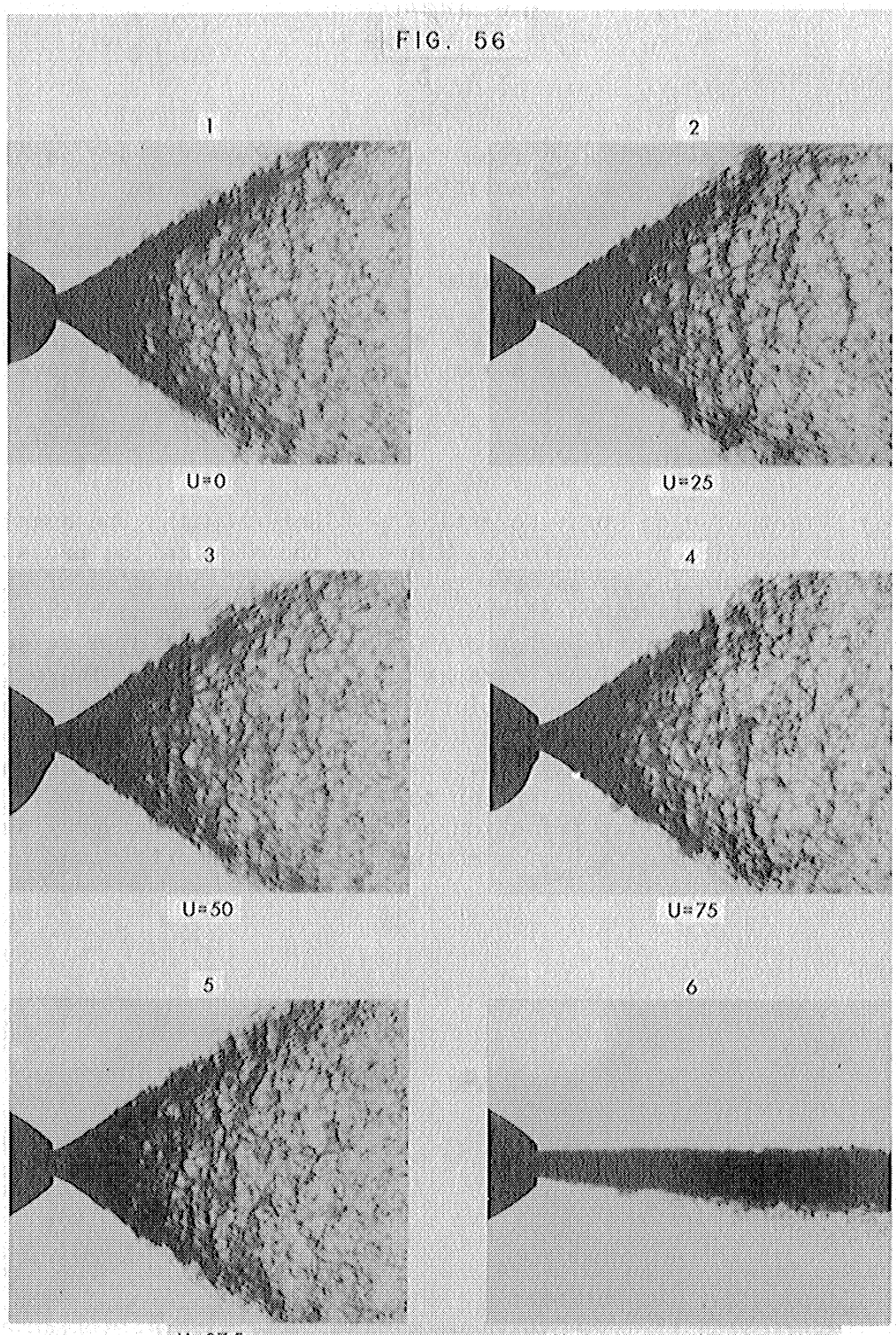

PHOTOGRAPHS OF SPRAY AND NOZZLE TIP
FOR VARIOUS AIRSTREAM VELOCITIES

7. CONCLUSIONS

7.1 Effect of Turbulence

It has been found from measurements of the total mass in the spray that an increase in turbulence intensity increases the evaporation rate of the spray. At a downstream distance of x = 18 inches, for example, 52 per cent of the injected mass will have evaporated when $(\sigma)_{avg}$ = 2.2 per cent, whereas 64 per cent will have evaporated when $(\sigma)_{avg}$ = 7.4 per cent.* This effect of turbulence does not appear to work through the Reynolds number but seems to be due rather to an increase in the coefficient of diffusion.

The results of tests with the closed duct in the test section do not give any conclusive information on the effect of scale of turbulence on the rate of evaporation. The reason for this deficiency lies in the fact that changes occurred in the turbulence intensity σ as well as in the scale L, and the two effects could not be separated. However, it can be said that the collection data in the closed duct indicate the same trend of increasing rate of evaporation with increasing σ as was found in the open-jet configuration.

Regarding its effect upon turbulence, the change from an open jet to a closed duct brought the flow closer to a state of true isotropy. This conclusion is based on measurements of the scale and of the decay of σ. In addition, the scale and σ are lower in the closed-duct arrangement.

It is assumed, in the derivation of the correction formula for evaporation out of the collector tube, that the temperature of the probe is the same during the two halves of a collection-evaporation test sequence. Actually, the tube temperature will rise slowly after the spray has been turned off. Hence the correction coefficient α, as determined by the present experiments, is conservative. The tests show that α increases with increasing σ. Therefore, when the collected masses are corrected for evaporation, the two characteristics of α just mentioned would tend to mask differences in spray evaporation due to turbulence, unless the last effect were appreciable, as indeed it proves to be.

The present study shows up the need to attack this problem for the much simpler case of a single evaporating drop. Until the effect of turbulence has been explored for a single drop, it will be difficult to devise a theory for sprays.

It appears, on the basis of the curves shown in Fig. 30, that the turbulence tends to broaden or spread the drop-size distribution.

---

* $(\sigma)_{avg}$ denotes the arithmetic mean of the values of σ at x = 9, 10, 14, and 18 inches.

7.2 Effect of Relative Velocity

The data show a strong dependence of rate of evaporation on relative velocity. The increase of rate of evaporation with wind speed was puzzling until it was determined that the speed of the mean drop shortly after injection is far less than the mean speed of the liquid before it leaves the nozzle. Good qualitative agreement was obtained with Frössling's equation. Previous checks of the equation have been carried out with single drops of low volatility. The results given here for a spray using the mean drop diameter in the equation indicate the desirability of checking the equation with single, highly volatile drops.

The drag coefficient derived for the mean drop is low compared with tests of solid spheres. Further, values of C_D for the mean drop do not coincide for different combinations of U and δ which produce the same Reynolds number. These discrepancies suggest that other parameters, such as v_n/U, where v_n is the velocity normal to the drop surface, may be important.

Photographs of the spray just as it leaves the nozzle indicate that no gross changes occur in the spray sheath as U is varied. However, the present equipment lacks the resolution to examine fine changes in the spray formation. No attempt was made to determine the effect of U on drop-size distribution, due to the large number of photographs required and limitations of time and personnel.

7.3 Drop Photography

In applying photography to the measurement of individual drops in the range of diameters from 0.0005 to 0.010 inch, it is found that considerable care must be exercised if even moderate accuracy and reproducibility are to be achieved. Errors which are inherent in the film and its processing do not appear to have been given enough consideration in earlier work on the photography of spray drops. The largest film error is that due to turbidity, which results in a strong dependence of measured drop diameter upon exposure, particularly for drops smaller than about 0.002 inch in diameter, for the present equipment.

Calculations of lens errors are especially useful in establishing the approximate lower limit to the size of drops which can be photographed and measured successfully. However, a more exact limit must be found by experiment, because the standard depth-of-field and resolving-power calculations involve criteria which are, in the practical sense, a trifle arbitrary. The fact that emulsion properties vary somewhat from one batch to another means that film errors must be controlled and measured by direct calibration. Such a calibration procedure was devised and tested, with results which appear to be reasonable and consistent. The tests showed that, if exposure and development are controlled to give a negative density of 1.8 to 2.0, it is possible to measure drops of diameter $0.002 \leq \delta \leq 0.010$ inch to within about 5 per cent, whereas for drops of such size that $0.0005 \leq \delta \leq 0.002$ inch the error will be 10 per cent or higher.

Based on the single set of comparative data available, the photographically determined mass ratio $(M)_{\sigma=7.2}/(M)_{\sigma=0.90}$ is within 10 per cent of that obtained from collector-tube data.

The tedium of manual drop counting and measurement strongly indicates that the data should be obtained from the negatives by an automatic device when many photographs are to be analyzed.

Distribution of this report is in accordance with CM Distribution List TG7-9.

NOMENCLATURE

A	constant, area
B	constant
C	constant
C_D	drag coefficient (p. 16)
C_p	specific heat at constant pressure
D	optical density (p. 38), diffusion coefficient (p. 52)
$\mathfrak{D}$	substantial differential operator (p. 52)
E	collector efficiency (p. 17), photographic exposure (p. 38)
F	focal length of lens (p. 36)
I	light intensity (p. 6)
J	per cent decrease of light intensity (p. 5)
L	length, scale of turbulence (p. 65)
M	mass, mesh length of turbulence screen (p. 65)
$\hat{M}$	molecular weight
N	number of drops
N.A.	numerical aperture of lens (p. 37)
Nu	Nusselt number (p. 84)
P	total pressure
Pr	Prandtl number (p. 84)
R	gas constant, resolving power of photographic films (p. 41), mass fraction (p. 48)
R_{ij}	correlation tensor (p. 63)
Re	Reynolds number based on drop diameter
R_M	Reynolds number based on mesh length (p. 66)
S	surface area, photographic sharpness (p. 40)
Sc	Schmidt number (p. 54)
S_f	frontal area of spherical drop (p. 89)
T	absolute temperature, light transmission (p. 38)
U	free-stream velocity, velocity at edge of boundary layer (p. 54)
a	constant, photographic parameter (p. 38), drop radius (p. 17), induced velocity fluctuation (p. 69)
b	constant, photographic parameter (p. 38)
c	radius or width of collector (p. 17), concentration (p. 52), photographic parameter (p. 38)
d	photographic parameter (p. 38)
f	correlation function (p. 64)
f	wind factor (pp. 53 and 58)
fn	function
f/	lens aperture
g	correlation function (p. 64)
h_g	heat-transfer coefficient (p. 82)
i	inertia of photographic emulsion (p. 39)
j	light absorption parameter (p. 5)
k	constant, collector-tube parameter (p. 17), thermal conductivity (p. 52)
k_g	mass-transfer coefficient (p. 82)

k_q thermal conductivity (p. 82)
l length, direction cosine (p. 16), line width (p. 41)
m mass, direction cosine (p. 16)
n constant, order of a diffraction ring (p. 7), index of refraction (p. 37), number of drops (p. 48), normal direction (p. 53)
p distance from lens (p. 36), vapor pressure (p. 53)
q constant
r radius
t time
u,v,w velocity components
w mass of spray per unit volume of air (p. 18)
x,y,z coordinates

α constant, correction factor for evaporation losses (p. 23), thermal diffusivity (p. 52)
β deposition efficiency (p. 17)
γ photographic contrast (p. 39)
Γ complete gamma function (pp. 3 and 62), photographic astrogamma (p. 40)
δ drop diameter, Kronecker delta (p. 64)
ϵ boundary-layer thickness (p. 55), rate of energy dissipation (p. 64)
θ angle
κ photographic parameter (p. 39)
λ wavelength of light (p. 7), eddy diameter (p. 64), latent heat of vaporization (p. 82)
μ viscosity, evaporation parameter (p. 77)
ν kinematic viscosity
ρ density, radius in lens theory (p. 36)
σ photographic turbidity (p. 41), turbulence number (p. 65)
ϕ collector-tube parameter (p. 17)
Φ function
Ψ function
∇^2 Laplacian operator

BIBLIOGRAPHY

1. Bevans, A.S., "Mathematical Expressions for Drop Size Distribution in Sprays", paper presented at the Conference on Fuel Sprays, University of Michigan, March, 1949.

2. York, J.L., Private Communication. A report on this work is in press as an annual report for Contract W-33-038-ac-21230 between the University of Michigan Engineering Research Institute and the Air Materiel Command of the U.S. Air Force.

3. Lee, D.W., The Effect of Nozzle Design and Operating Conditions on the Atomization and Distribution of Fuel Sprays, NACA TR 425, 1932.

4. Houghton, H.G., "The Size and Size Distribution of Fog Particles", Physics, 2, 467 (1932).

5. Houghton, H.G., and Radford, W.H., "On the Measurement of Drop Sizes and Liquid Water Content in Fogs and Clouds", Papers in Physical Oceanography and Meteorology, published by Mass. Inst. of Tech. and Woods Hole Oceanographic Institution, Vol. VI, No. 4, 1938.

6. Kinoshita, M., and Uchiyama, K., "On the Size of Fog Droplets", Scientific Papers of the Institute of Physical and Chemical Research, Tokyo, No. 391, 19, 144 (1932).

7. Sauter, J., "Die Grössenbestimmung der im Gemischnebel von Verbrennungskraftmaschinen vorhandenen Brennstoffteilchen", Zeits. d. V.D.I., 70, 1040 (1926). Available in translation as NACA TM 390.

8. Schmidt, J.M., Application of the Photoelectric Photometer to the Study of Atomization, JPL-GALCIT Progress Report No. 3-15, 1946.

9. Humphreys, W.J., Physics of the Air, McGraw-Hill, New York, 1940.

10. Wilson, J.G., "Note on Optical Methods of Measuring the Size of Small Water Drops", Camb. Phil. Soc., 32, 493 (1936).

11. Schmidt, J.M., Measurement of Droplet Sizes by the Diffraction Ring Method, JPL-GALCIT Progress Report No. 3-18, 1948.

12. Hausser, F., and Strobl, G.M., "Die Messung der Tropfengrösse bei zerstäubten Flüssigkeiten", Zeits. f. Tech. Physik, 5, 154 (1925).

13. Woeltjen, A., Über die Feinheit der Brennstoffzerstäubung in Ölmaschinen, Dissertation, Technische Hochschule, Darmstadt, 1925.

14. Rupe, J.H., A Technique for Investigation of Spray Characteristics of Constant Flow Nozzles, Paper presented at the Conference on Fuel Sprays, University of Michigan, March, 1949.

15. Guyton, A.C., "Electronic Counting and Size Determination of Particles in Aerosols", Jour. Ind. Hygiene and Toxicology, 28, No. 4, 133 (1946).

16. Vonnegut, B., Cunningham, R., and Katz, R., Report on Instruments for Measuring Atmospheric Factors Related to Ice Formation on Airplanes, AAF TR 5519, 1946.

17. Langmuir, I., and Blodgett, K., A Mathematical Investigation of Water Droplet Trajectories, AAF TR 5418, 1946.

18. Malkus, W.V.R., Bishop, R.H., and Briggs, R.O., Analysis and Preliminary Design of an Optical Instrument for the Measurement of Drop Size and Free-Water Content of Clouds, NACA TN 1622, 1948.

19. Tolman, R.C., et al., "Relation Between Intensity of Tyndall Beam and Size of Particles", Jour. Amer. Chem. Soc., 41, 575 (1919).

20. Anon., Description and Instruction Manual for NBS Portable Turbulence Measuring Apparatus, Model 1940.

21. Schubauer, G.B., and Klebanoff, P.S., Theory and Application of Hot Wire Instruments in the Investigation of Turbulent Boundary Layers, NACA ACR 5K27, 1946.

22. Glauert, H., The Elements of Aerofoil and Airscrew Theory, Cambridge University Press, 1947.

23. Kantrowitz, Arthur, Aerodynamic Heating and the Deflection of Drops by an Obstacle in an Air Stream in Relation to Aircraft Icing, NACA TN 779, 1940.

24. Brown, H.E., and Amstead, B.H., Droplet Dispersion in High Velocity Airstreams, paper presented at the Conference on Fuel Sprays, University of Michigan, March, 1949.

25. York, J.L., Photographic Analysis of Sprays, Ph.D. Thesis, University of Michigan, 1949.

26. Dodge, R., Hagerty, W., and York, J.L., Continuous Fuel Sprays, USAF TR 6067, 1950.

27. Lee, D.W., and Spencer, R.C., Photomicrographic Studies of Fuel Sprays, NACA TR 454, 1933.

28. Scheubel, F.N., "Über Zerstäubung in Vergasern", Jahrb. d. Wiss. Ges. f. Luftfahrt, 140 (1927). Translation, NACA TM 644, 1932.

29. Monk, G.S., Light, McGraw-Hill, New York, 1937.

30. Wood, R.W., Physical Optics, Macmillan, New York, 1934.

31. Hardy, A.C., and Perrin, R.H., The Principles of Optics, McGraw-Hill, New York, 1932.

32. Page, L., Introduction to Theoretical Physics, Van Nostrand, New York, 1935.

33. Myers, L.M., Electron Optics, Van Nostrand, New York, 1939.

34. Mees, C.E.K., The Theory of the Photographic Process, Macmillan, New York, 194

35. Ross, F.E., The Physics of the Developed Photographic Image, Rochester, N.Y., 1924.

36. Jakob, M., Heat Transfer, Wiley, New York, 1949, Vol. I.

37. Probert, R.P., "The Influence of Spray Particle Size and Distribution in the Combustion of Oil Drops", Lond. Phil. Mag., 37, 94 (1946).

38. Maxwell, J.C., "Diffusion", Scientific Papers, Cambridge University Press, 1890, Vol. II.

39. Langmuir, I., "The Evaporation of Small Spheres", Phys. Rev., 12, 368 (1918).

40. Morse, H.W., "On the Evaporation from the Surface of a Solid Sphere", Proc. Am. Acad. Arts and Sciences, 45, 361 (1910).

41. Houghton, H.G., "A Study of the Evaporation of Small Water Drops", Physics, 4, 419 (1933).

42. Namekawa, T., and Takahashi, T., "A Note on the Rate of Evaporation of Small Water-Drops such as Rain-Drops", Mem. Coll. Sci., Kyoto University, 20, 139 (1937).

43. Frössling, N., "Über die Verdunstung fallender Tropfen", Gerlands Beiträge d. Geophysik, 52, 170 (1938).

44. Eckert, E.R.G., Introduction to the Transfer of Heat and Mass, McGraw-Hill, New York, 1950.

45. Goldstein, S., Modern Developments in Fluid Dynamics, Oxford University Press 1938, Vol. I.

46. Luthander, S., and Rydberg, A., "Experimentelle Untersuchung über den Luftwiderstand bei einer um eine mit der Windrichtung parallele achse rotierenden Kugel", Physik. Zeits., 36, 552 (1935).

47. Krell, O., "Druckverteilung an der luftumströmten Kugel", Zeits. f. Flugtechnik u. Motorluftschiffahrt, 22, 97 (1931).

48. v. Kármán, T., "The Fundamentals of the Statistical Theory of Turbulence", Jour. Aero. Sci., 4, 131 (1937).

49. Schubauer, G.B., A Turbulence Indicator Utilizing the Diffusion of Heat, NACA TR 524, 1935.

50. Taylor, G.I., "Statistical Theory of Turbulence", Proc. Roy. Soc. A, 151, 421 (1935).

51. v. Kármán, T., and Howarth, L., "On the Statistical Theory of Turbulence", Proc. Roy. Soc. A, 164, 192 (1938).

52. Dryden, H.L., Schubauer, G.B., Mock, W.C., Jr., and Skramstad, H.K., Measurements of Intensity and Scale of Wind-Tunnel Turbulence and their Relation to the Critical Reynolds Numbers of Spheres, NACA TR 581, 1937.

53. Batchelor, G.K., and Townsend, A.A., "Decay of Vorticity in Isotropic Turbulence", Proc. Roy. Soc. A, 190, 534 (1947).

54. Batchelor, G.K., "Energy Decay and Self-Preserving Correlation Functions in Isotropic Turbulence", Quart. Jour. Appl. Math., 6, 97 (1948).

55. Batchelor, G.K., and Townsend, A.A., "Decay of Isotropic Turbulence in the Initial Period", Proc. Roy. Soc. A, 193, 539 (1948).

56. Batchelor, G.K., and Townsend, A.A., "Decay of Turbulence in the Final Period", Proc. Roy. Soc. A, 194, 527 (1948).

57. Anon., Selected Values of Properties of Hydrocarbons, U.S. Bureau of Standards Circular C461, 1947.

58. Perry, J.H., Chemical Engineers' Handbook, McGraw-Hill, New York, 1950.

59. Elabd, I.H.A., The Analysis of Fuel Sprays by Electrical Methods, Sc.D. Thesis, University of Michigan, 1950.

60. McAdams, W.H.,Heat Transmission, McGraw-Hill, New York, 1942.

61. Kramers, H., "Heat Transfer from Spheres to Flowing Media", Physica, 12 (1946).

62. Brinkman, H.C., "A Calculation of the Viscous Force Exerted by a Flowing Fluid on a Dense Swarm of Particles", Appl. Sci. Res. A, 1, 27 (1947).

63. Kuethe, A.M., and Schetzer, J.D., Foundations of Aerodynamics, Wiley, New York, 1950.